



<https://theses.gla.ac.uk/>

Theses Digitisation:

<https://www.gla.ac.uk/myglasgow/research/enlighten/theses/digitisation/>

This is a digitised version of the original print thesis.

Copyright and moral rights for this work are retained by the author

A copy can be downloaded for personal non-commercial research or study,
without prior permission or charge

This work cannot be reproduced or quoted extensively from without first
obtaining permission in writing from the author

The content must not be changed in any way or sold commercially in any
format or medium without the formal permission of the author

When referring to this work, full bibliographic details including the author,
title, awarding institution and date of the thesis must be given

Enlighten: Theses

<https://theses.gla.ac.uk/>
research-enlighten@glasgow.ac.uk

THE ANALYSIS OF RIDGE WAVEGUIDES
USING GREEN'S FUNCTIONS

A Thesis
submitted to the Faculty of Engineering
of the University of Glasgow

for the degree of
Master of Science in Electronics

by

Mustafa Nadeem Chima
B.Sc. (Hon) Electrical & Electronic Engineering

© Mustafa N. Chima, 1991

October 1991.

ProQuest Number: 11008056

All rights reserved

INFORMATION TO ALL USERS

The quality of this reproduction is dependent upon the quality of the copy submitted.

In the unlikely event that the author did not send a complete manuscript and there are missing pages, these will be noted. Also, if material had to be removed, a note will indicate the deletion.



ProQuest 11008056

Published by ProQuest LLC (2018). Copyright of the Dissertation is held by the Author.

All rights reserved.

This work is protected against unauthorized copying under Title 17, United States Code
Microform Edition © ProQuest LLC.

ProQuest LLC.
789 East Eisenhower Parkway
P.O. Box 1346
Ann Arbor, MI 48106 – 1346

This Thesis is dedicated to my wife

Naureen

and to my son

Khaleel al-Soubur

for their wonderful support and encouragement
for my research work carried out while we
were starting our lives together.

ACKNOWLEDGEMENTS

I wish to thank the following individuals who contributed enormously to the completion of the research work for this thesis.

I sincerely thank Professor John Lamb, Dean of the Department of Electronics and Electrical Engineering for the invaluable use of the computing facilities in the department. I would like to congratulate him for having built up such great computing department and I highly recommend anyone to study here for a degree which involves numerical study.

I am deeply grateful to my supervisor Dr. John M. Arnold, whose continued support and encouragement pushed me through difficult times and made me aware that there is more to numerical work than just computing. I thank him personally for his perseverance in having to answer my continual barrage of questions that never seem to end during my study.

I also thank the Science, Engineering and Research Council for supporting me through the years, without which life would have been impossible. I convey my sincere thanks to Professor Peter Laybourn and Mr. Tom Wright for allowing me to use the University facilities when I needed them the most.

I also wish to thank the computing staff, Miss Anne Mackinnon and Dr. David Muir, for their help with my computing queries and to Paul Rosenberg and Lesley Drysdale of Computing Services for their help with my Fortran programming and UNIRAS™ graphics.

CONTENTS

ACKNOWLEDGEMENTS	i
CONTENTS	ii
LIST OF ABBREVIATIONS AND NOMENCLATURE	vii
LIST OF FIGURES	ix
SUMMARY	1
CHAPTER 1 INTRODUCTION	2
1.1 Waveguide Optics	2
1.1.1 Dispersion	2
1.1.2 Cutoff Condition	3
1.1.3 Monomode Operation	3
1.2 Waveguiding Structures	4
1.2.1 Slab Waveguide	4
1.2.2 Embedded Strip Waveguide	4
1.2.3 Ridge/Rib Waveguide	4
1.3 Numerical Techniques	7
1.3.1 Effective Index Method	7
1.3.2 Scalar Finite Difference Method	9
1.3.3 Fourier Techniques	9
1.4 Green's Function Method	9
1.5 Conclusions and Intended Research	10
1.6 Layout of Thesis	10
CHAPTER 2 WAVEGUIDE THEORY	12
2.1 Maxwell's Equations	12
2.1.1 Wave Equation	13
2.1.2 Maxwell's Curl Equations	13
2.1.3 Eigenvalue β	14
2.1.4 Guidance	14
2.1.5 Cutoff Condition	15

2.2 Reflection at a Dielectric Interface	15
2.3 The Asymmetric Slab Waveguide	19
2.3.1 Guided TE Modes	19
2.3.2 Guided TM Modes	23
2.3.3 Fundamental Mode Solutions	24
2.3.4 First Order Mode	26
2.3.5 Conclusions	26
2.4 Ridge Waveguides	26
CHAPTER 3 NUMERICAL TECHNIQUES	31
3.1 Ridge Waveguide Structures	31
3.1.1 BT1 Structure	31
3.1.2 BT2 Structure	31
3.1.3 BT3 Structure	31
3.2 Effective Index Method	33
3.2.1 EIM Program	33
3.3 Scalar Finite Difference Method	36
3.3.1 Successive Over Relaxation	37
3.3.2 Finite Difference Program	38
3.3.2.1 Iterative Procedure	38
3.3.2.2 Choice of Acceleration/Relaxation Factor	38
3.3.2.3 FD Box Size	39
3.3.3 Results	39
3.4 Conclusions	46
CHAPTER 4 GREEN'S FUNCTION METHOD	49
4.1 Introduction	49
4.2 Existence of the Green's Function	49
4.2.1 Poisson's Equation	49
4.2.2 Green's Function for the Helmholtz Wave Equation	50
4.3 Green's Function Theory	52
4.3.1 Integral Theorems	52

4.3.2 Gauss's Theorem	52
4.3.3 Green's Theorem	52
4.3.4 Reciprocity Property of the GF	53
4.4 Boundary Conditions	54
4.4.1 Dirichlet Boundary Conditions	54
4.4.2 Neumann Boundary Conditions	54
4.4.3 Discontinuity Boundary Conditions	54
4.4.4 Further Boundary Conditions on the Green's Function	55
4.5 Definition of the Analytical Problem:	
Kirchhoff-Huygens Integral	58
4.5.1 Slab/Ridge Waveguide GF Problem	58
4.5.2 Kirchhoff-Huygens Line Integral	58
4.6 Choice of Numerical Method	59
4.6.1 Numerical Choice for the GF	59
4.6.2 Numerical Method for the Electric Field	59
4.6.3 Numerical Method for the Kirchhoff-Huygens Integral	60
4.7 Conclusions	60
CHAPTER 5 DERIVATION OF THE GREEN'S FUNCTION	61
5.1 Fourier Transform of the GF Wave Equation	61
5.2 Free Space (Unbounded) Green's Function	62
5.2.1 Forward Fourier Transform Solution	62
5.2.2 Inverse Fourier Transform	64
5.2.3 Cartesian Coordinate Resolution	65
5.2.4 Cartesian Contour Plot	65
5.3 Dielectric Slab GF Solution - Situation 1	67
5.3.1 Sign of η_n	67
5.3.2 Inverse Fourier Transform Solution	69
5.4 Dielectric Slab GF Solution - Situation 2	71
5.4.1 Singularity Nature of the Green's Function	72
5.5 Conclusions	73

CHAPTER 6	EIGENVALUE SOLUTION USING THE GREEN'S FUNCTION	74
6.1	Derivation of the GF Transcendental Equation	74
6.1.1	Solutions to the GF Transcendental Equation	74
6.2	Derivation of the Modal Contribution Spatial GF $g_m(x,y)$	77
6.2.1	Singularities of the GF	77
6.2.2	Pole Contribution of the Green's Function	78
6.2.3	Spatial GF $g_m(x,y)$	79
6.3	Derivation of the IFT Green's Function $g_n(x,y)$	81
6.4	Kirchhoff-Huygens Line Integral	82
6.4.1	Matrix Implementation	82
6.4.2	GF Matrix Elements	85
6.4.3	Iterative Procedure	85
6.5	Slab Waveguide Results	85
6.6	Rib Waveguide Results	89
6.7	Conclusions	89
CHAPTER 7	CONCLUSIONS AND FUTURE WORK	90
7.1	Waveguide Study	90
7.2	Green's Function Study	90
7.3	Improvements and Future Considerations	91
REFERENCES		92
APPENDIX A	Transcendental Equation Program	95
APPENDIX B	Effective Index Method Program	97
APPENDIX C	Finite Difference Method Program	100
APPENDIX D	Finite Difference Approximation	107
APPENDIX E	SOR Applied to Gauss-Seidel	111
APPENDIX F	Shifting Theory for Inverse Fourier Transform	114
APPENDIX G	Green's Function Program (Free Space)	115
APPENDIX H	Inverse Fourier Transform Program for GF	117
APPENDIX I	Green's Function Program (Situation 1)	119

APPENDIX J	GF Transcendental Equation Program	122
APPENDIX K	Modal Green's Function Program	125
APPENDIX L	Numerical Green's Function Program	128
APPENDIX M	Kirchhoff-Huygens Matrix Calculations	131

LIST OF ABBREVIATIONS AND NOMENCLATURE

DBC	Dirichlet Boundary Conditions
EIM	Effective Index Method
FD	Finite Difference
FDM	Finite Difference Method
FT	Fourier Transform
GF	Green's Function
IFT	Inverse Fourier Transform
KH	Kirchhoff-Huygens
NAG	Numerical Algorithms Group
NBC	Neumann Boundary Conditions
RF	Relaxation Factor
SOR	Successive Over Relaxation
TE	Transverse Electric
TIR	Total Internal Reflection
TM	Transverse Magnetic
$g(x,y)$	Scalar spatial GF
$G(k_x,y)$	Forward Fourier transformed GF
G_o	FT of free space GF
$g_n(x,y)$	Spatial GF derived from numerical FT
$g_m(x,y)$	Spatial contribution of GF
$\underline{E}, \underline{H}$	Electric and magnetic field vectors
\underline{B}	Magnetic flux density
\underline{D}	Electric flux density
\underline{J}	Current density
ρ	Charge density
μ_o, μ_r	Magnetic and relative magnetic permeability
ϵ_o, ϵ_r	Dielectric and relative dielectric permittivity
κ, k	Transverse wavenumber
λ	Wavelength
k_x	Fourier spatial frequency
k_q	Root of GF transcendental equation
b	Normalised effective index
n_e	Effective index of propagation
β	Propagation constant
$\delta(y-y')$	Dirac delta function
v	Frequency parameter (EIM)
α^{TE}	Asymmetry parameter

- ω Angular frequency
- $E_{i,j}$ Discrete scalar electric field (FDM)
- n_1, n_2, n_3 Cladding, guiding and substrate layer relative permittivities
- (x, y, z) Observational point coordinates
- (x', y', z') Source point coordinates

$$\nabla = \left[\frac{\delta}{\delta x}, \frac{\delta}{\delta y}, \frac{\delta}{\delta z} \right] \text{ del operator}$$

$$\nabla^2 = \nabla \cdot \nabla = \left[\frac{\delta^2}{\delta x^2} + \frac{\delta^2}{\delta y^2} + \frac{\delta^2}{\delta z^2} \right]$$

$$\nabla_t^2 = \left[\frac{\delta^2}{\delta x^2} + \frac{\delta^2}{\delta y^2} \right]$$

LIST OF FIGURES

CHAPTER 1

Figure 1.1 Slab Waveguide Geometry	5
Figure 1.2 Embedded Strip Waveguide Geometry	6
Figure 1.3 Ridge Waveguide Geometry	8

CHAPTER 2

Figure 2.1 Reflection at a Dielectric Interface	16
Figure 2.2 Allowed Values of β	17
Figure 2.3 Optical Paths For Different Values of β	18
Figure 2.4 Coordinate System for the Slab Waveguide	20
Figure 2.5 TE and TM Polarisation Vectors	21
Figure 2.6 Asymmetric Slab Waveguide Structures	25
Figure 2.7 Fundamental Mode Profiles	27
Figure 2.8 1st Order Mode Profile for Waveguide 1	28
Figure 2.9 Finite Difference Contour Plot of Cross Sectional Electric Field Distribution.	29

CHAPTER 3

Figure 3.1 BT Ridge Waveguide Structures	32
Figure 3.2 Effective Index Method Approximation	34
Figure 3.3 Normalised b versus v Diagram	35
Figure 3.4 Rate of Convergence for Different Values of ω	40
Figure 3.5 Rate of Convergence for $\omega \geq 2.0$	41
Figure 3.6 Cross Sectional Contour Plot of Mode Profile for BT3 Using Different Box Sizes	43
Figure 3.7 BT1 Mode Profile Contour Plot	44
Figure 3.8 BT2 Mode Profile Contour Plot	45
Figure 3.9 Convergence of FD Method Using Smaller Mesh Spacing	47

CHAPTER 4

Figure 4.1 Solution of Poisson's Equation	51
Figure 4.2 Green's Function's Domain	57

CHAPTER 5

Figure 5.1 Point Source in Free Space	63
Figure 5.2 2D and 3D Plot of Free Space Green's Function g_n	66
Figure 5.3 Green's Functions Situations	68
Figure 5.4 2D Contour Plot of Green's Function for Situation 1	70

CHAPTER 6

Figure 6.1 Graphical Solution of Transcendental Equation for WG2	75
Figure 6.2 Graphical Solution of Transcendental Equation for WG1	76
Figure 6.3 Plane of Integration for the Cauchy Integrals	80
Figure 6.4 Contour Plot of the Modal Green's Function $g_m(x,y)$	83
Figure 6.5 Contour Plot of the Numerical Green's Function $g_n(x,y)$	84
Figure 6.6 Kirchhoff-Huygens Line Integral Path	86
Figure 6.7 Plot of Contour Electric Field Using the KH Integral	88

APPENDIX

Figure D1 FD Approximation of the Tangent of a Curve	108
Figure D2 Finite Difference Grid	110

SUMMARY

In the theory of integrated optics, a central role is played by the rib waveguide geometry. The electromagnetics problems consists of the determination of the transverse mode profile and propagation constant of the dominant mode in the guide. Since this problem is not soluble in closed form by any known analytical methods, several numerical techniques have been used, amongst which the simple finite-difference (FD) method is very attractive because of the rectilinear geometry of the rib waveguide. However, the problem requires the imposition of a boundary condition at infinity in the transverse cross-section, which is not possible on a FD mesh of finite extent.

The Green's function (GF) is an alternative formulation for this open-boundary problem. A suitable GF for a planar waveguide (with no rib) can be found analytically by Fourier transform methods, which can then be used to transform the Helmholtz equation for the region outside the rib from an elliptical partial differential equation into an integral equation on a contour surrounding the rib only, via Kirchhoff's theorem. This integral equation is matched to a FD solution for the field inside the rib by an iterative method. In this way the correct boundary conditions at infinity are automatically incorporated. In actual implementation of the method, a fully discretised analogue of Green's theorem on the FD mesh is used, in which the GF is the true inverse of the discrete FD operator, rather than discretising the exact boundary integral equation, which permits a systematic treatment of the singularity of the GF to be carried out.

The method is explored fully by initially considering slab waveguides, i.e. with no rib. Application to the ridge waveguide is however not investigated to due time constraints, but a possible method is discussed.

1.1 WAVEGUIDE OPTICS

Waveguide optics has undergone massive investigation during the last decade, as researchers begin to exploit the propagating characteristics of light. With the promise accomplished of high transmission rates by fibre optics, the next step of semiconductor integrated optics does not seem too remote. Propagation of electromagnetic waves in semiconductor material had already been investigated in the 1950's by Marcuvitz¹ where the theory of wave propagation was established.

The main impetus for constructing integrated optical circuits came about when the design of an all-optical fibre circuit was devised by S.E. Millar² at Bell Laboratories. Although transmission of optical information in fibres yielded in high bit transmission rates, they suffered from signal degradation over several hundreds of kilometres. Optical fibre repeaters constructed from the current state-of-the-art electrical technology proved adequate but cumbersome. Because the operating wavelength was in the micron region, optical structures of these dimensions could yield small compact device circuits with lower loss than their bulk counterparts.

The majority of guided wave propagation problems are solved by employing the analytical separation of variables technique. This method, although powerful, becomes impossible whenever the boundary conditions are not simple. Dielectric slab waveguides³ have been analysed exactly. Other geometries considered are the strip or embedded strip waveguide geometry, and ridge waveguides. Confinement of the light in the strip waveguides is accomplished by the use of total internal reflections at the dielectric boundaries.

These various geometries may solve the problem of guiding the light, other problems can occur such as dispersion, cutoff conditions and multimode operation. Ideally monomode operation is desired and this can be attained by careful material design, geometry and dimensions.

1.1.1 Dispersion

One of the main causes of loss of waveguiding is that of material dispersion. This is due to the inherent property that the refractive index of optical materials is a function of wavelength. Therefore for minimum dispersion, a particular operating wavelength for the waveguide material is chosen⁴.

Another cause of loss of waveguiding is that caused by waveguide dispersion. This causes the optical pulse to spread out and become distorted as it travels down the length of the waveguide. Since the pulse spread is proportional to the difference in the refractive

indices of the guiding and substrate layers, this distortion can be reduced by considering a much smaller difference in refractive index step.

The other type of dispersion is that of intra-modal dispersion. For a given frequency of operation, the waveguide supports a finite number of modes, each of which travels at its own velocity. Thus the optical information can become irregular because of this. However, the problem can be solved by operating the waveguide with one mode, known as monomode operation.

1.1.2 Cutoff Condition

Confinement of the light inside a guiding dielectric layer is accomplished by surrounding this layer with other dielectric layers whose refractive index is lower. With this configuration, the optical signal is sandwiched between the dielectric interfaces by total internal reflection (TIR). When TIR is lost at one dielectric interface, the light escapes from the guiding region and subsequently disperses into the surrounding region. This mainly occurs at low frequencies in which the angle of incidence of the light at a dielectric interface is sufficiently high. As a consequence propagation of the light is not possible.

1.1.3 Monomode Operation

Monomode operation in optical devices is preferred. As mentioned above, an optical device which operates in multimode the optical information is dispersed due to the different group velocities of each mode and thus transmission of information becomes useless. Since the number of modes supported is directly dependant on the materials and geometry used, suppression of these unwanted modes can be accomplished by careful device design. The zero order or fundamental mode has a maximum at the centre of the guide, with the field decaying as one progresses to the dielectric boundaries. This field is easily generated by semiconductor lasers and can be detected by photo-diodes.

Hence for a waveguide to operate with particular modes it is important that these optical devices be accurately modelled so that the time and effort spent on material and geometry design of the device be reduced.

It can be seen that the development of optical devices is over-complicated by the tight tolerances of the small micronic structures. However it is envisaged that this technology can replace the 'electric systems' technology by superior performance and be cost effective⁵.

1.2 WAVEGUIDING STRUCTURES

1.2.1 Slab Waveguide

The slab waveguide is the simplest geometry that can be considered. Because of its simplicity, it can be described by simple mathematical equations that give exact analytical solutions. These waveguide solutions and properties have been useful in obtaining a better understanding of more complicated waveguiding structures.

Figure 1.1 shows the configuration of the dielectric slab waveguide. A layer of material with refractive index n_2 is deposited onto a substrate with refractive index n_3 . The cladding, n_1 , can either be another dielectric material with a refractive index lower than n_2 , or air, which has a refractive index of unity. Because $n_2 > n_1, n_3$, light is confined by total internal reflections on the dielectric interfaces.

If $n_1 = n_3$, we have a symmetrical slab waveguide structure. For $n_1 \neq n_3$, it is called an asymmetric slab waveguide. The symmetric structure supports many modes which are mathematically expressed as odd and even modes. The lowest order mode is capable of propagation down to very low frequencies. Modes in the asymmetric slab waveguide are fewer and mathematically more complicated. However they are more widely used since the higher modes can easily be suppressed.

Fabrication of slab waveguides is made easier by the simple geometry of the structure. Deposition of glass/plastic films onto similar substrates is accomplished by evaporation, sputtering or by epitaxial growth techniques. Another method called ion-implantation, utilises the method of creating a separate layer on a substrate by bombarding the surface with ions. This alters the refractive index of the surface layer and hence a guiding film is created. The depth of the layer can be altered by accelerating the ions to a higher or lower velocity.

1.2.2 Embedded Strip Waveguide⁶

Restricting the area of the ion implantation, a smaller or narrower structure can be built. As the name suggests, a waveguide with a higher refractive index is embedded into the substrate as shown in figure 1.2a. The rays of light are again confined in the lateral direction by the reflection at the bottom and top dielectric interfaces, but they are also confined in the transverse direction thus restricting another degree of freedom. The propagation of the rays can be visualised as a zig-zag fashion along the length of the guide (figure 1.2b) which can be bent to channel the light along a predetermined path.

1.2.3 Ridge/Rib Waveguide

A simple solution to confine a mode in a dielectric slab waveguide is to introduce

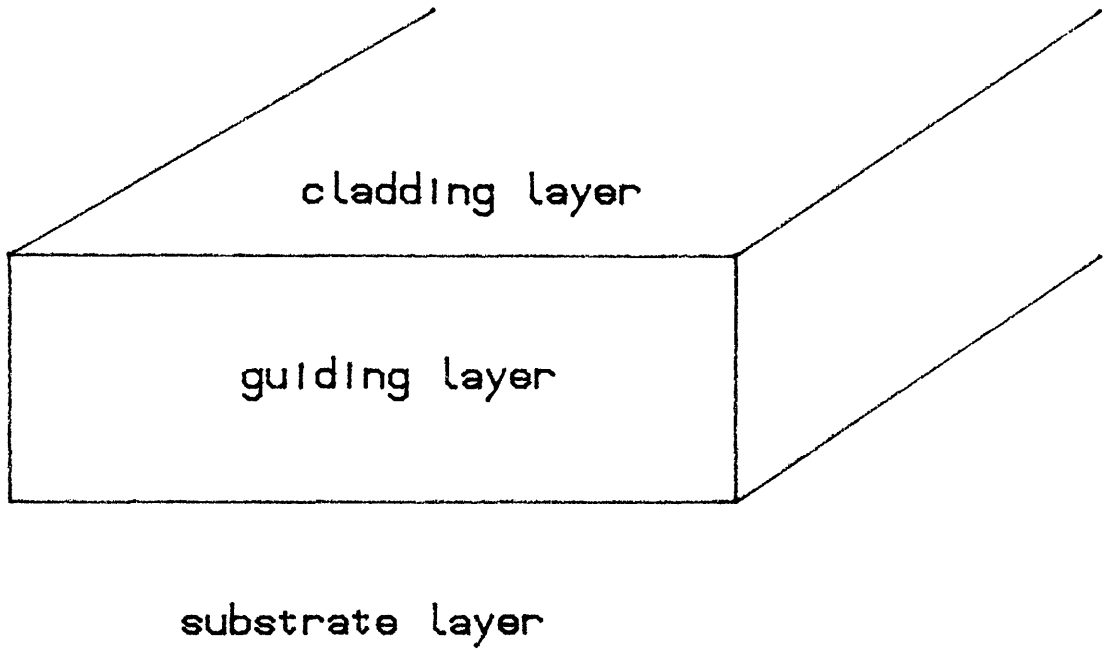


Figure 1.1 Slab Waveguide Geometry

Original in colour

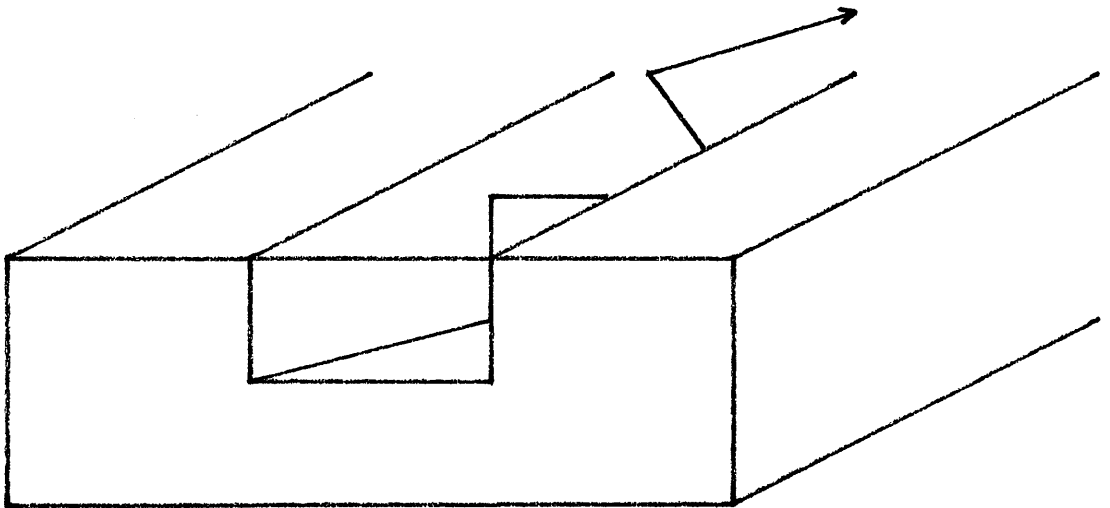
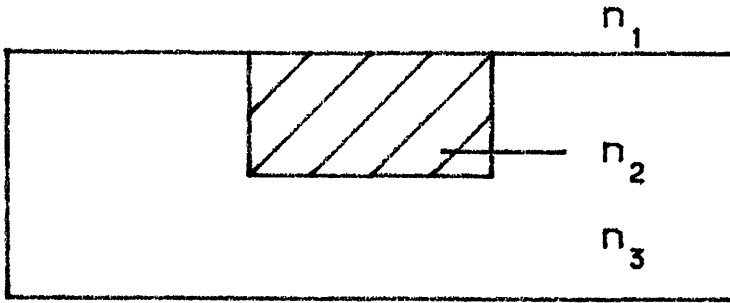


Figure 1.2 Embedded Strip Waveguide Geometry

a ridge/rib into which extends part of the modal field (figure 1.3). This structure is useful because it can control the effective index of propagation of the mode by altering the rib height. A guide consisting of a rib height h greater than the depth layer d will give strong guiding in the rib part as the mode would be operating at cutoff in the thinner slab region. Such a device with strong guiding characteristics can easily incorporate bends or curves as in the embedded waveguide. A structure with $h \ll (h+d)$ would cause the mode to extend laterally as the vertical confinement is weak. This configuration can be used for transferral of modal power into another rib waveguide in close proximity. This directional coupler can be ultimately used as a logic switch.

1.3 NUMERICAL TECHNIQUES

Because of the complexities of the waveguide structure, an analytical solution of the wave equation is not possible, so an approximate numerical solution is sought.

Over the last two decades, researchers have devised many approximate numerical techniques in order to model waveguiding characteristics. A solution to an eigenvalue equation will give an effective index value of the propagation wave, and a physical representation of the modal field. These can be used to determine the guiding characteristics of the structure, how well/weakly confined the wave mode is etc.. The number of propagating modes and their effective indices of propagation can consequently be calculated and by altering the dimensions of the waveguide, suppress any unwanted modes. Other ways of suppressing modes is to alter the waveguide material composition or the operating wavelength. Optimum devices can therefore be designed from the results of the numerical analysis.

The main method of determining optical waveguide characteristics is to use Maxwell's equations. These equations involve the electromagnetic components of the optical field \underline{E} and \underline{H} , whose properties ultimately lead to a wave equation which is solved for the particular waveguide structure.

The wave equation is readily determined for simple slab waveguides, where the boundary conditions are simple and yield exact solutions to the electric field profile and effective index of propagation. However this analytical technique breaks down whenever the waveguide geometry becomes complicated e.g. when a vertical dielectric boundary is introduced as in the embedded and ridge waveguides. As a consequence an approximate numerical technique is pursued.

1.3.1 Effective Index Method

The Effective Index method⁷ (EIM) is an approximate technique which attempts to solve the effective index by considering slab modes. This is accurate if the adjacent slabs

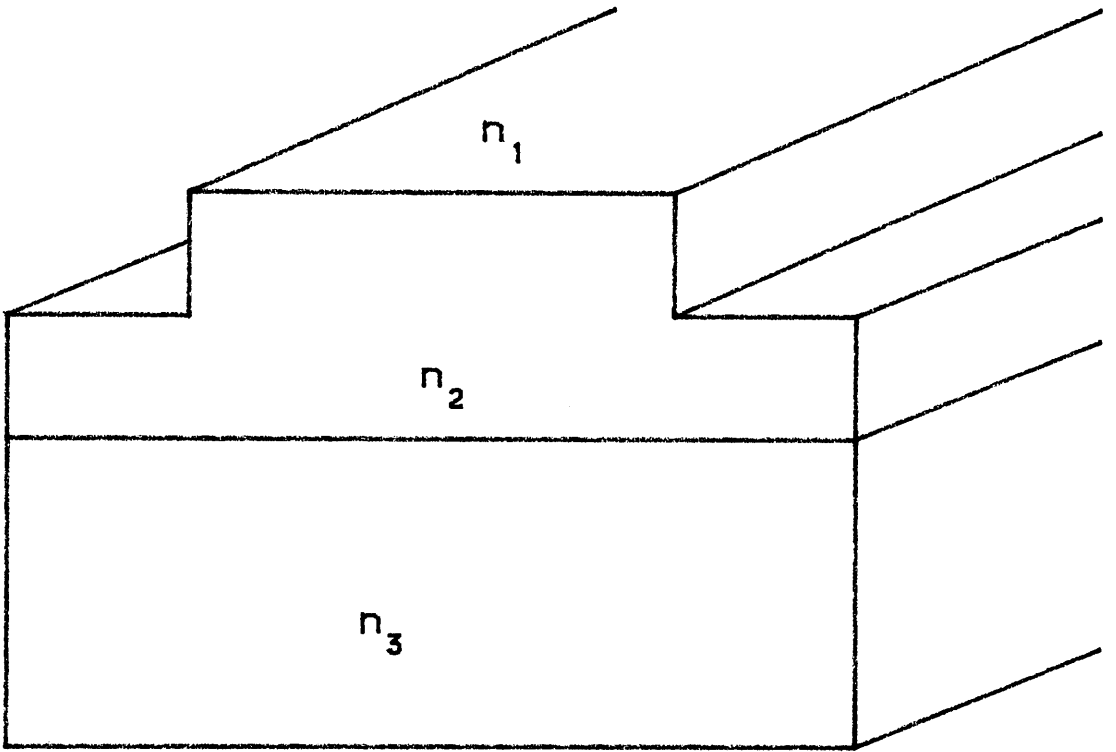


Figure 1.3 Ridge Waveguide Geometry

do not differ considerably in height and this method could break down if the rib was very much pronounced. However the over estimation puts an upper limit to the effective index.

1.3.2 Scalar Finite Difference Method⁸

This method is suitable for rectangular waveguides such as the ridge waveguide. The cross section of the waveguide is covered by a rectangular mesh/grid, the points on this grid representing the electric field component of the optical field. The second order derivatives in the wave equation are replaced by the finite difference (FD) approximation and the equation is rearranged to be solved for the electric field at each grid point. The FD approximation is applied in a pagewise manner across the cross section of the waveguide, with the effective index being updated by the Rayleigh quotient using the corrected field values. Convergence is usually attained when the difference between successive effective index values is small or that the effective index no longer improves.

The error involved in this method is $(\Delta h)^2$ where h is the mesh spacing between adjacent points. This is a simple technique which gives an acceptable representation of the field profile and the effective index estimate.

The major limitation to this technique is that the boundary conditions at infinity cannot be modelled. To solve this, one would have to consider a larger box to include the field further along the lateral direction. Alternatively the finite mesh/grid can also be graded, so that smaller mesh points are used within the vicinity of the modal field, and a larger mesh as the field gets weaker.

1.3.3 Fourier Techniques

As most waveguides have a planar stratification, elementary Fourier techniques can be implemented. The advantage of this is that the Fourier transform (FT) would eliminate the coordinate variable in the direction of the FT, thus simplifying the wave equation to be solved. As shown in chapter 4, this reduces the partial differential wave equation into an ordinary differential equation, whose solutions are simple.

1.4 GREEN'S FUNCTION METHOD

The Green's function (GF) method has been mainly applied to microwave problems⁹ but recently has been used for optical waveguide problems^{10, 11}. The GF is a solution of Poisson, wave and Helmholtz equations, and as the boundary conditions are exact, makes the GF a very powerful technique.

The GF basically gives the impulse response of a system. The inhomogeneous Helmholtz wave equation contains the Dirac delta function $\delta(y-y')$ which can be thought

of as being a pulse of laser light in the guiding region. Thus we can determine the modal distribution of the waveguide caused by this point source. For the other surrounding regions, the homogeneous Helmholtz wave equation is solved, and with the reduction to an ordinary differential equation with the application of the Fourier transform, gives a simple known solution.

The GF can also be used with other analytical techniques such as the Kirchhoff–Huygen's line integral. This method explicitly incorporates the field conditions at infinity, which is of course, advantageous to our problem.

1.5 CONCLUSIONS AND INTENDED RESEARCH

Waveguiding can be accomplished in many ways and is dependent on many factors like material composition and geometry. These parameters can be determined by the numerical modelling of the optical device, hence an accurate numerical method is sought.

Initially the Effective Index Method and Finite Difference methods are studied and the results compared to results published by other authors who have used these methods.

To obtain an analytical solution to the field of dielectric waveguides, the scalar GF is determined. This is the main focus of research for the thesis. Since the slab waveguide solution is known to be exact, the results of the GF derived will be compared to this.

1.6 LAYOUT OF THESIS

A review of the basic waveguide structures to be considered has been given. The complication of the exact analytical solution for other waveguide geometries has given impetus to construct another numerical technique for the evaluation of waveguide characteristics of rib structures.

Chapter 2 will discuss the background theory of wave propagation in dielectric films in more detail. The concepts discussed will include Maxwell equations, total internal reflection and of exact solutions of the electric field for slab waveguides.

A full chapter is devoted to the Effective Index and the Finite Difference methods for slab and ridge waveguides, and particular ridge waveguide structures of interest will be introduced and solved with the numerical techniques mentioned. The finite difference approximation is introduced here to facilitate an understanding to the discretized method used in the Kirchhoff–Huygens line integral.

In chapter 4, an introduction is given to the scalar Green's Function which is to be applied to the waveguide problem. The properties and relevant boundary conditions applicable to the GF method are discussed. The analytical tool, the Kirchhoff–Huygens (KH) line integral is derived, whose components includes the GF.

The derivation of the GF will be given in chapter 5. In this chapter, the GF for free space and the dielectric slab structure are determined. These exercises are performed so that the calculated GF can be compared to solutions given in the literature.

In chapter 6, the solution of the GF for a point source inside the guiding layer of the slab waveguide is extended to derive a transcendental equation, which when solved, gives the effective index of the structure. As this GF is a component of the KH line integral, the integral is performed for a chosen path in the slab waveguide. Numerical results using the KH integral and any limitations of the GF method are discussed.

Conclusions about the research work and future considerations and improvements are given in chapter 7.

Before attempting to solve the propagation characteristics of ridge waveguides, this chapter introduces Maxwell's equations, the concept of total internal reflection of light in dielectric media, transverse electric (TE) and transverse magnetic (TM) propagation of electromagnetic waves in slab waveguides and eigenvalues of such structures. Since the treatment of the slab structure is exact, it will be used as a reference for the calculation of the Green's function for the slab waveguide.

2.1 MAXWELL'S EQUATIONS

Propagation of electromagnetic waves is described by the electrical and magnetic field vectors $\underline{E}(x,y)$ and $\underline{H}(x,y)$, the vectors being derived from the electric and magnetic fields produced by the motion of electrostatic charges. The electric and magnetic field components of electromagnetic wave propagation are expressed from Faraday's and Ampere's Laws respectively

$$\nabla \times \underline{E} = -\delta \underline{B} / \delta t \quad (2.1)$$

$$\nabla \times \underline{H} = \delta \underline{D} / \delta t + \underline{J} \quad (2.2)$$

where \underline{B} is the magnetic flux density, \underline{D} is the electric flux density and \underline{J} is the current density. Assuming that there are no sources in the region containing the fields, then $\underline{J} = 0$ and $\rho = 0$, thus

$$\nabla \cdot \underline{B} = 0 \quad (2.3)$$

$$\nabla \cdot \underline{D} = \rho = 0 \quad (2.4)$$

$$\nabla \cdot \underline{J} = \delta \rho / \delta t = 0 \quad (2.5)$$

$$\underline{D} = \epsilon \underline{E} = \epsilon_0 \epsilon_r \underline{E} \quad (2.6)$$

$$\underline{B} = \mu \underline{H} = \mu_0 \mu_r \underline{H} \quad (2.7)$$

where ρ is the charge density, ϵ_r is the permittivity of the medium, ϵ_0 is the permittivity of free space, μ_r is the relative permeability of the material (usually equal to 1) and μ_0 is the permeability of free space.

For time harmonic fields, propagation of the electromagnetic wave along the z-direction is assumed as $\exp j(\omega t - \beta z)$. Therefore the above equations are expanded to give

$$\nabla \times \underline{E} = -j\omega \underline{B} \quad (2.8)$$

$$\nabla \times \underline{H} = j\omega \underline{D} \quad (2.9)$$

from (2.6), (2.7) assuming a source free region, i.e. $\rho = 0$, we obtain

$$\nabla \times \underline{E} = -j\omega \mu \underline{H} \quad (2.10)$$

$$\nabla \times \underline{\mathbf{H}} = j\omega\epsilon \underline{\mathbf{E}} \quad (2.11)$$

$$\nabla \cdot \underline{\mu \mathbf{H}} = 0 \quad (2.12)$$

$$\nabla \cdot \underline{\epsilon \mathbf{E}} = 0 \quad (2.13)$$

These are the reduced Maxwell's Equations for time harmonic fields.

2.1.1 Wave Equation

Taking the curl of (2.10) and (2.11) we obtain

$$\nabla \times \nabla \times \underline{\mathbf{E}} = \nabla(\nabla \cdot \underline{\mathbf{E}}) - \nabla^2 \underline{\mathbf{E}} = -j\omega\mu \nabla \times \underline{\mathbf{H}} = \omega^2 \epsilon \underline{\mu \mathbf{E}}$$

and
$$\nabla \times \nabla \times \underline{\mathbf{H}} = \nabla(\nabla \cdot \underline{\mathbf{H}}) - \nabla^2 \underline{\mathbf{H}} = j\omega\mu \nabla \times \underline{\mathbf{E}} = \omega^2 \epsilon \underline{\mu \mathbf{H}}$$

i. e.
$$\nabla^2 \underline{\mathbf{E}} + k_C^2 \underline{\mathbf{E}} = 0 \quad (2.14)$$

$$\nabla^2 \underline{\mathbf{H}} + k_C^2 \underline{\mathbf{H}} = 0 \quad (2.15)$$

$$k_C^2 = \omega^2 \mu \epsilon \quad (2.16)$$

Equations (2.14) and (2.15) represent the reduced Helmholtz wave equation for electromagnetic waves for macroscopic media, which will be used extensively for the evaluation of slab waveguides.

2.1.2 Maxwell's Curl Equations

Using the definition of the curl operator on the vector $\underline{\mathbf{U}} = u(x,y,z)$

$$\begin{aligned} \nabla \times \underline{\mathbf{U}} &= \begin{vmatrix} \mathbf{i} & \mathbf{j} & \mathbf{k} \\ \partial/\partial x & \partial/\partial y & \partial/\partial z \\ U_x & U_y & U_z \end{vmatrix} \\ &= \left[\frac{\partial U_z}{\partial y} - \frac{\partial U_y}{\partial z} \right] \mathbf{i} + \left[\frac{\partial U_x}{\partial z} - \frac{\partial U_z}{\partial x} \right] \mathbf{j} + \left[\frac{\partial U_y}{\partial x} - \frac{\partial U_x}{\partial y} \right] \mathbf{k} \end{aligned} \quad (2.17)$$

in equations (2.10) and (2.11), we obtain the expanded Maxwell's equations in component form

$$\frac{\partial E_z}{\partial y} + j\beta E_y = -j\omega\mu H_x \quad (2.18)$$

$$-j\beta E_x - \frac{\partial E_z}{\partial x} = -j\omega\mu H_y \quad (2.19)$$

$$\frac{\partial E_y}{\partial x} - \frac{\partial E_x}{\partial y} = -j\omega\mu H_z \quad (2.20)$$

$$\frac{\partial H_z}{\partial y} + j\beta H_y = j\omega\epsilon E_x \quad (2.21)$$

$$-j\beta H_x - \frac{\partial H_z}{\partial x} = j\omega\epsilon E_y \quad (2.22)$$

$$\frac{\partial H_y}{\partial x} - \frac{\partial H_x}{\partial y} = j\omega\epsilon E_z \quad (2.23)$$

The above equations explicitly relate the transverse electric field and the transverse magnetic field components. However, we need not solve the above for all components, since we can make use of the redundancy in Maxwell's equations to get the transverse field components from solutions for the longitudinal component E_z and H_z (section 2.3).

2.1.3 Eigenvalue β

To describe each mode propagating in the dielectric medium, a distinct value of eigenvalue β (or effective index n_e) is designated. Each mode has this distinct eigenvalue unless two modes are degenerate (these modes have equal phase velocities but their transverse field profiles are not always identical). Thus having defined a propagating mode, it is then assumed to have a translational invariance as $\exp j(\omega t - \beta z)$, which describes a mode travelling in the positive z -direction, with a propagation index of β and at a frequency ω ($\omega = 2\pi f$) radian/second, i.e.

$$\begin{aligned} \underline{E}_i(x, y, z) &= \underline{e}_i(x, y) e^{j(\omega t - \beta_i z)} \\ \underline{H}_i(x, y, z) &= \underline{h}_i(x, y) e^{j(\omega t - \beta_i z)} \end{aligned} \quad (2.24)$$

Since we have written the time and space variation of the field in terms of the complex exponential, the only physically meaningful part of this complex expression is the real part i.e. $\xi = \text{Re}(\underline{E})$. This equality relates the real measurable field ξ to the theoretically derived field \underline{E} . The principle advantage of this is that the complex exponential expression is more readily manipulated than the equivalent expressions involving sine and cosine functions.

2.1.4 Guidance

For a mode to propagate in a dielectric medium, it is necessary that the effective index $\beta = k_0 n_e$ be such that

$$k_0 n_2 \gg \beta \gg k_0 n_3 \gg k_0 n_1 \quad (2.25)$$

where $k_0 = 2\pi/\lambda_0$ is the free space wave number, λ_0 being the free space wavelength. n_1 and n_3 are the refractive indices of the surrounding cladding and substrate regions respectively. A mode is said to be strongly guided if the value of n_e is close to that of the film refractive index n_2 , and weakly guided if n_e is close to n_3 . A value of effective index between these two extremes ensures that total internal reflection occurs at both dielectric boundaries. This is described in more detail below. It is therefore envisaged that the solution of the eigenvalue equations derived for slab waveguides will yield effective index values within this range of propagating modes.

2.1.5 Cutoff Condition

If the value β of a mode satisfies the relation

$$\beta = k_0 n_3 \quad (2.26)$$

the mode is said to be operating at the cutoff condition. As described in section 1.2, this occurs when total internal reflection (TIR) is lost at a dielectric boundary and the mode propagates into the surrounding medium. The concept of TIR is described below.

2.2 REFLECTION AT A DIELECTRIC INTERFACE

Consider a ray of light at an interface between a dense medium with refractive index n_2 , and a less dense medium which has a refractive index of n_1 , i.e. $n_2 > n_1$. This is shown in figure 2.1. By the application of Snell's law

$$n_2 \sin \theta_2 = n_1 \sin \theta_1 \quad (2.27)$$

It can be seen that for the critical condition $\theta_1 = 90^\circ$ (i.e. no light escapes into the n_1 region) we require

$$n_2/n_1 = \sin \theta_c \quad (2.28)$$

Once the critical condition is met, $\sin \theta_1 > 1.0$, therefore the $\pi/2 - \theta_1$ is imaginary. The ray is reflected back into the n_2 medium. For a three layer problem, we require the condition

$$\sin \theta > n_3/n_2 \quad (2.29)$$

at the lower interface. For the cutoff conditions $n_2 \sin \theta > n_1$ and $n_2 \sin \theta > n_3$, multiplying by k_0

$$n_2 k_0 \sin \theta > k_0 n_1$$

$$n_2 k_0 \sin \theta > k_0 n_3$$

$$\text{Thus } n_2 k_0 > \beta > k_0 n_3 > k_0 n_1 \quad (2.30)$$

as mentioned previously in equation (2.25). A graphical representation of the above inequality is shown in figure 2.2.

It can be seen that for a given value of frequency ω , there exists a continuum range of values for β for each mode. Each value of β gives a different value of bounce angle at the interface (figure 2.3a).

Simple guide analysis suggests that β can take on a continuum of values between $n_2 k_0$ and $n_3 k_0$ for a given frequency. Since a given value of β corresponds to one value of bounce angle, this implies that the bounce angle has a continuum of values once critical conditions have been met.

Figure 2.3b shows loss of TIR – light escapes into the cladding (air). Figure 2.3c

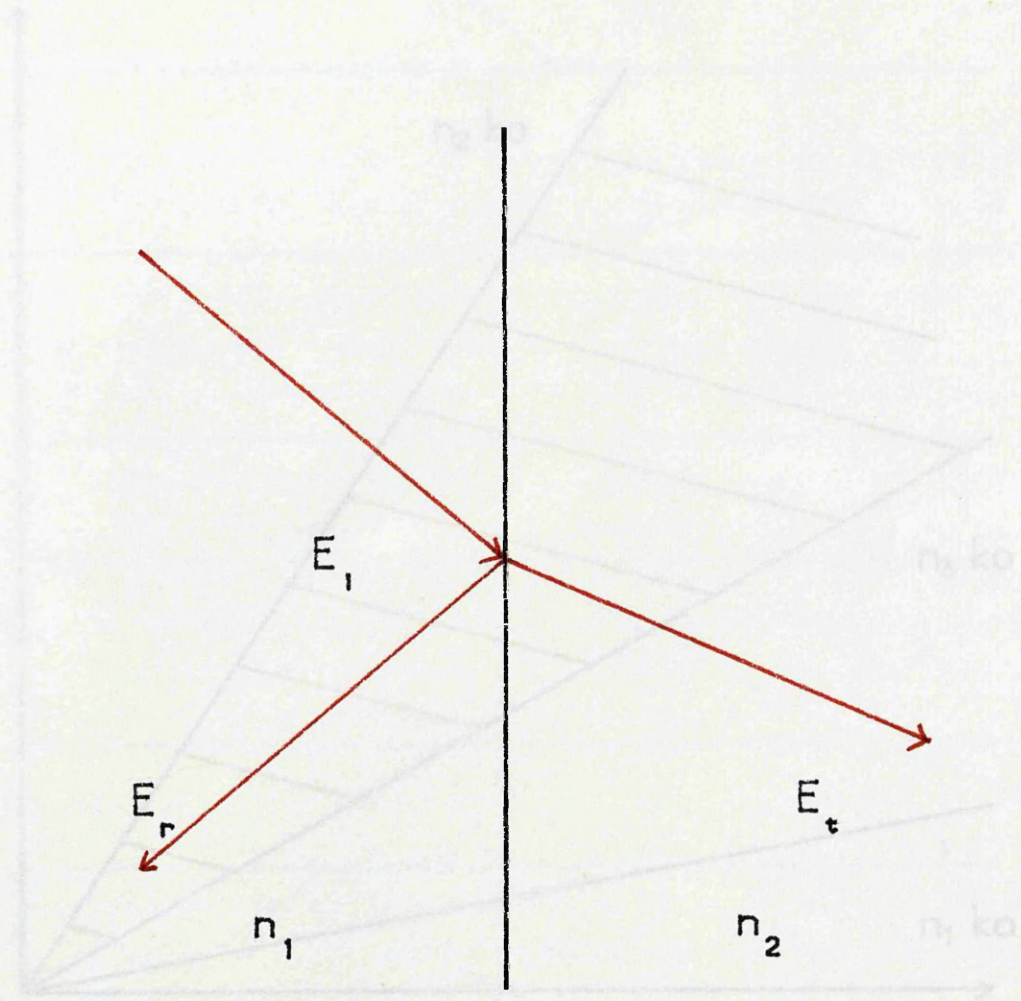


Figure 2.1 Reflection at a Dielectric Interface

Original in colour

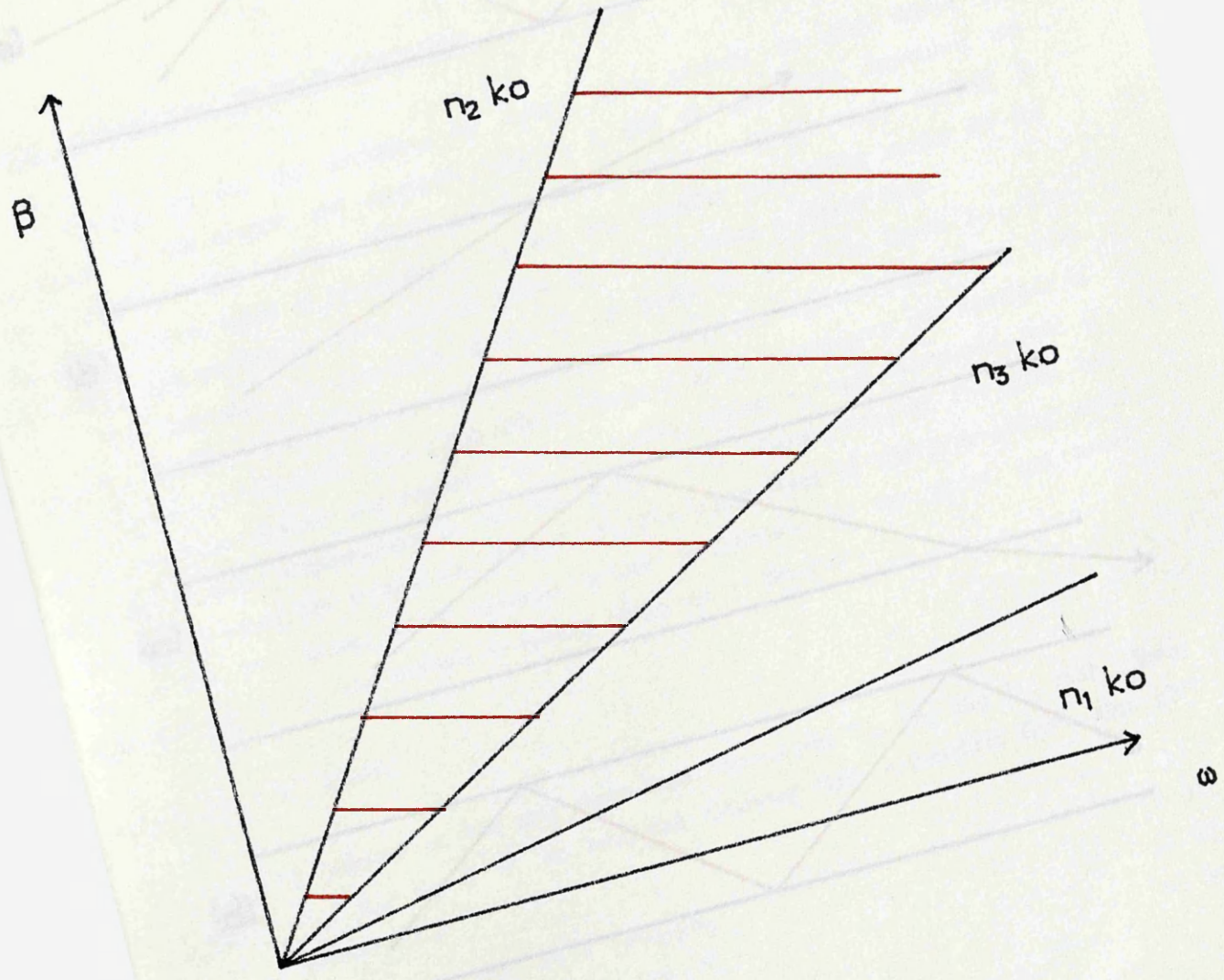


Figure 2.2 Allowed Values of β

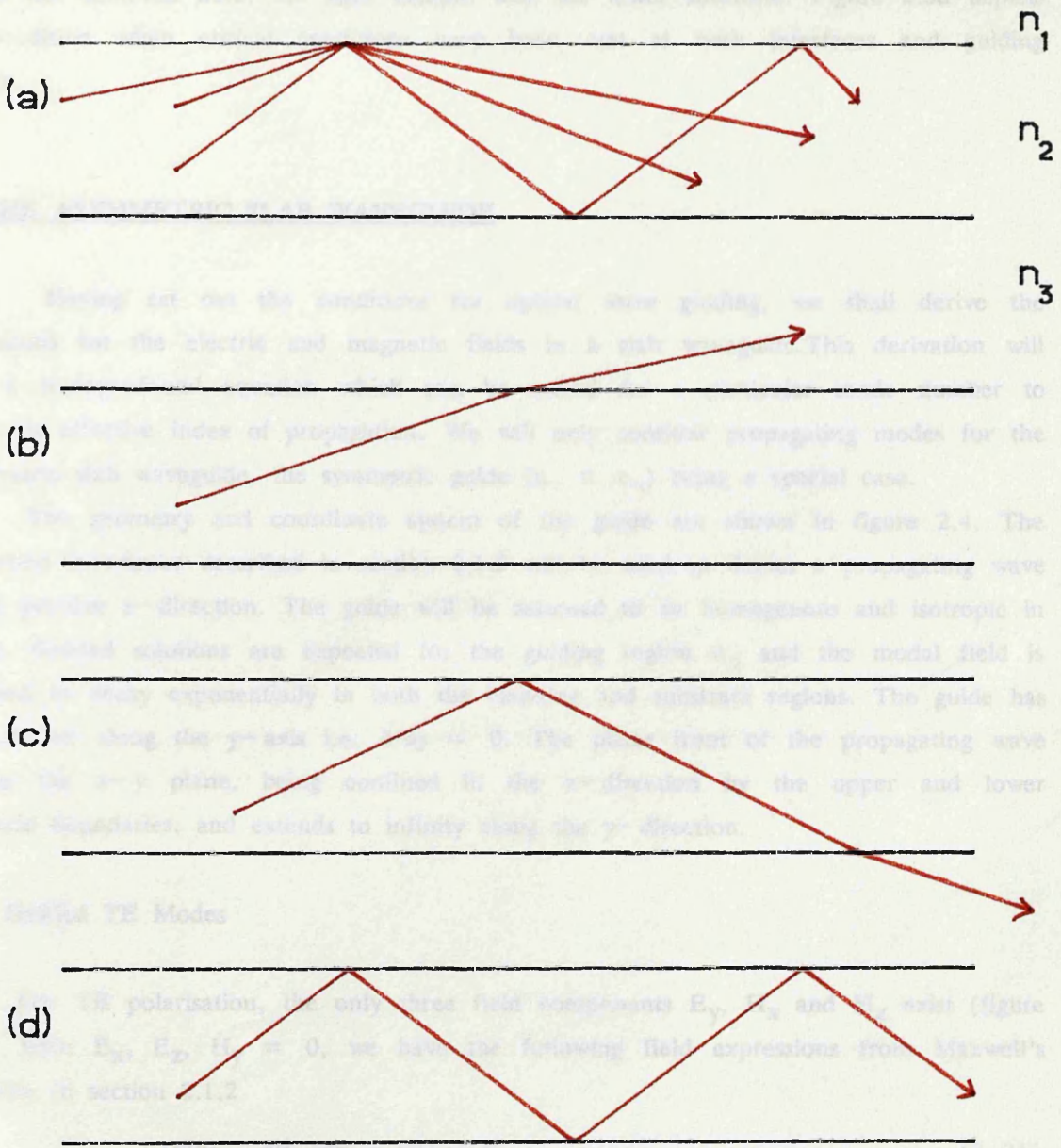


Figure 2.3 Optical Paths for Different Values of β

$$\text{curl } \mathbf{H} = \mathbf{j} + \partial \mathbf{D} / \partial t \quad (2.31)$$

$$j \partial E_y / \partial z = -j \omega \epsilon_0 E_x \quad (2.32)$$

$$\partial E_y / \partial x = -j \omega \epsilon_0 E_z \quad (2.33)$$

$$E_x = -j / \omega \epsilon_0 \partial E_y / \partial z = -\beta \omega \epsilon_0 E_y \quad (2.34)$$

$$E_z = j / \omega \epsilon_0 \partial E_y / \partial x \quad (2.35)$$

$$\nabla_{\perp}^2 E_y + (\epsilon_0 \epsilon - \beta^2) E_y = 0 \quad (2.36)$$

shows TIR conditions satisfied at the n_2/n_1 interface but not at the n_2/n_3 interface. Since TIR is not achieved here, the light escapes into the lower substrate. Figure 2.3d depicts the condition when critical conditions have been met at both interfaces and guiding persists.

2.3 THE ASYMMETRIC SLAB WAVEGUIDE

Having set out the conditions for optical wave guiding, we shall derive the expressions for the electric and magnetic fields in a slab waveguide. This derivation will yield a transcendental equation which can be solved for a particular mode number to obtain its effective index of propagation. We will only consider propagating modes for the asymmetric slab waveguide, the symmetric guide ($n_1 = n_3$) being a special case.

The geometry and coordinate system of the guide are shown in figure 2.4. The translation invariance described in section 2.1.2 will be used to depict a propagating wave in the positive z -direction. The guide will be assumed to be homogenous and isotropic in nature. Guided solutions are expected for the guiding region n_2 and the modal field is expected to decay exponentially in both the cladding and substrate regions. The guide has no variation along the y -axis i.e. $\partial/\partial y = 0$. The phase front of the propagating wave lies in the x - y plane, being confined in the x -direction by the upper and lower dielectric boundaries, and extends to infinity along the y -direction.

2.3.1 Guided TE Modes

For TE polarisation, the only three field components E_y , H_x and H_z exist (figure 2.5a). With E_x , E_z , $H_y = 0$, we have the following field expressions from Maxwell's equations in section 2.1.2

$$-j\beta H_x - \partial H_z / \partial x = j\omega \epsilon_0 \epsilon_r E_y \quad (2.31)$$

$$j\beta E_y = -j\omega \mu_0 H_x \quad (2.32)$$

$$\partial E_y / \partial x = -j\omega \mu_0 H_z \quad (2.33)$$

Thus the \underline{H} components can be expressed in terms of the E_y component

$$H_x = -j/\omega \mu_0 \partial E_y / \partial z = -\beta \omega \mu_0 E_y \quad (2.34)$$

$$H_z = j/\omega \mu_0 \partial E_y / \partial x \quad (2.35)$$

Substitution of (2.34) and (2.35) into (2.31) yields the one-dimensional reduced wave equation for the E_y component

$$\frac{\partial^2 E_y}{\partial x^2} + (n^2 k_0^2 - \beta^2) E_y = 0 \quad (2.36)$$

The problem of determining the TE modes of the slab waveguide has now become very

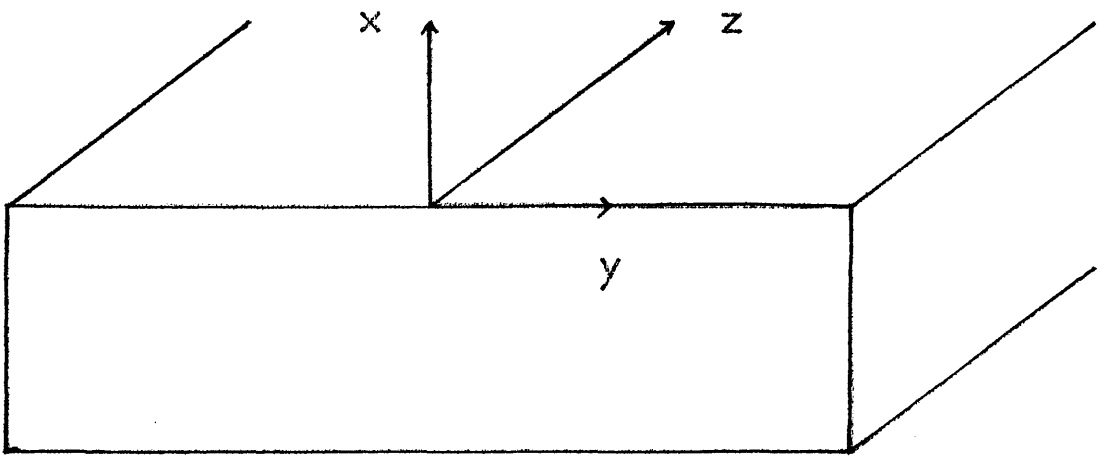


Figure 2.4 Coordinate System for the Slab Waveguide

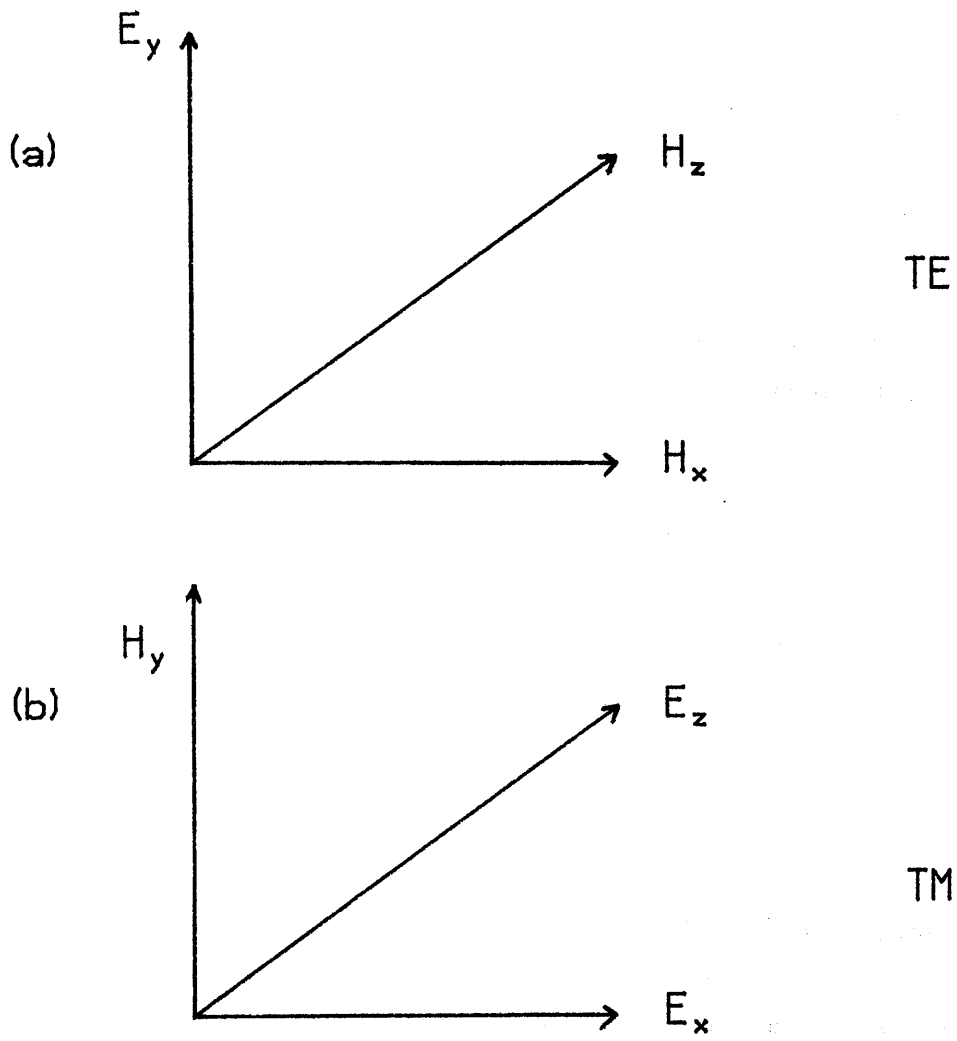


Figure 2.5 TE and TM Polarisation Vectors

simple since we now have to find solutions of the one dimensional reduced wave equation, the magnetic field components being readily calculated from equations (2.31)–(2.33). The above equation can be solved for each dielectric region, subject to the following conditions.

1. The tangential \underline{E} and \underline{H} fields are continuous at the boundary $x = 0$ and $x = -d$.
2. As we require a solution of a mode confined within the film layer, the solution of the wave equation must yield an oscillatory solution for that region.
3. With the above assumptions, the field is expected to decay outside the film region i.e. an exponential decay of the field occurs in the cladding and substrate regions as $x \rightarrow \infty$. Hence the field has an evanescent 'tail' in these regions.

Solutions which satisfy these conditions for the E_y component are

$$E_y(x, z) = \begin{cases} A e^{-\kappa_1 x} & x > 0 \\ B \cos(\kappa_2 x + \psi) & -d < x < 0 \\ C e^{\kappa_3 x} & x < -d \end{cases} e^{-j\beta z} \quad (2.37)$$

where

$$\kappa_1 = (\beta^2 - n_1^2 k_0^2)^{\frac{1}{2}} \quad (2.38)$$

$$\kappa_2 = (n_2^2 k_0^2 - \beta^2)^{\frac{1}{2}} \quad (2.39)$$

$$\kappa_3 = (\beta^2 - n_3^2 k_0^2)^{\frac{1}{2}} \quad (2.40)$$

The term $e^{j\omega t}$ has been omitted for convenience. It has been assumed that all the dielectric regions are magnetically equivalent i.e. $\mu_1 = \mu_2 = \mu_3 = 1.0$. The phase constant ψ has been introduced since the solutions in general will be neither odd nor even as is the case for a symmetric slab. The amplitude coefficients A, B and C will be determined by applying the boundary conditions.

From equation (2.35), the magnetic field component H_z can be expressed as

$$H_z(x, z) = \begin{cases} -j\frac{\kappa_1}{\omega} A e^{-\kappa_1 x} & x > 0 \\ -j\frac{\kappa_2}{\omega} B \sin(\kappa_2 x + \psi) & -d < x < 0 \\ j\frac{\kappa_3}{\omega} C e^{\kappa_3 x} & x < -d \end{cases} e^{-j\beta z} \quad (2.41)$$

Applying the boundary conditions at $x = 0$

$$\underline{E}_{\text{tan}} : A = B \cos(\psi)$$

$$\underline{H}_{\text{tan}} : A = \kappa_2 / \kappa_1 B \sin(\psi)$$

Taking the ratio of these two equations to eliminate A and B gives

$$\tan(\psi) = \kappa_1 / \kappa_2 \quad (2.42)$$

A similar expression is obtained at the other boundary $x = -d$

$$\tan(\psi - \kappa_2 d) = -\kappa_3/\kappa_2 \quad (2.43)$$

Taking the inverse tangents of equations (2.42) and (2.43), noting that

$$\tan(x) = \tan(x \pm n\pi) \quad n = 0, 1, 2, \dots$$

we obtain

$$\psi = \frac{1}{2}\Psi_1^{\text{TE}} \pm n\pi \quad n = 0, 1, 2, \dots \quad (2.44)$$

$$\psi - \kappa_2 d = \frac{1}{2}\Psi_3^{\text{TE}} \pm m\pi \quad m = 0, 1, 2, \dots \quad (2.45)$$

where

$$\Psi_1^{\text{TE}} = 2 \tan^{-1}(\kappa_1/\kappa_2) \quad (2.46)$$

$$\Psi_3^{\text{TE}} = 2 \tan^{-1}(\kappa_3/\kappa_2) \quad (2.47)$$

Adding equations (2.44) and (2.45) we obtain the transcendental equation

$$2\kappa_2 d - \Psi_1^{\text{TE}} - \Psi_3^{\text{TE}} = 2q\pi \quad q = 0, 1, 2, \dots \quad (2.48)$$

The above equation can be solved numerically or graphically to obtain the eigenvalue β for a particular mode q .

Using the boundary conditions expressed for $\underline{E}_{\text{tan}}$ and $\underline{H}_{\text{tan}}$, the E_y field component can thus be written down as

$$\mathbf{E}_y(x, z) = B \left\{ \begin{array}{l} \cos(\psi) e^{-\kappa_1 x} \\ \cos(\kappa_2 x + \psi) \\ \cos(\psi - \kappa_2 d) e^{\kappa_3(x+d)} \end{array} \right\} e^{-j\beta z} \quad \begin{array}{l} x > 0 \\ -d < x < 0 \\ x < -d \end{array} \quad (2.49)$$

The expressions for H_x and H_z can be obtained directly from equations (2.34) and (2.35).

2.3.2 Guided TM Modes

For TM polarisation, the only non-zero field components are H_y , E_x and E_z (figure 2.5b). By following the above derivation for the TE field component E_y and using the equations from section 2.1.2, expressions for the H_y component can be written down as

$$\mathbf{H}_y(x, z) = B \left\{ \begin{array}{l} \cos(\psi') e^{-\kappa_1 x} \\ \cos(\kappa_2 x + \psi') \\ \cos(\psi' - \kappa_2 d) e^{\kappa_3(x+d)} \end{array} \right\} e^{-j\beta z} \quad \begin{array}{l} x > 0 \\ -d < x < 0 \\ x < -d \end{array} \quad (2.50)$$

where ψ' is given by

$$\psi' = \frac{1}{2}\Psi_1^{\text{TM}} \pm n\pi \quad n = 0, 1, 2, \dots \quad (2.51)$$

$$\psi' - \kappa_2 d = \frac{1}{2}\Psi_3^{\text{TM}} \pm m\pi \quad m = 0, 1, 2, \dots \quad (2.52)$$

and

$$\Psi_1^{\text{TM}} = 2 \tan^{-1}(\epsilon_2 \kappa_1 / \epsilon_1 \kappa_2) \quad (2.53)$$

$$\Psi_3^m = 2 \tan^{-1}(\epsilon_2 \kappa_3 / \epsilon_3 \kappa_2) \quad (2.54)$$

The transcendental equation is thus given as

$$2\kappa_2 d - \Psi_1^m - \Psi_3^m = 2q\pi \quad q = 0, 1, 2, \dots \quad (2.55)$$

2.3.3 Fundamental Mode Solutions

Having obtained the TE and TM solutions one can determine the modal propagation constants of various slab structures. In this section, we will calculate the propagation constants of the slab structures shown in figure 2.6. Note that the calculated eigenvalue will be used to plot the fundamental TE mode profile, which will be compared to later with other numerical evaluation techniques to be discussed later. These values will be used as a reference to determine the validity of the transcendental equation that will be obtained from the derivation of the slab waveguide Green's function.

The figure shows a slab structure with a guiding layer of depth $d = 1.3\mu\text{m}$ with a refractive index $n_2 = 3.44$ and the operating wavelength is $\lambda = 1.55\mu\text{m}$. It is surrounded by air ($n_1 = 1.0$) and an infinite substrate layer of refractive index n_3 . The above configuration will be tailored to give confinement of the fundamental TE only ($q = 0$ in equation (2.48)).

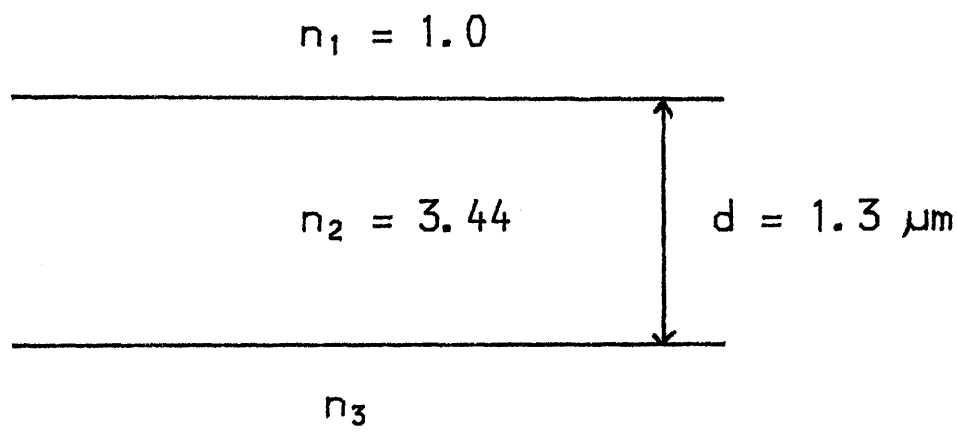
Structure	n_3	Fundamental TE		First order TE	
		n_e	(b)	n_e	(b)
1.	3.305	3.407608578	(0.7564)	3.319209796	(0.1034)
2.	3.34	3.409401428	(0.6909)	-	-
3.	3.39	3.414288868	(0.4839)	-	-
4.	3.40	3.416097973	(0.4010)	-	-
5.	3.42	3.422500118	(0.1247)	-	-
6.	3.435	-	-	-	-

Table 2a

Table 2a lists the solutions to the TE transcendental equation (2.48), the program to solve equation (2.48) is listed in appendix A. The normalised index b is given by the expression

$$b = \frac{n_e^2 - n_3^2}{n_2^2 - n_3^2} \quad (2.56)$$

which will be used as a guide to how strongly the mode is confined. As can be seen, the value of the effective index lies in the range $n_3 < n_e < n_2$. This is the case for the first five structures. Guides 1 and 2 constitute a strongly guided mode since b is greater than the order of 0.5. Guides 3 and 4 on the other hand show slightly less strongly confined modes, whereas guide 5 shows a mode which is very near to cutoff. Guide 6



- | | | |
|----|---------------|-----------------------------|
| 1. | $n_3 = 3.305$ | $\lambda = 1.3 \mu\text{m}$ |
| 2. | 3.34 | |
| 3. | 3.39 | |
| 4. | 3.40 | |
| 5. | 3.42 | |
| 6. | 3.435 | |

Figure 2.6 Asymmetric Slab Waveguide Structures

has no solution and therefore no modes propagate.

Figure 2.7 shows the cross sectional field profile of the electric field for each slab structure. As expected for the first two waveguides, most of the electric field is confined within the guiding layer since the effective index of propagation is relatively high. As a consequence, the field hardly penetrates into the surrounding regions.

However since guides 3, 4 and 5 have lower effective indices, the mode is still confined within the guiding layer, but exhibit a larger evanescent tail into the substrate region. This is due to the angle of incidence of the ray approaching critical conditions at the n_2/n_3 interface.

2.3.4 First Order Mode

The effective index of the first order TE mode can be calculated by setting $q = 1$ in equation (2.48).

Guide 1 has a solution for the first order mode as its thickness can support two modes. The solution of the next higher mode is not possible. Figure 2.8 shows the cross sectional field profile of the first order mode. Several observations can be made.

The mode profile exhibits a zero near the centre of the dielectric slab. The mode profile on one side of the zero is a rotated image of the other profile but is not identical, this being due to the differences in the dielectric boundary refractive indices. However, since the refractive index difference between the n_2/n_3 is small, the field penetrates into the substrate. The large penetration into this region is reminiscent of a mode near cutoff (c.f. solution for the fundamental mode for guide 5).

2.3.5 Conclusions

Due to the simplicity of the slab waveguide structure, an exact solution for the Helmholtz wave equation is achieved. Development of the E_y field component solutions has led to a transcendental equation (2.48) which when solved, gives an indication as to how many modes are supported in the slab and their relative effective indices. Using Maxwell's equations, we can determine all the relevant field components for the particular polarisation of the field.

Simple guide analysis has laid the constraints to which electromagnetic propagation is possible within dielectric structures.

2.4 RIDGE WAVEGUIDES

Confinement of the mode can be achieved in the vertical direction by the use of abrupt refractive index changes. Figure 2.9 shows a cross sectional contour plot of the

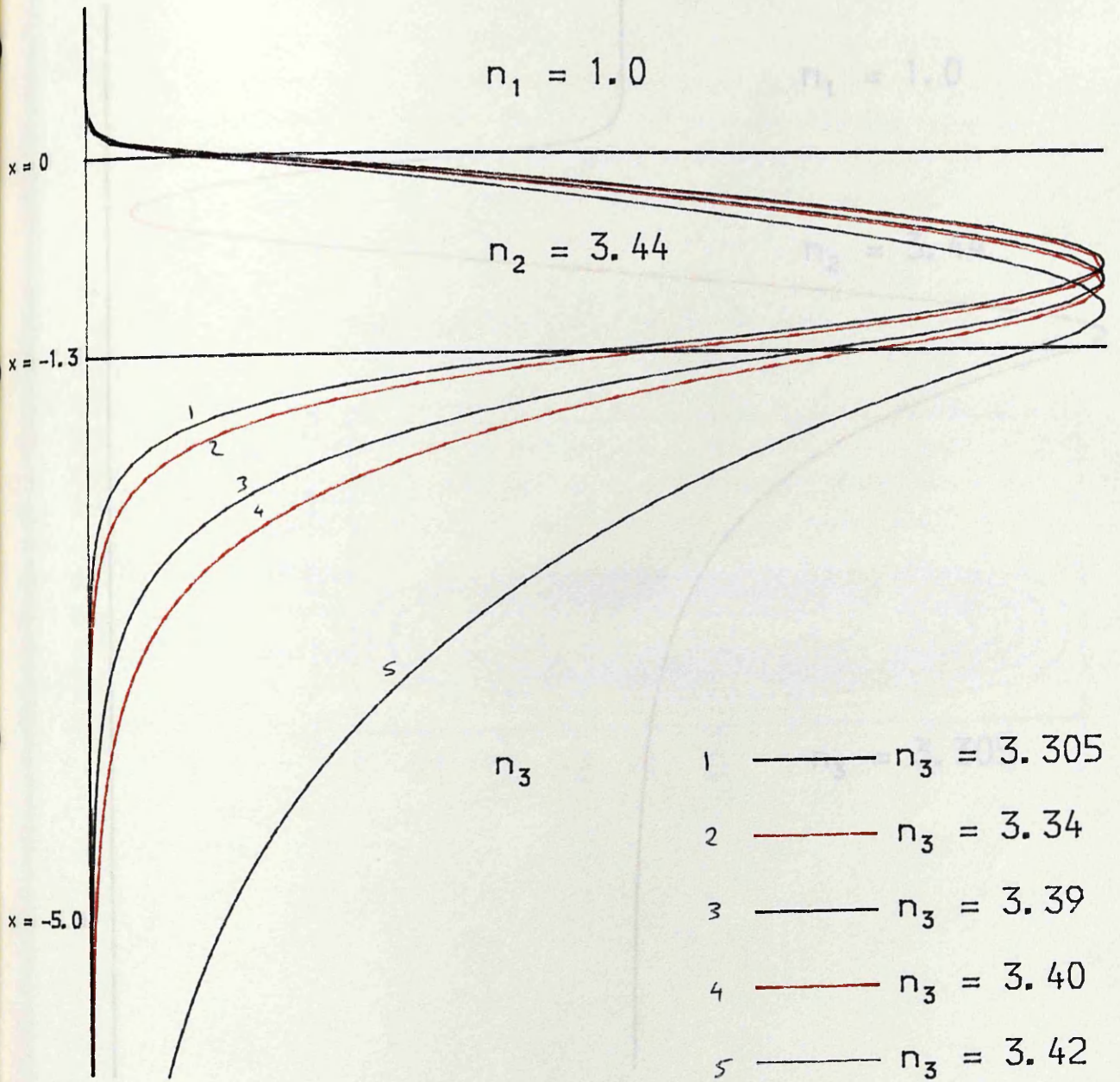


Figure 2.7 Fundamental Mode Profiles

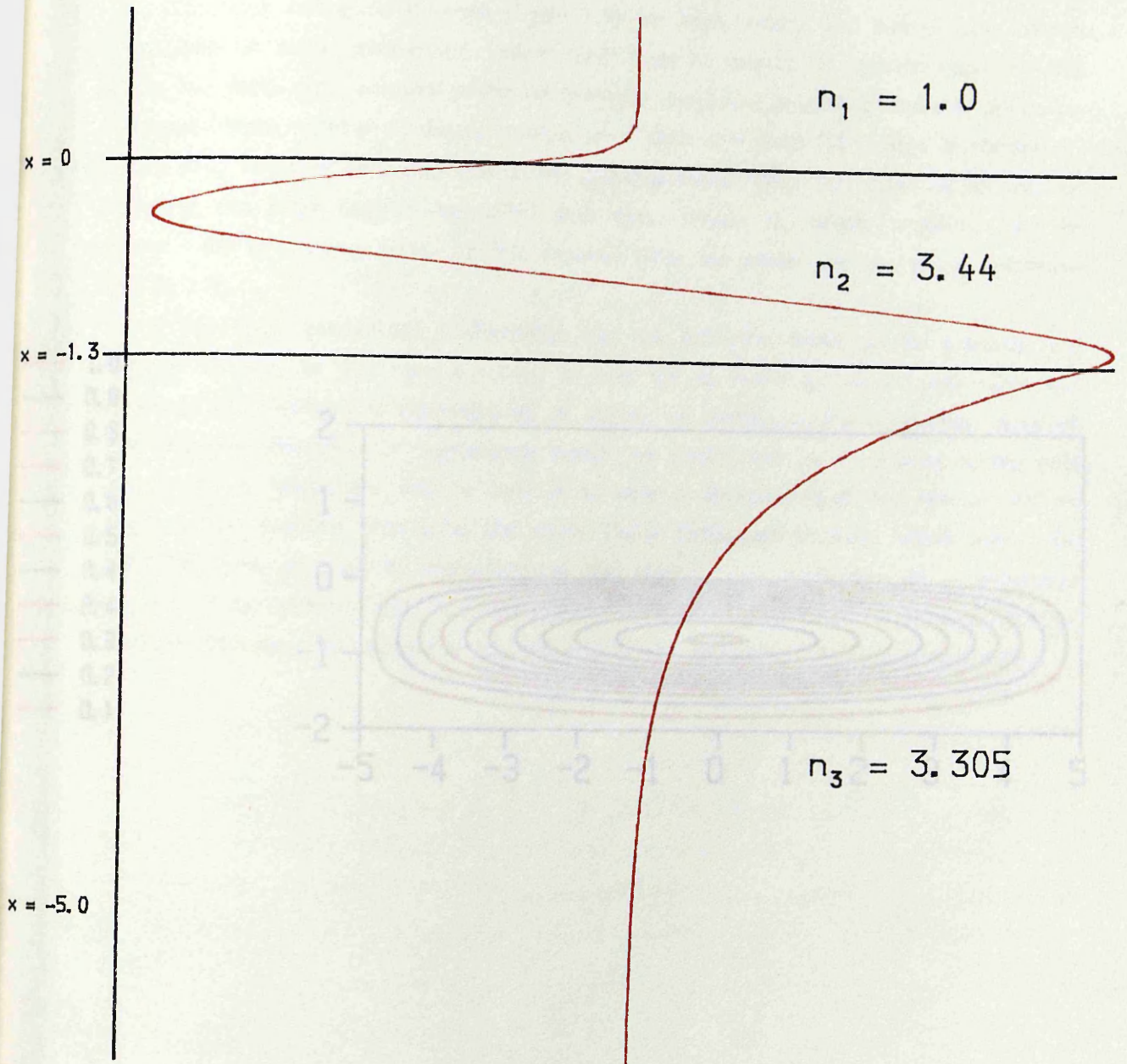


Figure 2.8 1st Order Mode Profile for Waveguide 1

Sectional Electric Field Distribution

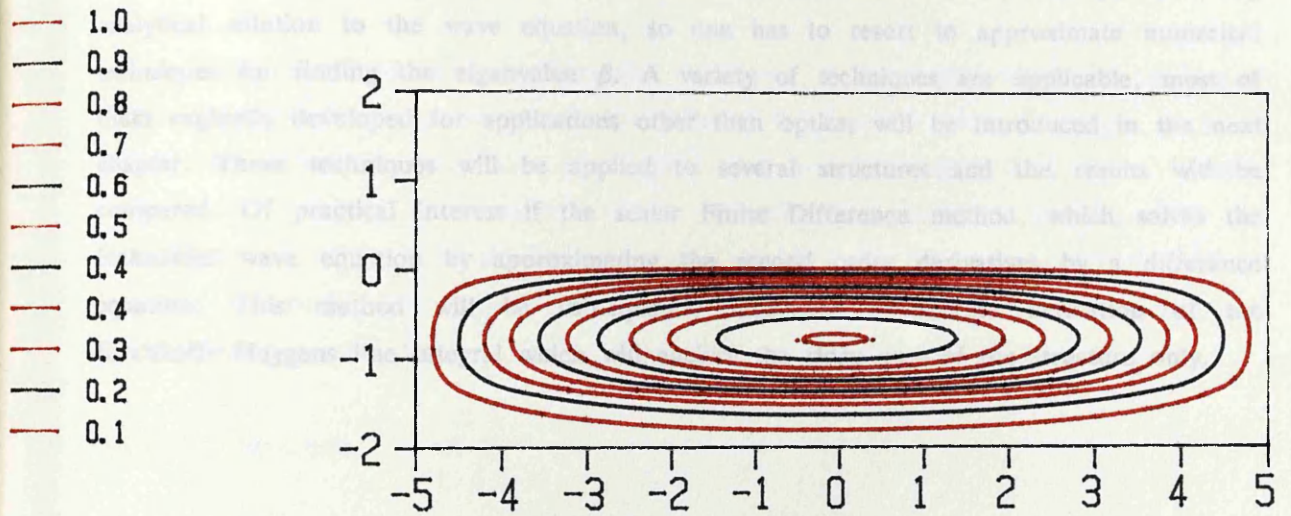


Figure 2.9 Finite Difference Contour Plot of the Cross Sectional Electric Field Distribution

electric field for the slab structure 2 (at $z = 0$). As the field decays rapidly in the outer two regions, n_1 and n_3 , the decay in the lateral y -direction is slow.

The ridge waveguide structure (figure 1.3) has been studied with considerable interest as a means of mode confinement and control. Ease of control of geometry and material doping has made this structure preferable for such purposes. A guiding layer is grown on a substrate layer, similar to the fabrication of a slab waveguide. The ridge is formed by etching away the film on either side to the required depth. Thus the height of the guiding layer and the ridge can be controlled with ease. Finally the whole structure may be covered with a cladding layer, or left exposed (thus surrounded by air whose refractive index is 1.0).

The ridge geometrical configuration and the refractive index profile preclude any analytical solution to the wave equation, so one has to resort to approximate numerical techniques for finding the eigenvalue β . A variety of techniques are applicable, most of them originally developed for applications other than optics, will be introduced in the next chapter. These techniques will be applied to several structures and the results will be compared. Of practical interest is the scalar Finite Difference method, which solves the Helmholtz wave equation by approximating the second order derivatives by a difference equation. This method will be subsequently used for a discrete derivation of the Kirchhoff-Huygens line integral which will enclose the ridge part of the structure only.

As an analytical solution cannot be obtained for the ridge waveguide, we shall investigate two numerical techniques which attempt to solve the eigenvalue equation. Although there are many techniques available^{1,2} for our purpose, we shall limit our investigation to the Effective Index Method (EIM) and the scalar Finite Difference Method (FDM).

3.1 RIDGE WAVEGUIDE STRUCTURES

Having defined the two numerical techniques to be implemented, we shall now define the particular ridge waveguide structures to be analysed. M.J. Robertson et al.^{1,3} define three structures which have been widely used by other authors M.S. Stern et al.^{1,4}, M.S. Stern et al.^{1,5} and by C. Vassallo^{1,6}. These are referred to as structures BT1, BT2 and BT3 (figure 3.1). The three structures have been designed for single mode operation at an operating wavelength of $1.55\mu\text{m}$. The refractive indices of the materials are typical values for those of bulk GaAs/AlGaAs.

3.1.1 BT1 Structure

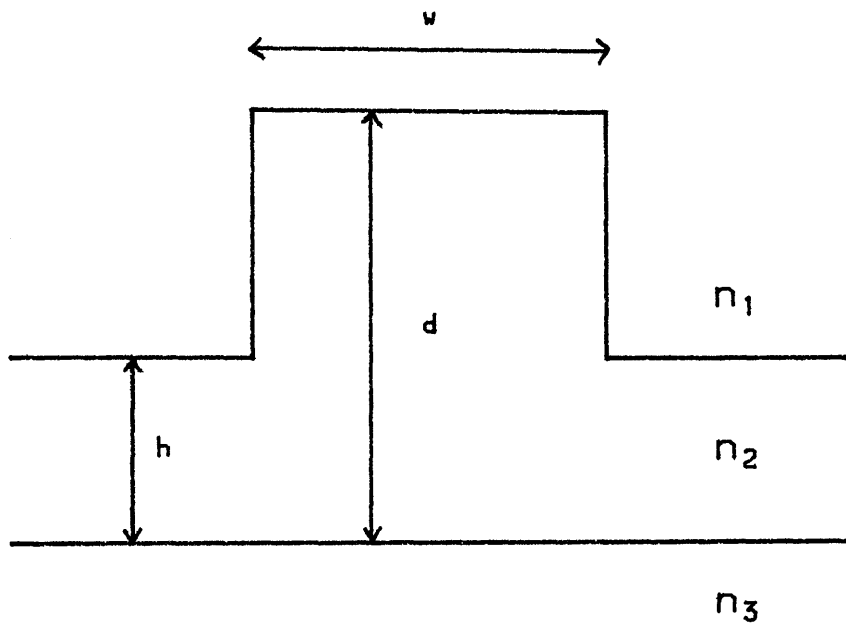
As described in section 2.4, the ridge structures can be tailored for a variety of purposes. In figure 3.1 structure BT1 has a very large difference in refractive indices ($\Delta n = 2.44$ and 0.1). Strong confinement is accomplished by the relatively large ridge height and narrow width. Such a structure is useful for curved waveguides since radiation loss is minimal.

3.1.2 BT2 Structure

For directional couplers, the requirement that the electric field extend laterally means a small ridge height is required. Structure BT2 is a weakly guiding waveguide in which a small ridge height allows very small vertical confinement, but allows the field to extend laterally.

3.1.3 BT3 Structure

Figure 3.1 shows a larger structure in which the mode profile is tailored to fit the mode profile of an optical fibre. Such a structure would be essential for an optical fibre to integrated circuit coupler configuration.



	n_1	n_2	n_3	d	h	w
BT1	1.0	3.44	3.34	1.3	0.2	2.0
BT2	1.0	3.44	3.36	1.0	0.1	3.0
BT3	1.0	3.44	3.435	6.0	2.5	4.0

Figure 3.1 BT Ridge Waveguide Structures

Appendices B and C show the computer programs used to calculate the effective index of the ridge waveguides using the Effective Index Method and the Finite Difference Method. A comparison will be made to the results obtained by M. J. Robertson et al.¹³.

3.2 EFFECTIVE INDEX METHOD^{8, 17}

This method solves the propagation constants semi-analytically, the solution being that of a transcendental equation for two slab waveguides, one representing the guiding layer slab and the other representing the ridge slab (see figure 3.2). Having obtained the effective indices of these two regions, the transcendental equation is again solved in the transverse direction, the solution of which is a good approximation to the true propagation constant. The following describes the method.

Initially, a normalised parameter v is introduced

$$v = k_0 d (n_2^2 - n_3^2)^{\frac{1}{2}} \quad (3.1)$$

where d is the depth of the slab, k_0 is the free space wavenumber, and n_2, n_3 are the refractive indices of the guiding layer and substrate respectively. Next an asymmetry parameter

$$\alpha^{TE} = \frac{n_3^2 - n_1^2}{n_2^2 - n_3^2} \quad (3.2)$$

is defined which varies from 0 for the symmetric waveguide to ∞ in the limit of very strong asymmetry. Using the normalised $b-v$ diagram shown in figure 3.3, one can obtain the normalised effective index of the slab

$$b = \frac{n_e^2 - n_3^2}{n_2^2 - n_3^2} \quad (3.3)$$

The values of b range from 0 to 1, corresponding to the modal effective indices over the allowed range n_3 to n_2 . This allows easier comparison between the different structures. Rearranging the above equation, we solve for the effective index

$$n_e^2 = n_3^2 + b(n_2^2 - n_3^2) \quad (3.4)$$

This method is accurate for slab structures but since the ridge waveguide is solved by investigating slab modes, discrepancies can occur for large etch step.

3.2.1 EIM Program¹⁸

The ridge structure is divided into the three slab structures as shown in figure 3.2. For our purposes, solutions for TE modes are considered. The effective indices of the two (three) slab modes are calculated using the EIM subroutine and are consequently used for

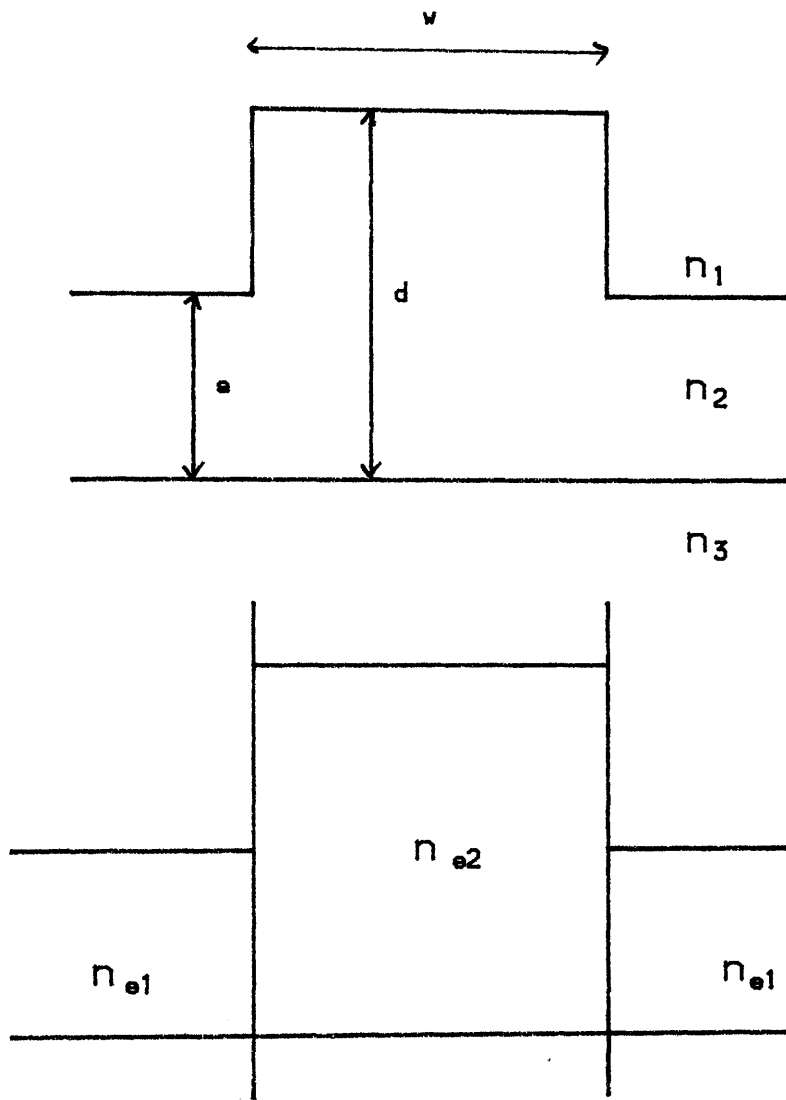


Figure 3.2 Effective Index Method Approximation

ϵ_2/ϵ_0	ϵ_3/ϵ_0	ϵ_1/ϵ_0	ϵ_4/ϵ_0
3.0	1.0	2.0	1.5
3.0	1.0	2.0	1.5
3.0	1.0	2.0	1.5

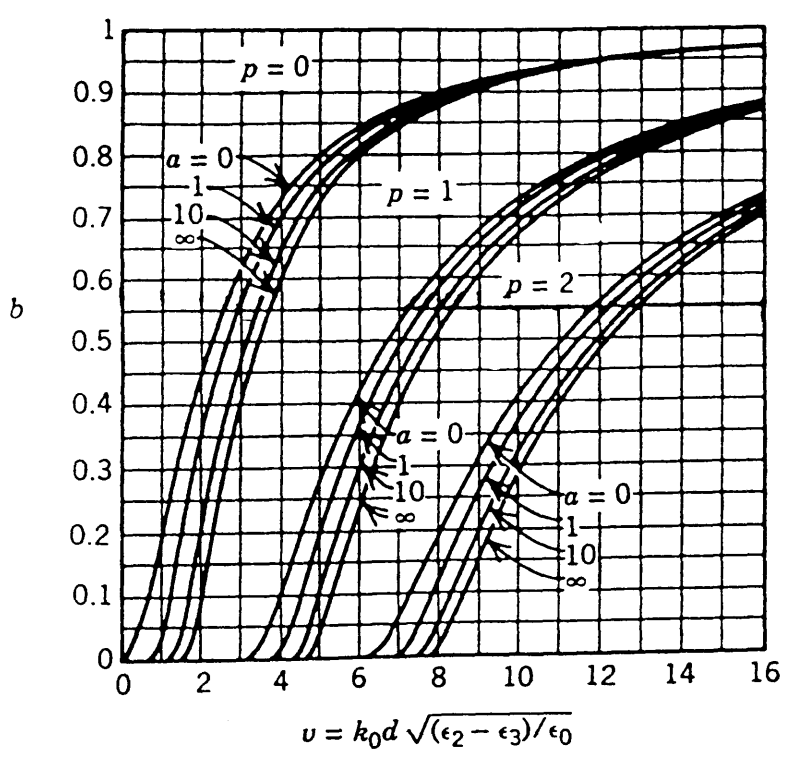


Figure 3.3 Normalised b versus v Diagram

the second EIM calculation in the longitudinal direction. The calculated effective values for the three structures are

Structure	n_e	b	[13]
BT1	3.396321732	0.4995	0.4995
BT2	3.395483971	0.4406	0.4407
BT3	3.437391281	0.4781	0.4783

Table 3a

The normalised modal refractive index b is given by equation (3.3).

These results compare favourably with the published results of M. J. Robertson et al.¹³ which discusses the validity of the results obtained. The value for BT1 is expected to be low since the slab mode is at cutoff. In this case an effective index of 1.0 is chosen in this region, thus the overall resulting effective index will be lower than the true value.

The value for BT2 is expected to be much more accurate as the etch step is very small and both rib/slab modes are propagating. However the effective index value is expected to be higher than the true value.

Again for BT3, the effective index is anticipated to be high since the slab mode is near cutoff and the rib height is twice the height of the slab thickness and the rib width is less than the rib height, giving a much higher result.

3.3 SCALAR FINITE DIFFERENCE METHOD⁸

The finite difference method approximates the second order derivatives of the scalar Helmholtz wave equation by a difference equation. Arranging the equation to solve for the electric field at a particular point it is applied to all points across a mesh which surrounds the waveguide cross-section geometry. The boundary conditions are enforced by enclosing the waveguide by an arbitrary box on which the electric field tends to or is equal to zero. Advantage is taken of the symmetry of the structure, so that only half of the waveguide cross-section is considered.

As discussed in appendix D, the finite difference approximation for the 2nd order derivative has an error of $(\Delta x)^2$, Δx being the difference step between adjacent points in the x-direction. It is envisaged that the error can be reduced by considering a smaller difference step.

The method involves an iterative technique which solves the electric field at each mesh point, and the effective index is updated after each pass through the structure with the newly calculated field values. Convergence is determined when the difference between

successive effective indices is small, or the effective index no longer improves.

Starting from the scalar Helmholtz wave equation for TE modes⁸

$$\frac{\partial^2 E}{\partial x^2} + \frac{\partial^2 E}{\partial y^2} + k_0(n^2(i, j) - n_e^2)E = 0 \quad (3.5)$$

where $n(i, j)$ is the local refractive index of the waveguide at the point (i, j) , and n_e is the estimated refractive index of the structure. Then approximating the second order derivatives by the difference equations (D7), (D8) in appendix D, at the point (i, j) and rearranging for $E_{i, j}$, we obtain the following discrete equation

$$E_{i, j} = \frac{E_{i+1, j} + E_{i-1, j} + R^2(E_{i, j+1} + E_{i, j-1})}{2(1+R^2) - k_0^2(\Delta x)^2[n^2(i, j) - n_e^2]} \quad (3.6)$$

where $R = \Delta x/\Delta y$. For a square grid, $\Delta x = \Delta y$, therefore $R = 1$. So the electric field at the point $P(ih, jk)$ can be represented by equation (3.6).

With an initial guess of the field, together with an estimate of the propagation constant (usually n_3), an iterative routine is used to calculate the field distribution by applying the FD approximation equation (3.6) at each field point. After each iteration through the structure, the variational expression

$$\beta^2 = \frac{\iint_{\text{xsect}} \left[\frac{\partial^2 E}{\partial x^2} + \frac{\partial^2 E}{\partial y^2} + k_0^2 n^2 E \right] E \, dx \, dy}{\iint_{\text{xsect}} E^2 \, dx \, dy} \quad (3.7)$$

or in discrete form

$$n_e^2 = \frac{\sum [E_{i+1, j} + E_{i-1, j} + E_{i, j+1} + E_{i, j-1} - 4E_{i, j} + (\Delta x)^2 k_0^2 n^2 E_{i, j}] E_{i, j}}{\sum (E_{i, j})^2 (\Delta x)^2 k_0^2} \quad (3.8)$$

is applied using the updated field values to calculate the resulting effective index of the structure. Here we have used $\Delta x = \Delta y$, i.e. each mesh point is on a square grid.

Because of the simplicity of the FD method, a computer program can easily be written to implement the many calculations required for the iterative method. Since we are dealing with a matrix structure, the process can be accelerated by the use of a vector facility (or array processor).

3.3.1 Successive Over Relaxation

The convergence of the result can be speeded up by using an acceleration factor. The difference between any two successive $E_{i, j}$ values corresponds to a correction term to the current estimate, and convergence may be accelerated by overcorrecting at each stage. This process is known as Successive Over Relaxation (SOR). An SOR factor of 1 does

guarantee convergence, but it was found that a convergence factor of 1.6 was an improvement (convergence was three times faster). The SOR method is described in appendix E.

3.3.2 Finite Difference Program

The program written for the FDM consists of a 2 dimensional array in which the elements are configured to represent the refractive cross-sectional area of the waveguide structure. A corresponding array for the electric field at each mesh point is also used. The electric field is set to zero at the box boundary. The size of the box is alterable and is chosen so that the waveguide and the electric field some distance away from the waveguiding region is enclosed. Since the value of the difference between successive array elements is unity, the meshspacing to be implemented can be dynamically incorporated, giving the program greater flexibility. For our analysis, three meshsizes will be used as in reference 13 with the exception of the meshsize of $\Delta x = 0.0333\mu\text{m}$ which does not adequately fit any of the structures.

3.3.2.1 Iterative Procedure

Together with an initial guess of the electric field and of the effective index n_e the finite difference approximation is applied to the waveguide cross section in three distinct stages.

Stage one applies the FD approximation with a relaxation factor of 1.0. This allows an initial field representation given the estimated value of the effective index. This crude representation is subsequently used in the second iteration sequence (consisting of 20 iterations) in which the FD approximation is applied with a relaxation factor. The value of the chosen relaxation factor is given in section 3.3.2.2. The effective index is updated after each pass through the structure and it is expected that the value of the effective index converges rapidly with the application of the acceleration parameter. Finally the field is smoothed out with another further 20 iterations using a relaxation factor of 1.0 and the effective index of the final waveguide field is calculated.

3.3.2.2 Choice of Acceleration/Relaxation Factor

Appendix E describes the method of S.O.R. as applied to the Gauss-Seidel method of iteration. Implementing expression (E9) on the FD approximation equation (3.6), we obtain

$$E_i^{(n+1)} = \omega(\text{R.H.S. of eqn. 3.6}) - (\omega-1)E_i^{(n)} \quad (3.9)$$

The iterative calculations can therefore be applied with a choice of an acceleration parameter ω .

A RF between the range $1.0 < \omega < 2.0$ is shown to be convergent³². Although a

factor of 1.0 does guarantee convergence, a value greater than this would improve convergence significantly. The difficulty arises because it is not possible to dynamically choose an optimum value within the program.

Figure 3.4 shows the rate of convergence for the effective index for the BT1 structure for a choice of relaxation factors. A RF of 1.0 does show convergence to a final value, but the convergence is slow. However a RF of 1.5 accelerates convergence significantly as the final value is reached at the third iteration. This essentially has given an improvement by a factor of 3. The same occurs for a RF of 1.6. A RF of 1.8 gives a good estimate in the second iteration but as before does not converge until after the third iteration.

A RF greater than or equal to 2.0 however gives quite different results (figure 3.5). For a RF of $\omega = 2.0$ the effective index converges to a lower value of 3.3920, hence the RF should be in the range $1.0 < \omega < 2.0$. Applying the RF of 1.0 in the third iterative sequence, the correct effective index is achieved. Increasing the RF gives unpredictable results. For a RF of 2.01, the result converges to a value close to that of the substrate refractive index ($n_e = 3.340$). A further increase to 2.02 leads to a total breakdown of the program. Hence the SOR method becomes unstable for $\omega > 2$.

In conclusion, a relaxation factor of 1.6 will be used.

3.3.2.3 FD Box Size

One interesting aspect of finite differences is the size of the box which encloses the waveguide structure. As figures 3.6a and 3.6b show for the BT3 structure, the box has to be big enough not only to adequately cover the structure, but to also extend further to cover the region where the field falls to zero. Figure 3.6a shows that the field extends further along the x-direction, and this is accommodated by using a box of $30\mu\text{m} \times 20\mu\text{m}$. Figure 3.6b shows the same structure using a much smaller box, and as can be seen, there is a poor representation of the field inside the structure, and hence a poor value of the effective index ($b = 0.2719$ for a box size of $10\mu\text{m} \times 10\mu\text{m}$ ($\Delta x, \Delta y = 0.25\mu\text{m}$)).

In conclusion, the enclosing box is increased in size until the value of the effective index no longer improves. The chosen box size for the BT1 structure is $5\mu\text{m} \times 5\mu\text{m}$ and for the BT2 structure, the box size chosen is $10\mu\text{m} \times 6\mu\text{m}$.

However, due to an increased box size, more mesh points result. Therefore a greater accuracy is achieved at the expense of computer storage and execution time.

3.3.3 Results

The following table summarises the results obtained by performing the finite difference method on the three structures. The effective index and b value are the results obtained by M. J. Robertson et al.¹³, with the corresponding values obtain by the FD

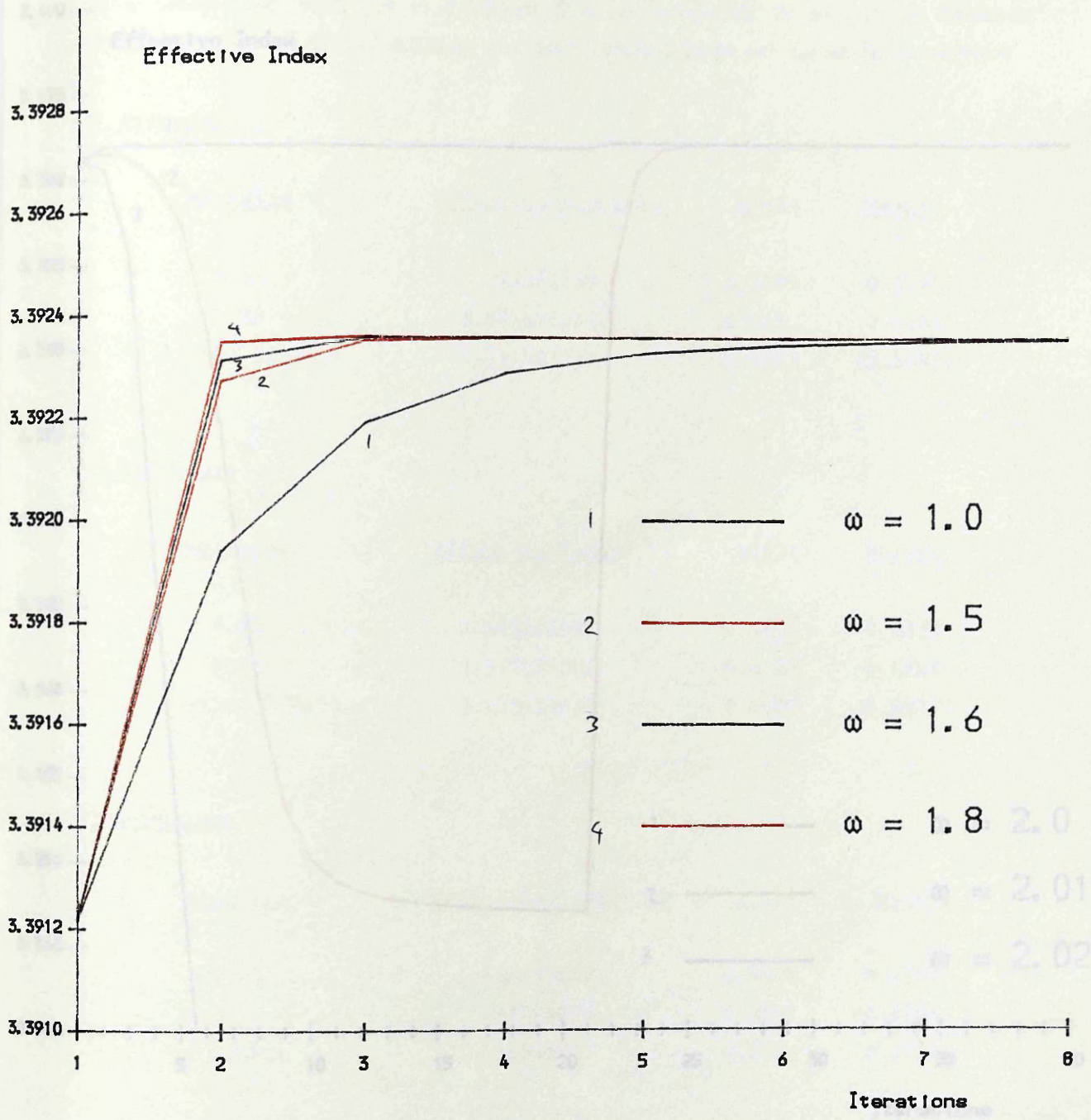


Figure 3.4 Rate of Convergence for Different Values of ω

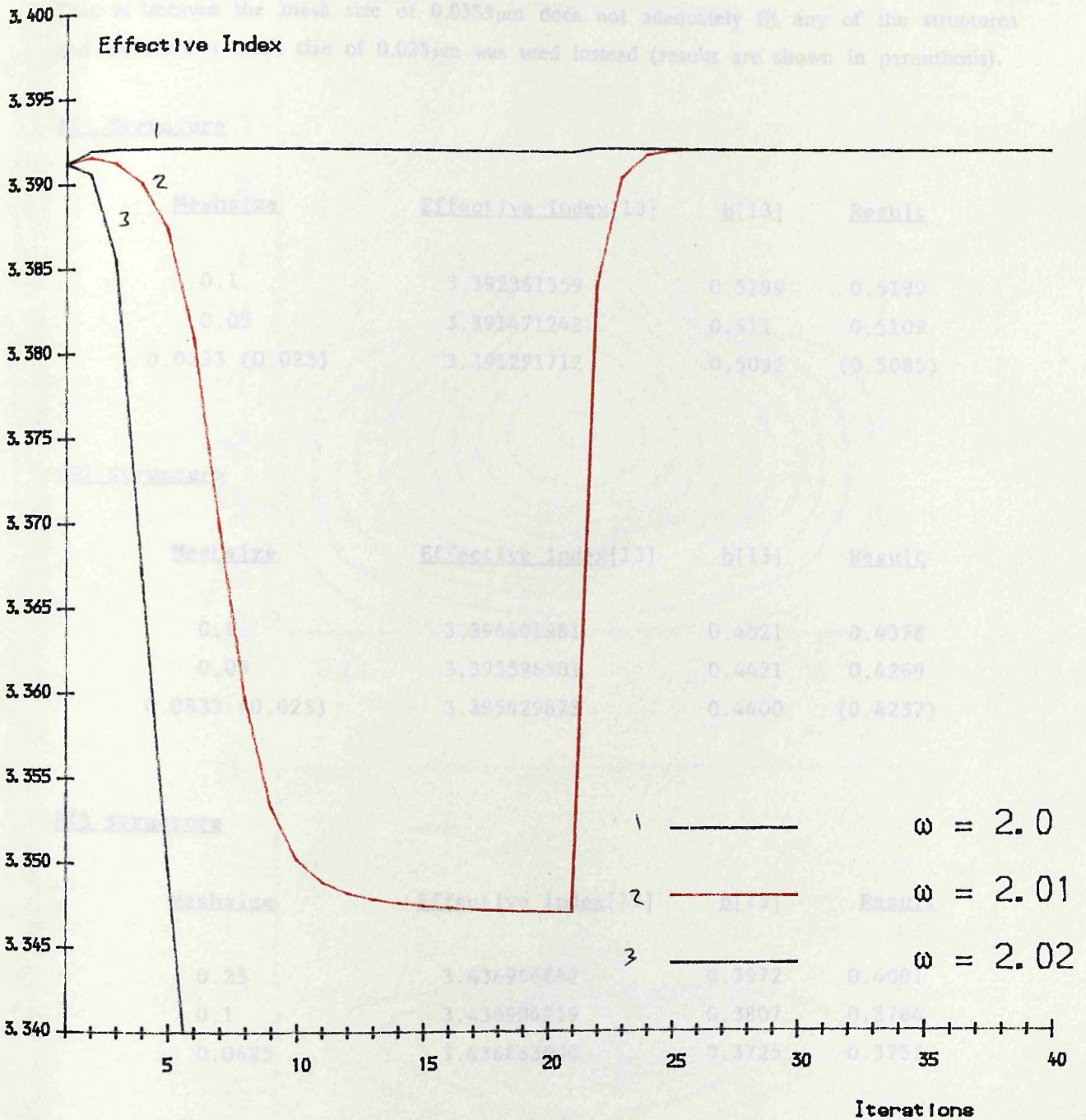


Figure 3.5 Rate of Convergence for $\omega \geq 2.0$

program listed under the 'Result' column.

A mesh spacing of $\Delta x, \Delta y = 0.0333 \mu\text{m}$ was not used as by M. J. Robertson et al.¹³. This is because the mesh size of $0.0333 \mu\text{m}$ does not adequately fit any of the structures and therefore a mesh size of $0.025 \mu\text{m}$ was used instead (results are shown in parenthesis).

BT1 Structure

<u>Meshsize</u>	<u>Effective Index</u> [13]	<u>b</u> [13]	<u>Result</u>
0.1	3.392361359	0.5199	0.5199
0.05	3.391471242	0.511	0.5109
0.0333 (0.025)	3.391291712	0.5092	(0.5085)

BT2 Structure

<u>Meshsize</u>	<u>Effective Index</u> [13]	<u>b</u> [13]	<u>Result</u>
0.1	3.396401981	0.4521	0.4378
0.05	3.395596501	0.4421	0.4269
0.0333 (0.025)	3.395429873	0.4400	(0.4237)

BT3 Structure

<u>Meshsize</u>	<u>Effective Index</u> [13]	<u>b</u> [13]	<u>Result</u>
0.25	3.436986842	0.3972	0.4001
0.1	3.436904219	0.3807	0.3784
0.0625	3.436863500	0.3725	0.3752

Table 3b

It can be seen from the above, that the results obtained are in close agreement. This is particularly true for the BT1 structure. The FD applied to this structure with a box size of $5 \mu\text{m} \times 5 \mu\text{m}$ gives a good representation of the field since the entire waveguide mode profile is confined within the rib, and hence the close agreement with the published results. Figure 3.7 shows a contour plot of the modal field.

The results for the BT2 structure are somewhat different from the published results. Again a large enough box was used ($10 \mu\text{m} \times 6 \mu\text{m}$) to obtain a good representation of

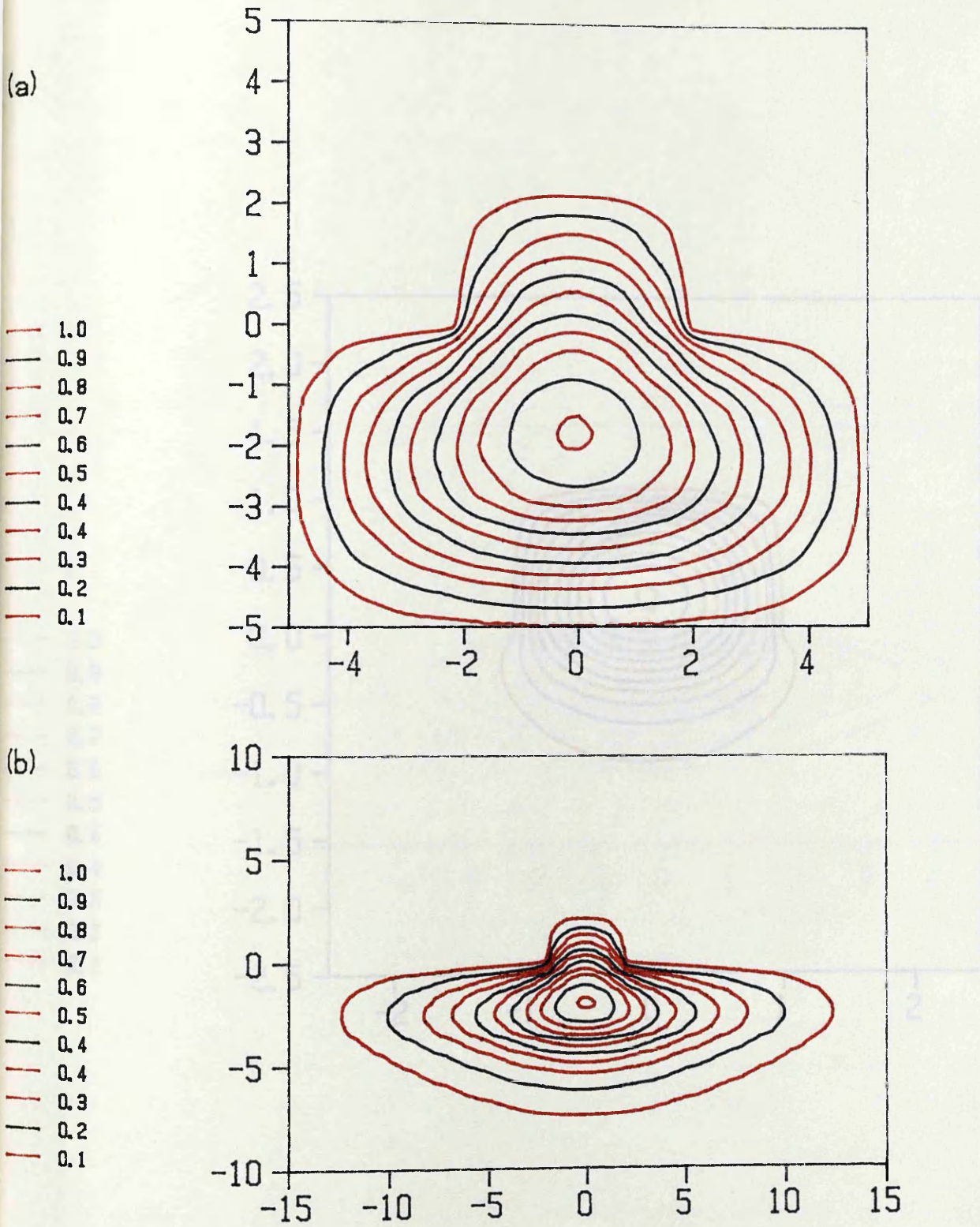


Figure 3.6 Cross Sectional Contour Plot of Mode Profile for BT3 Using Different Box Sizes

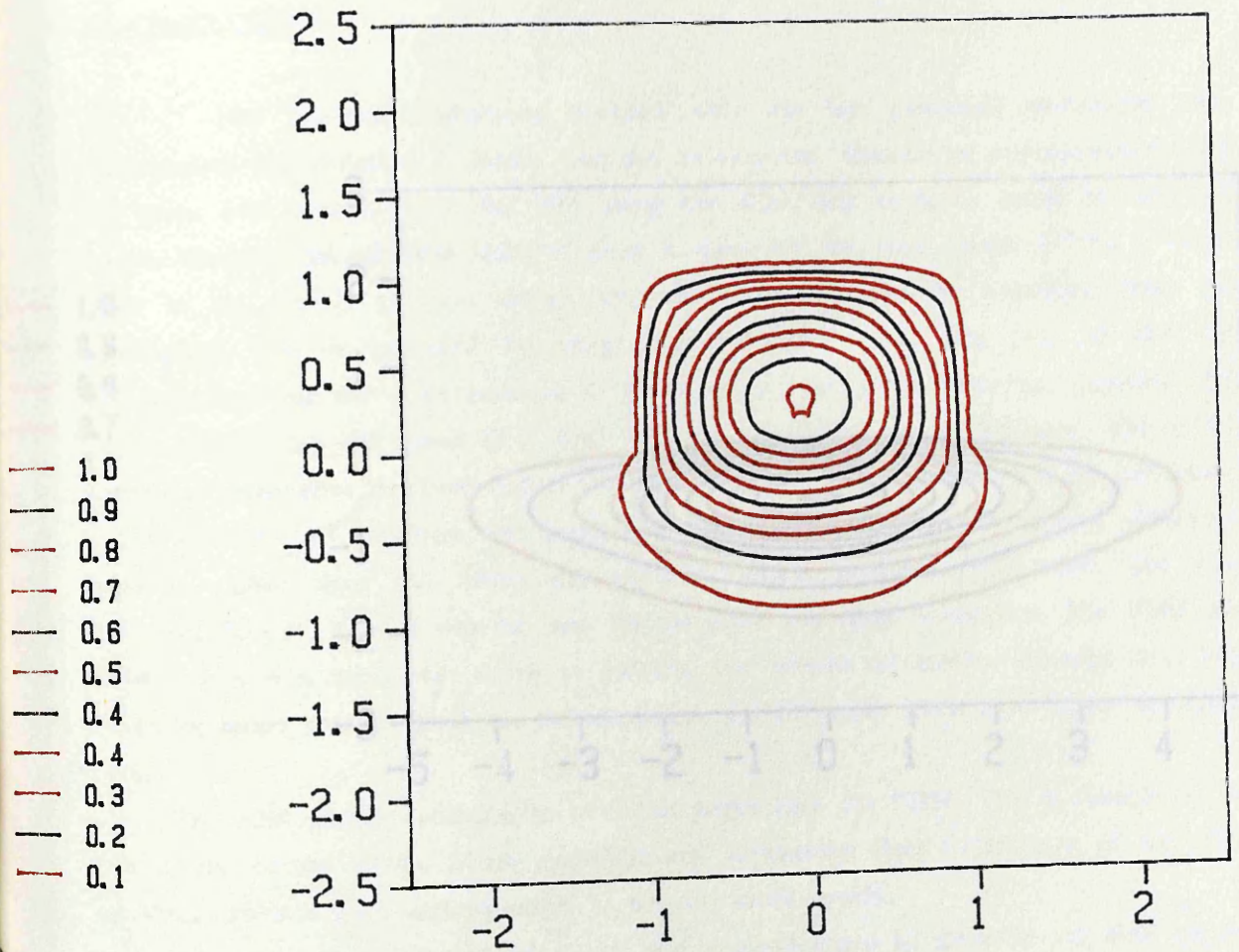


Figure 3.7 BT1 Mode Profile Contour Plot

the field, but the structure is weakly guiding and hence the finite difference codes work well. Due to the weakly guiding nature of BT2, the finite difference method is more sensitive, and hence the discrepancy of the results. The cross-sectional mode profile is shown in figure 3.6.

The results for BT3 compare very well with a difference of about 0.7%, and this was accomplished by using the larger box as in figure 3.6a as opposed to the box size in figure 3.5b.

3.4 CONCLUSIONS

The waveguide structures analysed with the two numerical techniques have demonstrated the variation in results that can be expected. Because of approximations that are taken into account (e.g. for BT1 using the EIM, the mode is cutoff in the slab region, therefore an effective index of unity is taken for this part, hence yielding a lower value to the overall effective index), the true values can only be postulated from the convergence that is expected by using, say, a smaller mesh size (or) in the FDM approximation. As the error involved in the FDM is $(\Delta x)^2$, it is therefore expected that the effective index will come to a final value as the mesh size is decreased. Figure 3.9 shows the three effective index values for the three structures. The FDM results are more accurate (rather than the difference method) for the BT1 structure. The FDM has also the case for the BT2 and BT3 waveguides. The FDM has converged with a mesh size down to $0.01 \mu\text{m}$, but because of smaller element size, this is larger than the BT1 structure.

The EIM predicts effective index values larger than the FDM. This is thought to be due to the corner effects where sinusoidal and exponential field dependences of the EIM are larger gives a good approximation to the real mode profile.

The removal of geometrical factors and approximations as made in the EIM above, could eliminate or minimize the doubt of the accuracy of the final result. As most structures to be analysed are of a planar nature, a Fourier analysis can be implemented. This has three distinct advantages.

1. Fourier transforms along the planar simplification simplifies the problem by eliminating the coordinate component in that direction. Thus the solution becomes that of a simple ordinary differential equation with only one coordinate variable.

2. Fourier analysis with efficient numerical code and fine mesh size gives more accurate results.

Figure 3.8 BT2 Mode Profile Contour Plot

the field, but the structure is weakly guiding. Structure BT1 is strongly guiding and hence the finite difference coped well. Due to the weakly guiding nature of BT2, the finite difference method is more sensitive, and hence the discrepancy of the results. The cross-sectional mode profile is shown in figure 3.8.

The results for BT3 compare very well with a difference of about 0.7%, and this was accomplished by using the larger box as in figure 3.6a as opposed to the box size in figure 3.6b.

3.4 CONCLUSIONS

The waveguide structures analysed with the two numerical techniques have demonstrated the variation in results that can be expected. Because of approximations that are taken into account (e.g. for BT1 using the EIM, the mode is cutoff in the slab region, therefore an effective index of unity is taken for this part, hence yielding a lower value to the overall effective index), the true value can only be postulated from the convergence that is expected by using, say, a smaller mesh size (Δx) in the FD approximation. As the error involved in the FDM is $(\Delta x)^2$, it is therefore expected that the effective index will come to a final value as this mesh size is decreased. Figure 3.9 shows the three effective index values for each structure against decreasing mesh size (Δx).

For the BT1 structure, the graph converges due to the error in using a difference equation rather than the differential equation, which increases with mesh size (the difference factor). This is also the case for the other two ridge waveguides. The FDM has converged with a mesh size down to $0.01 \mu\text{m}$, but because of smaller element size, this results in larger storage space on the computer, and ultimately leads to a larger execution time.

The EIM predicts effective index values larger than the FDM. This is thought to be due to the corner effects where sinusoidal and exponential field dependence of the EIM no longer gives a good approximation to the real mode profile.

The removal of geometrical factors and approximations as made in the EIM above, could eliminate or minimize the doubt of the accuracy of the final result. As most structures to be analysed are of a planar nature, a Fourier analysis can be implemented. This has three distinct advantages.

1. Fourier transforms along the planar stratification simplifies the problem by eliminating the coordinate component in that direction. Thus the solution becomes that of a simple ordinary differential equation with only one coordinate variable.
2. Fourier transform techniques are simple to program with efficient numerical code and give much more accurate results.

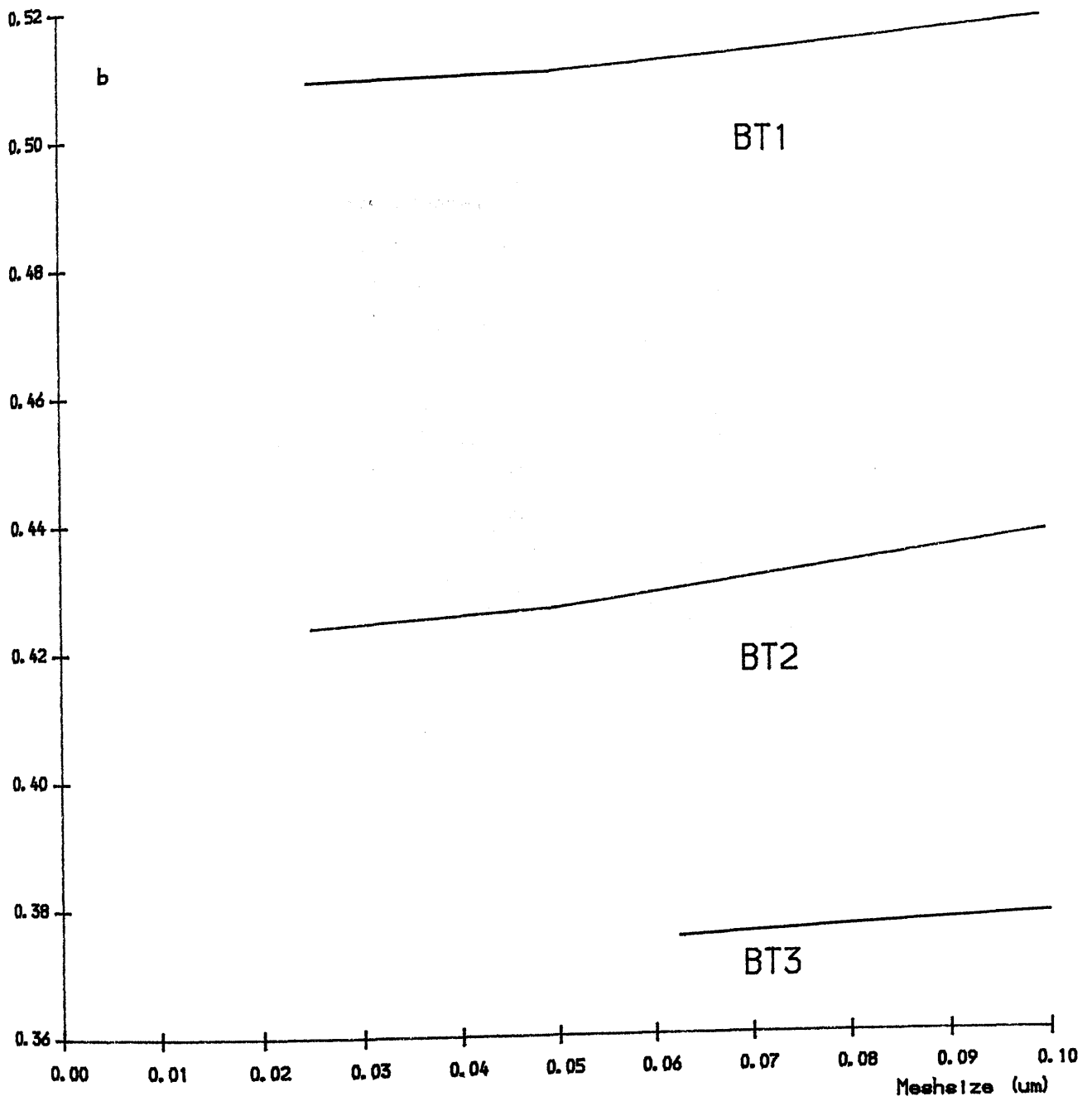


Figure 3.9 Convergence of FD Method Using Smaller Mesh Spacing

3. Most important of all, boundary conditions along the planar stratification are exact and intrinsic, thus minimising errors in the final result.

The Green's Function method is proposed and discussed in the next chapter. Using the elementary Fourier technique, the GF can be calculated for the planar geometry, the boundary conditions at the dielectric interfaces and at infinity are incorporated, thus yielding a much more accurate representation of the waveguide mode. The effective index is a solution to a transcendental equation that will be extracted from the GF equation of the structure. This is discussed in chapter 6.

2.2.1. THE GREEN'S FUNCTION

Scalar Equation

is the differential equation of Poisson's equation

$$\nabla^2 \phi(r) = -\rho(r)/\epsilon_0$$

where ϕ is the scalar potential at the point r , and $\rho(r)$ is the charge density

4.1 INTRODUCTION

As discussed in the previous chapter, a mathematical method is required for the planar stratified dielectric medium. The limitations imposed by the previous numerical techniques gives impetus for the derivation of a much more accurate method which is tailored to incorporate the exact boundary conditions posed by the problem. The conditions at infinity which were difficult to manipulate in the Finite Difference method, are explicitly incorporated into our solution. For our analysis, we shall assume the following.

1. Because we are considering a stratified medium, we shall assume translational invariance as $\exp j(\omega t - \beta z)$, i.e. travelling waves in the positive z -direction, with an effective index of propagation of $\beta = n_e k_0$, at a frequency of ω rads/sec.
2. The stratified media are isotropic and magnetically equivalent.
3. Again we shall consider the scalar wave equation, hence we ignore any polarisation dependence of the waveguide modes.
4. Solutions of the GF in media containing sources (inhomogeneous equations) will yield travelling/standing wave solutions. Source free media (homogeneous equations) will constitute solutions with a decaying nature of the GF. The layer containing the source is assumed to be the guiding layer.

4.2 EXISTENCE OF THE GREEN'S FUNCTION

4.2.1 Poisson's Equation

Consider the differential equation of Poissons equation

$$\nabla^2 \Phi(\mathbf{r}) = -\rho(\mathbf{r})/\epsilon_0 \epsilon_r \tag{4.1}$$

where $\Phi(\mathbf{r})$ is the scalar potential at the point \mathbf{r} , and $\rho(\mathbf{r})$ is the charge density. For the homogeneous case $\rho(\mathbf{r}) = 0$ and the above equation simplifies to the form of Laplaces equation

$$\nabla^2 \Phi(\mathbf{r}) = 0 \tag{4.2}$$

If q is a point charge at \mathbf{r}' , then the potential at \mathbf{r} is given as

$$\Phi(\mathbf{r}) = \frac{q}{4\pi(\mathbf{r}-\mathbf{r}') \epsilon_0 \epsilon_r} \quad (4.3)$$

Alternatively, the solution of (4.1) can be obtained by integrating around a volume which contains the charge density. Consider figure 4.1. The region P of volume V encloses the charge density $\rho(\mathbf{r}')$, which is broken up into small elements, each element contributing a point source of $q = \rho(\mathbf{r}') d^3\mathbf{r}'$. The total charge within the cube at \mathbf{r}' is $\rho(\mathbf{r}') d^3\mathbf{r}'$ and using equation (4.3) this makes a contribution to the potential \mathbf{r} of

$$\frac{1}{4\pi} \frac{\rho(\mathbf{r}')}{\epsilon_0 \epsilon_r |\mathbf{r}-\mathbf{r}'|} d^3\mathbf{r}' \quad (4.4)$$

Integrating or summing over all elements to find the total potential, we have

$$\Phi(\mathbf{r}) = \int \frac{\rho(\mathbf{r}')}{4\pi |\mathbf{r}-\mathbf{r}'| \epsilon_0 \epsilon_r} d^3\mathbf{r}' \quad (4.5)$$

This can be written as

$$\Phi(\mathbf{r}) = \int g(\mathbf{r}, \mathbf{r}') \frac{\rho(\mathbf{r}')}{\epsilon_0 \epsilon_r} d^3\mathbf{r}' \quad (4.6)$$

where the Green's Function for Poisson's equation is given by

$$g(\mathbf{r}, \mathbf{r}') = \frac{1}{4\pi |\mathbf{r}-\mathbf{r}'|} \quad (4.7)$$

4.2.2 Green's Function for the Helmholtz Wave Equation

Rewrite Poisson's equation (4.1) as

$$-\nabla^2 \Phi(\mathbf{r}) = \rho(\mathbf{r}) / \epsilon_0 \epsilon_r \quad (4.8)$$

the solution of which is given by (4.6). Operating ∇^2 on equation (4.6) remembering that this affects the \mathbf{r} variable only and not \mathbf{r}'

$$-\nabla^2 \Phi(\mathbf{r}) = \int \left[-\nabla^2 g(\mathbf{r}, \mathbf{r}') \right] \frac{\rho(\mathbf{r}')}{\epsilon_0 \epsilon_r} d\mathbf{r}' \quad (4.9)$$

But Poisson's equation (4.1) shows that the left hand side is equal to $\rho(\mathbf{r}') / \epsilon_0 \epsilon_r$. This is possible only if

$$-\nabla^2 g(\mathbf{r}, \mathbf{r}') = \delta(\mathbf{r} - \mathbf{r}') \quad (4.10)$$

where $\delta(\mathbf{r} - \mathbf{r}')$ is the dirac delta function defined as³³

$$\iiint_{-\infty}^{\infty} \delta(\mathbf{r}') d^3\mathbf{r}' = 1 \quad (4.11)$$

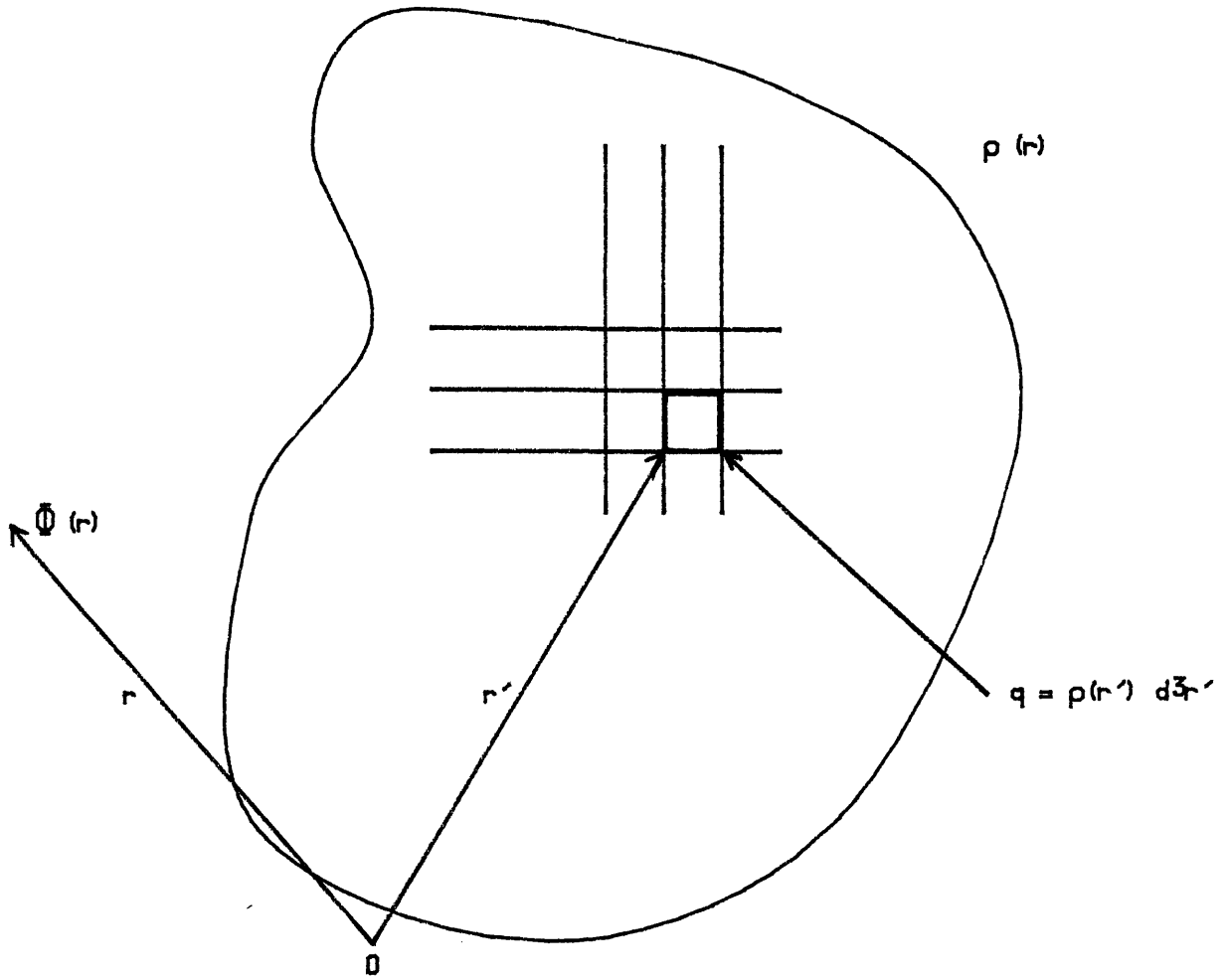


Figure 4.1 Solution of Poisson's Equation

Expressing equation (4.10) as the homogeneous wave equation which involves a derivative with respect to time i.e.

$$\nabla^2 g - \frac{1}{c^2} \frac{\partial^2}{\partial t^2} g = 0 \quad (4.12)$$

and using the translational invariance as described in equation (2.26) we obtain the homogeneous Helmholtz wave equation for the GF

$$\nabla^2 g + k^2 g = 0 \quad (4.13)$$

where $k = \omega/c$. The reason for solving the Helmholtz equation for the GF instead of the wave equation is because the solution of the elliptical Helmholtz wave equation subject to Dirichlet/Neumann boundary conditions on a closed surface results in a stable solution¹⁹.

4.3 GREEN'S FUNCTION THEORY

4.3.1 Integral Theorems

For subsequent analysis of the GF, we shall use a variant of Gauss's theorem called Green's theorem which will play an important role in the derivation of the reciprocity relations of the GF and of the Kirchhoff–Huygens integral.

4.3.2 Gauss's Theorem

Below is a derivation of a relation between a surface integral of a vector and the volume integral of the divergence of that vector. Assuming that the vector $\underline{\mathbf{F}}$ and its first derivatives are continuous over the region of interest, then

$$\iint_{\mathbf{S}} \underline{\mathbf{F}} \cdot d\mathbf{s} = \iiint_{\mathbf{V}} \nabla \cdot \underline{\mathbf{F}} \, dv$$

Hence the above equation states that the surface integral of a vector over a closed surface equals the volume integral of the divergence of that vector, integrated over the volume enclosed by the surface.

4.3.3 Green's Theorem

If φ and ψ are scalar fields, then by¹⁹

$$\nabla \cdot (\varphi \nabla \psi) = \varphi \nabla \cdot (\nabla \psi) + \nabla \varphi \cdot \nabla \psi$$

i.e.

$$\nabla \cdot (\varphi \nabla \psi) = \varphi \nabla^2 \psi + \nabla \varphi \cdot \nabla \psi$$

We now integrate throughout a region \mathbf{V} bounded by the closed surface \mathbf{S} and, using

Gauss's theorem above, we obtain

$$\iint_S \varphi \nabla \psi \cdot \underline{n} \, ds = \iiint_V \varphi \nabla^2 \psi \, dV + \iiint_V \nabla \varphi \cdot \nabla \psi \, dV$$

\underline{n} being the unit outward-drawn normal to the surface. Writing $\varphi \nabla \psi \cdot \underline{n}$ as $\varphi (\partial \psi / \partial n)$, we have

$$\iint_S \varphi \frac{\partial \psi}{\partial n} \, ds = \iiint_V \varphi \nabla^2 \psi \, dV + \iiint_V \nabla \varphi \cdot \nabla \psi \, dV + -\nabla \cdot (\psi \nabla \varphi)$$

whence

$$\iint_S \left[\varphi \frac{\partial \psi}{\partial n} - \psi \frac{\partial \varphi}{\partial n} \right] ds = \iiint_V \left[\varphi \nabla^2 \psi - \psi \nabla^2 \varphi \right] dV \quad (4.14)$$

The above equation is the Green's theorem. Having used Gauss's theorem, we require that φ , ψ and their partial derivatives of the first and second order be continuous functions of x , y , and z .

4.3.4 Reciprocity Property of the GF¹⁹

An important property of the GF is the symmetry of its two variables, i.e.

$$g(r_1, r_2) = g(r_2, r_1) \quad (4.15)$$

where r_1 can be classified as the source point and r_2 the observation point. First, let $g(r, r_1)$ satisfy

$$\nabla^2 g(r, r_1) + k^2 g(r, r_1) = -\delta(r - r_1) \quad (4.16)$$

corresponding to a mathematical point source at $r = r_1$. $g(r, r_2)$ satisfies the same equation

$$\nabla^2 g(r, r_2) + k^2 g(r, r_2) = -\delta(r - r_2) \quad (4.17)$$

Then $g(r, r_2)$ is a sort of potential at r , created by a unit point source at r_2 . We multiply the equation for $g(r, r_1)$ by $g(r, r_2)$ and the equation for $g(r, r_2)$ by $g(r, r_1)$ and subtract the two

$$\begin{aligned} g(r, r_2) \nabla^2 g(r, r_1) - g(r, r_1) \nabla^2 g(r, r_2) \\ = -g(r, r_2) \delta(r - r_1) + g(r, r_1) \delta(r - r_2) \end{aligned} \quad (4.18)$$

Integrating with respect to \underline{r} over whatever volume is involved

$$\begin{aligned} \iiint_V g(r, r_2) \nabla^2 g(r, r_1) - g(r, r_1) \nabla^2 g(r, r_2) \, dV \\ = \iiint_V -g(r_1, r_2) + g(r_2, r_1) \, dV \end{aligned}$$

Using Green's theorem (4.14) the above integral becomes

$$\iint_S \left[g(r, r_2) \nabla g(r, r_1) - g(r, r_1) \nabla g(r, r_2) \right] dS = -g(r, r_2) + g(r, r_1) \quad (4.19)$$

The terms on the right hand side appear when we use the Dirac delta functions and carry out the volume integration. Under the requirement that GF's $g(r, r_1)$ and $g(r, r_2)$ or their normal derivatives vanish over the surface S , the surface integral vanishes and

$$g(r_1, r_2) = g(r_2, r_1)$$

which shows that the GF is symmetric. This property shows that however asymmetrically the points r and r' are situated relative to the boundary, the potential at r due to point source placed at r' equals the potential at r' due to the same source placed at r .

4.4 BOUNDARY CONDITIONS

Before attempting to solve the partial/ordinary differential equations for our given region of interest, boundary conditions must be imposed to ensure that a unique solution is obtainable. Furthermore, as in section 2.3.1, the tangential components of the Green's function must be matched across any dielectric boundaries in order to obtain the value of the coefficients in the general solution of the partial/ordinary differential equation.

4.4.1 Dirichlet Boundary Conditions

When the function $U = u(x, y)$ is specified at/on the boundary, we refer to this as Dirichlet boundary conditions (DBC). DBC are often used for closed boundary situations.

4.4.2 Neumann Boundary Conditions

When the normal derivative (or gradient) of the function U is specified, i.e. dU/dn , on the boundary, we refer to this as Neumann boundary conditions (NBC). For the homogeneous case, the function U or the derivative dU/dn is set to zero on the boundary and for inhomogeneous boundary conditions, the value of U or dU/dn is specified for the DBC and NBC respectively.

4.4.3 Discontinuity Boundary Conditions²⁰

The Green's function is defined everywhere except at the source point (x', y') . This is a direct consequence of the singularity nature of the Dirac delta function. From equation (4.13), we consider the inhomogeneous one dimensional Helmholtz equation

$$\frac{\partial^2 g}{\partial y^2} + k^2 g = -\delta(y-y') \quad (4.20)$$

Integrating both sides with respect to y , from $y'^- - \gamma$ to $y'^+ + \gamma$, and let $\gamma \rightarrow 0$. Using this convention we are essentially integrating from y'^- to y'^+ , hence we obtain

$$\begin{aligned} \text{LHS} \quad & \int_{y'^-}^{y'^+} \left(\frac{\partial^2 g}{\partial y^2} + k^2 g \right) dy = \left. \frac{\partial g(y, y')}{\partial y} \right|_{y=y'^+} - \left. \frac{\partial g(y, y')}{\partial y} \right|_{y=y'^-} \\ \text{RHS} \quad & \int_{y'^-}^{y'^+} -\delta(y-y') dy = -1 \end{aligned}$$

The jump condition at the source point $y = y'$ is given as

$$\left. \frac{\partial}{\partial y} g(y, y') \right|_{y=y'^+} - \left. \frac{\partial}{\partial y} g(y, y') \right|_{y=y'^-} = -1 \quad (4.21)$$

For dielectric boundaries, we require that the Green's function be continuous i.e.

$$g(y=d^+, y') = g(y=d^-, y') \quad (4.22)$$

where d is the coordinate of the dielectric boundary with respect to some origin, the dielectric boundary lying in a plane perpendicular to the y -axis. This continuity condition is also applicable to the GF at the source point i.e.

$$g(y=y'^+, y') = g(y=y'^-, y') \quad (4.23)$$

4.4.4 Further Boundary Conditions on the Green's Function

The GF required for our analysis is the solution of the scalar inhomogeneous Helmholtz wave equation

$$\nabla^2 g(r, r') + k^2 g(r, r') = -\delta(r-r') \quad (4.24)$$

for a point source at r' , at an observation point $r = (x, y, z)$. This equation satisfies homogeneous Dirichlet ($G = 0$) or Neumann ($\partial G / \partial n = 0$) boundary conditions on the boundary surface S , and also in the source coordinates, on S' which surrounds the source point (figure 4.2). The Dirac delta function on the right hand side is defined in equation (4.11).

Next we show that the inhomogeneous equation

$$\nabla^2 \psi + k^2 \psi = -\rho(r) \quad (4.25)$$

subject to the same Dirichlet/Neumann boundary conditions on the surface S , may be

expressed in terms of g . Multiplying (4.24) by ψ and (4.25) by $g(r,r')$ and subtracting the two, exchanging r and r' at the same time

$$g(r',r)\nabla^2\psi(r') - \psi(r')\nabla^2g(r',r) = -[\psi(r')\delta(r'-r) - g(r',r)\rho(r')] \quad (4.26)$$

Integrating this over the source coordinates $r' = (x',y',z')$ in the definition domain P (figure 4.2b) we obtain,

$$\begin{aligned} & \iiint_{C_\infty} g(r',r)\nabla^2\psi(r') - \psi(r')\nabla^2g(r',r) \, dV' + \iiint_{C_\infty} \rho(r')g(r',r) \, dV' \\ & + \iiint_C g(r',r)\nabla^2\psi(r') - \psi(r')\nabla^2g(r',r) \, dV' + \iiint_C \rho(r')g(r',r) \, dV' \end{aligned}$$

The first integral vanishes due to Sommerfeld's radiation condition. With this together with the unique property of the delta function, the first integral at C_∞ is equal to $\psi(r)$. Changing the volume integral at C to V , we obtain

$$\begin{aligned} & \iiint_V g(r',r)\nabla^2\psi(r') - \psi(r')\nabla^2g(r',r) \, dV' + \iiint_V \rho(r')g(r',r) \, dV' \quad (4.27) \\ & = \begin{cases} \psi(r) & \text{if } r \text{ inside } S \\ 0 & \text{if } r \text{ outside } S. \end{cases} \end{aligned}$$

Using Green's theorem (equation (4.14)), we can reduce the first integral to a surface integral

$$\begin{aligned} & \iint_S [g(r',r)\nabla\psi(r') - \psi(r')\nabla g(r',r)] \cdot dS + \iiint_V \rho(r')g(r',r) \, dV' \quad (4.28) \\ & = \begin{cases} \psi(r) & \text{if } r \text{ inside } S \\ 0 & \text{if } r \text{ outside } S. \end{cases} \end{aligned}$$

For the inhomogeneous equation ($\rho \neq 0$), using the homogeneous boundary conditions stated above ($g = 0$) on S , the surface integral over S is zero and

$$\psi(r) = \iiint_V \rho(r')g(r,r') \, dV' \quad (4.29)$$

for r inside or on S . This function automatically satisfies the homogeneous Dirichlet boundary conditions ($\psi = 0$ on S) and is solution of equation (4.25). Again this function holds for Neumann boundary conditions. In conclusion, equation (4.29) is a solution of the inhomogeneous equation (4.25) for homogeneous boundary conditions when $g(r,r')$ satisfies the same conditions as does ψ .

Hence for subsequent analysis, the GF wave equation (4.24) will be solved for our

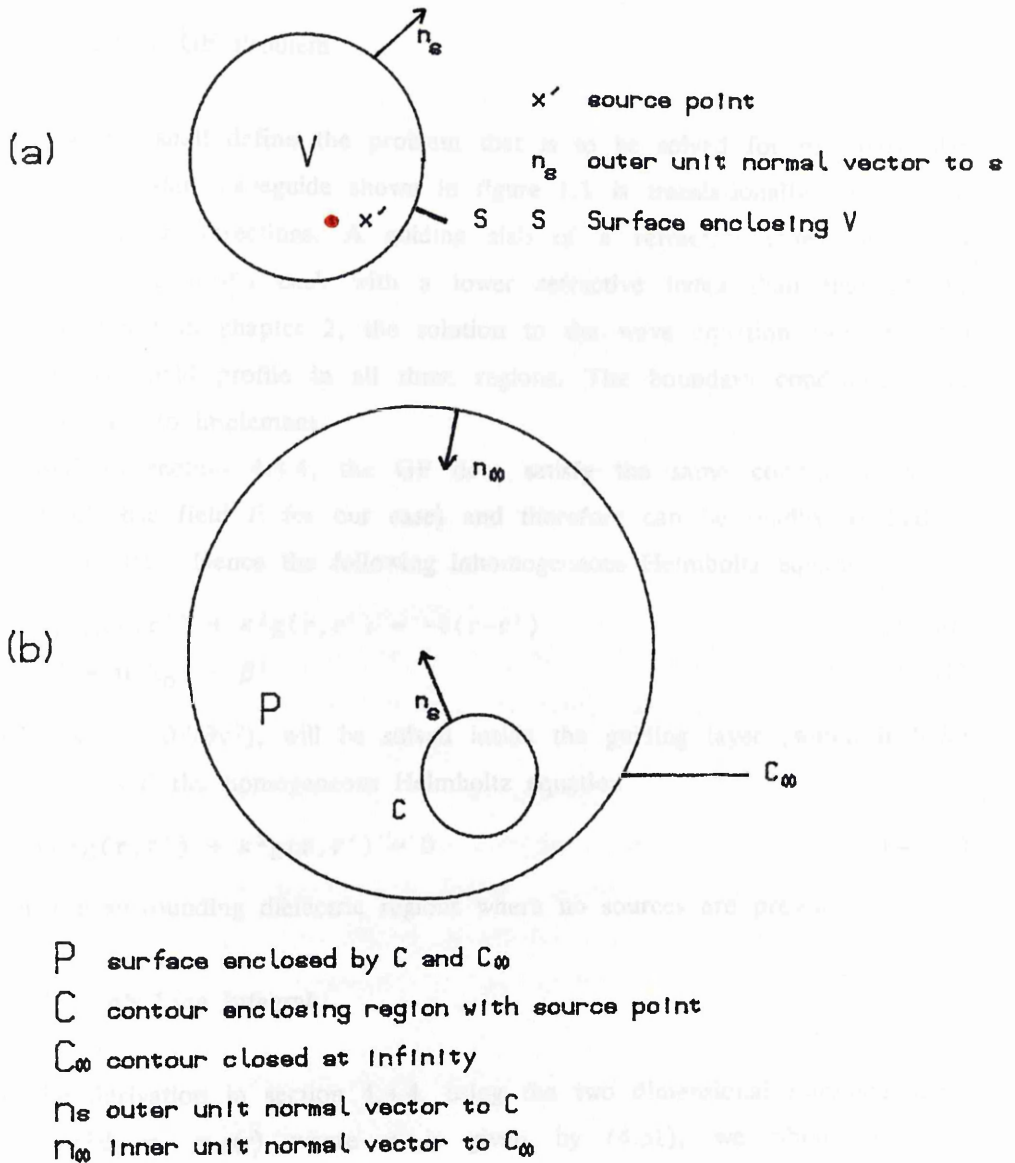


Figure 4.2 Green's Function Domain

particular problem to determine the required Green's function.

4.5 DEFINITION OF THE ANALYTICAL PROBLEM: Kirchhoff– Huygen's Integral

4.5.1 Slab/Ridge Waveguide GF Problem

As a preview, we shall define the problem that is to be solved for our particular waveguide structure. The slab waveguide shown in figure 1.1 is translationally invariant in the longitudinal and lateral directions. A guiding slab of a refractive index of n_2 is surrounded by two infinite media each with a lower refractive index than that of the guiding layer. As discussed in chapter 2, the solution to the wave equation yielded exact solutions to the electric field profile in all three regions. The boundary conditions were simple and therefore easy to implement.

As discussed in section 4.4.4, the GF does satisfy the same conditions as the function ψ (or the electric field E for our case) and therefore can be readily applied to our slab waveguide problem. Hence the following inhomogeneous Helmholtz equation

$$\nabla_t^2 g(r, r') + \kappa^2 g(r, r') = -\delta(r-r') \quad (4.30)$$

$$\kappa^2 = n^2 k_0^2 - \beta^2 \quad (4.31)$$

where $\nabla_t^2 = (\partial^2/\partial x^2 + \partial^2/\partial y^2)$, will be solved inside the guiding layer (which includes the source term at r') and the homogeneous Helmholtz equation

$$\nabla_t^2 g(r, r') + \kappa^2 g(r, r') = 0 \quad (4.32)$$

will be solved for the surrounding dielectric regions where no sources are present.

4.5.2 Kirchhoff– Huygen's Line Integral

Following the derivation in section 4.4.4, using the two dimensional inhomogeneous equation $\nabla^2 \psi + \kappa^2 \psi = -\rho(r)$ where κ is given by (4.31), we obtain for the homogeneous problem ($\rho(r) = 0$)

$$\iint_S g(r', r) \nabla_t^2 \psi(r') - \psi(r') \nabla_t^2 g(r', r) ds' = -\psi(r) \quad (4.33)$$

where the surface integration is performed in the x - y plane. Using Green's theorem in the plane using the reciprocity property, we obtain

$$\psi(r) = \int_C \left[g(r, r') \frac{\partial}{\partial n} \psi(r') - \psi(r') \frac{\partial}{\partial n} g(r, r') \right] dl \quad (4.34)$$

The path of integration is taken along a path enclosing the region of interest. The negative sign is eliminated by taking $\partial/\partial n$ as the normal inward on the surface boundary.

Equation (4.34) is the Kirchhoff–Huygens line integral which will be used for our analytical study of the rib/slab waveguide. The three components of the integral are therefore required. $\psi(r')$ is the general solution for the homogeneous wave equation at the source point r' . $\psi(r)$ is the scalar field at the observation point r . Finally the GF $g(r,r')$ is the GF for our particular region, which will be formulated in the next chapter.

4.6 CHOICE OF NUMERICAL METHOD

4.6.1 Numerical Choice for the Green's Function

The choice for calculating the GF are many, e.g. Fikioris⁹ (Watson transformation), R.C. Stevenson²¹ (Integral equations), Sphicopoulos et al.²² (Dyadic GF), Kolk²³ (Domain integral equation), C.C. Su²⁴ (Principle value integral) etc.. Although the majority of these authors discuss the vectorial dyadic GF, we have simplified our problem to solving the scalar GF.

To further simplify our problem, we consider solving an ordinary differential equation. As the planar stratification is invariant in the lateral directions, a Fourier transform in these directions reduces the two dimensional Helmholtz wave equation (4.30) and (4.32) to a one dimensional ordinary differential equation with only the one coordinate variable, the solutions of which are readily derivable.

Using the singularity nature of the GF at the source point, we can calculate analytically the spatial GF by the use of Cauchy's residue theorem. Thus the choice of the Fourier transform method has resulted in a simpler equation to solve. The presence of the singularity can also be used to derive a transcendental equation. As our GF calculations will require complex arithmetic to be performed, the GF program is implemented in Fortran 77.

Thus the GF for our case can be solved analytically and can be determined for any spatial coordinate within the waveguide.

4.6.2 Numerical Method for the Electric Field

The electric field within the region of interest is primarily determined by solutions to Maxwell's equations. Figure 2.9 shows the electric field profile of a slab waveguide using the exact field solutions obtained in chapter 2 and the solution as determined by the scalar FD method. As we are interested in an initial guess of the electric field for the Kirchhoff–Huygens integral, either field solution can be used. The object is that the field profile should converge using the Kirchhoff–Huygens integral in an iterative method. However, the effective index of the waveguide is required at each iteration, and the FD method is therefore most appealing.

4.6.3 Numerical Method for the Kirchhoff–Huygen's Integral

Given the GF at any point, and the electric field at discrete points, we can enclose a region of the waveguide of interest by the line integral and calculate the new electric field on this contour. Since we are using the discrete representation of the electric field, the integral (4.34) can be transposed via the rectangular rule into a matrix, the elements of which are the GF and the electric field. As in the FD method used in chapter 3, the vector processor facility can be used to accelerate the matrix calculations.

4.7 CONCLUSIONS

From simple solutions like Poisson's equation, we have shown that the GF is indeed a solution of this elliptic equation. Since the Helmholtz wave equation is also elliptic, it is therefore well-posed under the same conditions, and is suitable for our waveguide problem.

The integral theorems have been extensively used to demonstrate the properties of the GF. The theorems are further developed to derive the Kirchhoff–Huygens line integral which will be our analytical tool for the rib/slab waveguide.

Considering the waveguide structure, the stratification has allowed us to calculate the GF by an elementary Fourier transform method, which has the added advantage of simplifying the Helmholtz equation to an ordinary differential equation. The Fourier method is easily implemented on the computer. Having investigated the FD method in chapter 3, the Kirchhoff–Huygens line integral and its elements can be approximated by this method, thus leading to a final matrix problem which can be used in an iterative procedure.

From the previous considerations discussed in chapter 4, we shall now formulate the GF for our problem. The GF required is to satisfy the boundary conditions at infinity and at any dielectric discontinuities. As mentioned in section 4.1, the GF must constitute of sinusoidal solutions for the guiding layer and an evanescent decaying solution is required in the surrounding regions. These restrictions ensure that the GF satisfies the wave equation and Sommerfeld's radiation condition. Furthermore, we expect to observe other properties of the GF, e.g. the symmetry of the GF (the GF is an even function) and the large singularity that is to be expected at the source point where the GF is not defined. Only when the GF has been formulated for several situations and properties confirmed with the theory, will we then confidently use the GF for our problem.

As an initial exercise, the free space GF is determined in order to compare the solution to that with say, the Hankel function solution. The free space GF can also be used for Poissons equation, or for the purpose of diffraction theory.

The GF for the slab waveguide solution is determined for two different situations. The first considers the situation where the point source is located a finite distance above the dielectric slab, i.e. the point source is in free space within the proximity of a dielectric structure. The second situation, which is relevant to our problem, is when the point source is present within the guiding region, so resulting in a GF for the guiding slab. The homogenous solution for the GF wave equation (4.32) is however, formulated for the outer cladding and substrate regions.

5.1 FOURIER TRANSFORM OF THE GF WAVE EQUATION

The Green's function is a solution to the Helmholtz wave equation except at the source point. The 2D wave equation is reproduced below

$$\frac{\partial^2 g}{\partial x^2} + \frac{\partial^2 g}{\partial y^2} + \kappa^2 g = -\delta(x-x')\delta(y-y') \quad (5.1)$$

$$\kappa^2 = n^2 k_0^2 - \beta^2 \quad (5.2)$$

As the waveguide slab structure is translationally invariant in the x -direction, a Fourier transform in this coordinate variable reduces the partial differential equation (5.1) to an ordinary differential equation with y as the only variable, i.e.

$$\frac{\partial^2 G}{\partial y^2} + (\kappa^2 - k_x^2)G = -\delta(y-y') \quad (5.3)$$

The forward one dimensional Fourier transform is defined as

$$G(k_x, y) = \int_{-\infty}^{+\infty} g(x, y) e^{-ik_x x} dx \quad (5.4)$$

where k_x is the Fourier spatial frequency. The inverse Fourier transform is defined as

$$g(x, y) = \frac{1}{2\pi} \int_{-\infty}^{+\infty} G(k_x, y) e^{ik_x x} dk_x \quad (5.5)$$

By reducing the partial differential equation to an ordinary differential equation, we shall apply equation (5.3) to the particular situations.

5.2 FREE SPACE (UNBOUNDED) GREEN'S FUNCTION

5.2.1 Forward Fourier Transform Solution.

Figure 5.1 shows the situation where the source point is located in free space in the absence of any dielectric boundaries. The unbounded GF G_0 is readily derivable from the homogeneous wave equation (4.32). The simplicity of this solution can be used to formulate more complicated expressions for the GF in bounded regions. For the unbounded case, with the surface of integration at infinity, DBC and NBC are the same, therefore, for a fixed point source at r' , we expect G_0 and its derivatives to vanish as the observation point $r \rightarrow \infty$. Moreover, the decay of the GF is expected to be exponential as a function of $r-r'$ ($r-r' = \sqrt{(x-x')^2 + (y-y')^2}$), when $\kappa_1^2 < k_x^2$.

The equations to be solved are

$$\frac{\partial^2 G}{\partial y^2} - \eta_1^2 G = 0 \quad y > y' \quad (5.6a)$$

$$\frac{\partial^2 G}{\partial y^2} - \eta_1^2 G = 0 \quad y < y' \quad (5.6b)$$

where $\eta_1^2 = k_x^2 - \kappa_1^2$ (5.7)

The general solution to equation (5.6) for each region can be written down as

$$G_0 = A e^{-\eta_1 y} + B e^{\eta_1 y} \quad y > y' \quad (5.8)$$

$$G_0 = C e^{-\eta_1 y} + D e^{\eta_1 y} \quad y < y' \quad (5.9)$$

As there are no boundaries, an incoming wave solution $Be^{\eta_1 y}$ is not valid for $y > y'$,

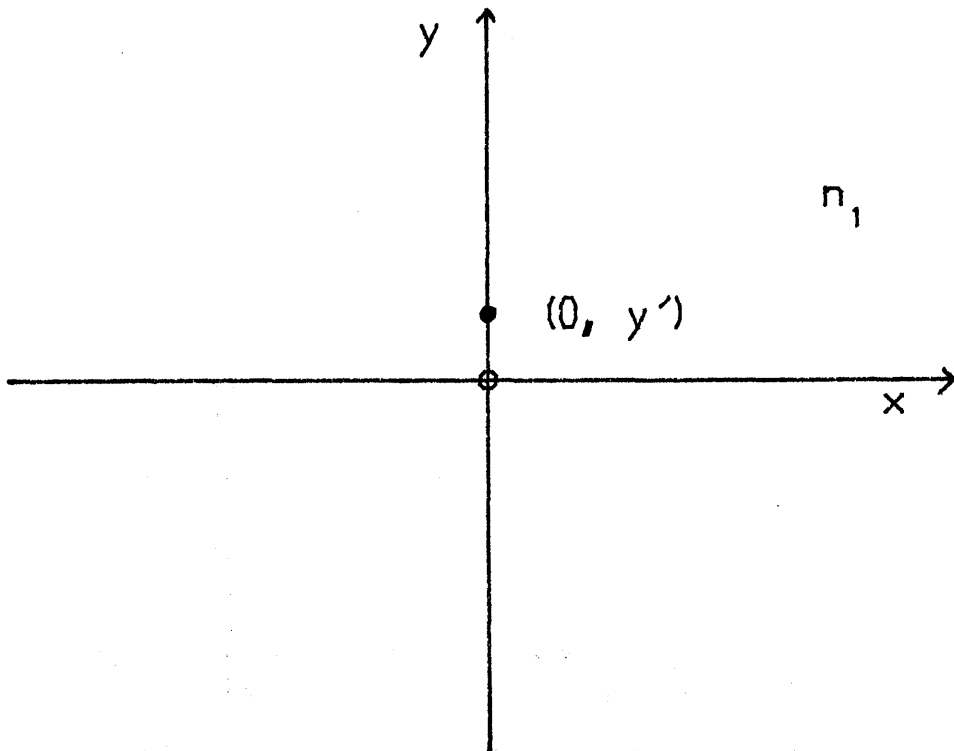


Figure 5.1 Point Source in Free Space

therefore we can assume $B = 0$. Similarly for the region $y < y'$, $C = 0$. The remaining terms for each region therefore constitutes an impulse at the source which decay exponentially as the observation point y tends to infinity.

Next, we apply the discontinuity boundary conditions (section 4.4.3) to the above general solutions, to determine the coefficients A and D . Since there is no dielectric boundary, the discontinuity of the GF across the source point is applicable only. Hence the boundary conditions for the GF and its derivative yield the following, with the source point located at the origin ($y' = 0$)

$$G_o (y = 0) : \quad A = D \quad (5.10)$$

$$\frac{dG_o}{dy} (y = 0) : \quad -\eta_1 A - \eta_1 D = -1 \quad (5.11)$$

$$\text{i.e.} \quad A = \frac{1}{2\eta_1} \quad (5.12)$$

$$D = \frac{1}{2\eta_1} \quad (5.13)$$

Therefore the GF for the two regions is then given as

$$G_o = \frac{e^{-\eta_1 y}}{2\eta_1} \quad y > y' \quad (5.14)$$

$$G_o = \frac{e^{\eta_1 y}}{2\eta_1} \quad y < y' \quad (5.15)$$

From direct observation of the GF expression, it can clearly be seen that the GF decays as $|y - y'| \rightarrow \infty$. Therefore the radiation condition in the y -direction is satisfied immediately. The GF is also even, i.e. $G_o(y - y') = G_o(-y - y')$.

5.2.2 Inverse Fourier Transform

The x -coordinate can be reintroduced by performing the inverse Fourier transform (IFT) of the GF from equation (5.5). However, for computer applications, we shall determine the spatial GF $g(x, y)$ numerically. This has the added advantage in that we can calculate the IFT quickly and efficiently. The resulting spatial GF will give a good approximation to the required analytical GF. For this case, the discrete inverse Fourier transform (DIFT) of (5.5) is written as

$$g_j(x, y) = \frac{1}{\sqrt{N}} \sum_{k=0}^{N-1} G_k(k_x, y) e^{i j k / N} \quad j = 0, N-1 \quad (5.16)$$

For our purposes, the NAG²⁵ routine C06FCF is used to calculate the IFT. Since the above NAG routine only calculates the forward Fourier transform, the IFT is calculated by taking the complex conjugate, performing the Fourier transform with C06FCF, and then

taking the complex conjugate of the result.

The difficulty arises since the NAG Fourier transform is only applicable for positive frequencies i.e. $j = 0..N-1$. Appendix F discusses the formulation of the shifting property of the Fourier transform.

Because the GF in the frequency domain is real valued ($\text{Im}(G) = 0$), the IFT will form a Hermitian sequence (i.e. for $0 < k < N/2$, $\text{Real}(g)$ is contained in $X(k)$, and $\text{Im}(g)$ is contained in $X(n-k)$, X being the array to store the values of the discrete GF values).

Fortran computer listings of the GF program and the IFT calculations are given in appendices G and H.

5.2.3 Cartesian Coordinate Resolution

As we are dealing with a discrete solution of the GF, we require that the GF can be defined for particular spatial coordinates (x,y) . The intermediate GF can therefore be determined by interpolation if necessary. For a resolution of Δx , the forward Fourier transform (5.4) must be band-limited. Using the identity

$$\Delta x \Delta k_x = 2\pi/N \quad (5.17)$$

where N is a positive power of 2, we can determine the actual frequency range required for the desired resolution Δx in the IFT. For the integration range $-Mk_0 < k_x < Mk_0$ in equation (5.4), divided into N equal steps, the interval step Δk_x in the discrete forward Fourier transform is given as

$$\Delta k_x = 2Mk_0/N \quad (5.18)$$

Hence

$$\Delta x = \frac{2\pi}{2Mk_0/N \cdot N} \quad (5.19)$$

i.e.

$$\Delta x = \lambda/2M \quad (5.19)$$

Therefore the resolution step can be dynamically chosen by band-limiting the interval range of the forward Fourier transform for the particular operating wavelength λ .

5.2.4 Cartesian Contour Plot

Figure 5.2 shows the two dimensional contour and three dimensional plot of the spatial GF $g(x,y)$ for free space. As expected there exists a singularity at the source point, where the GF is not defined. The GF radiates away from the source point and decays as $1/R$ (where $R = (r-r') = \sqrt{\{(x-x')^2 + (y-y')^2\}} \rightarrow \infty$). This is expected since the observation point and the source point are infinitely removed from each other. This solution is similar to that for a Hankel function²⁵.

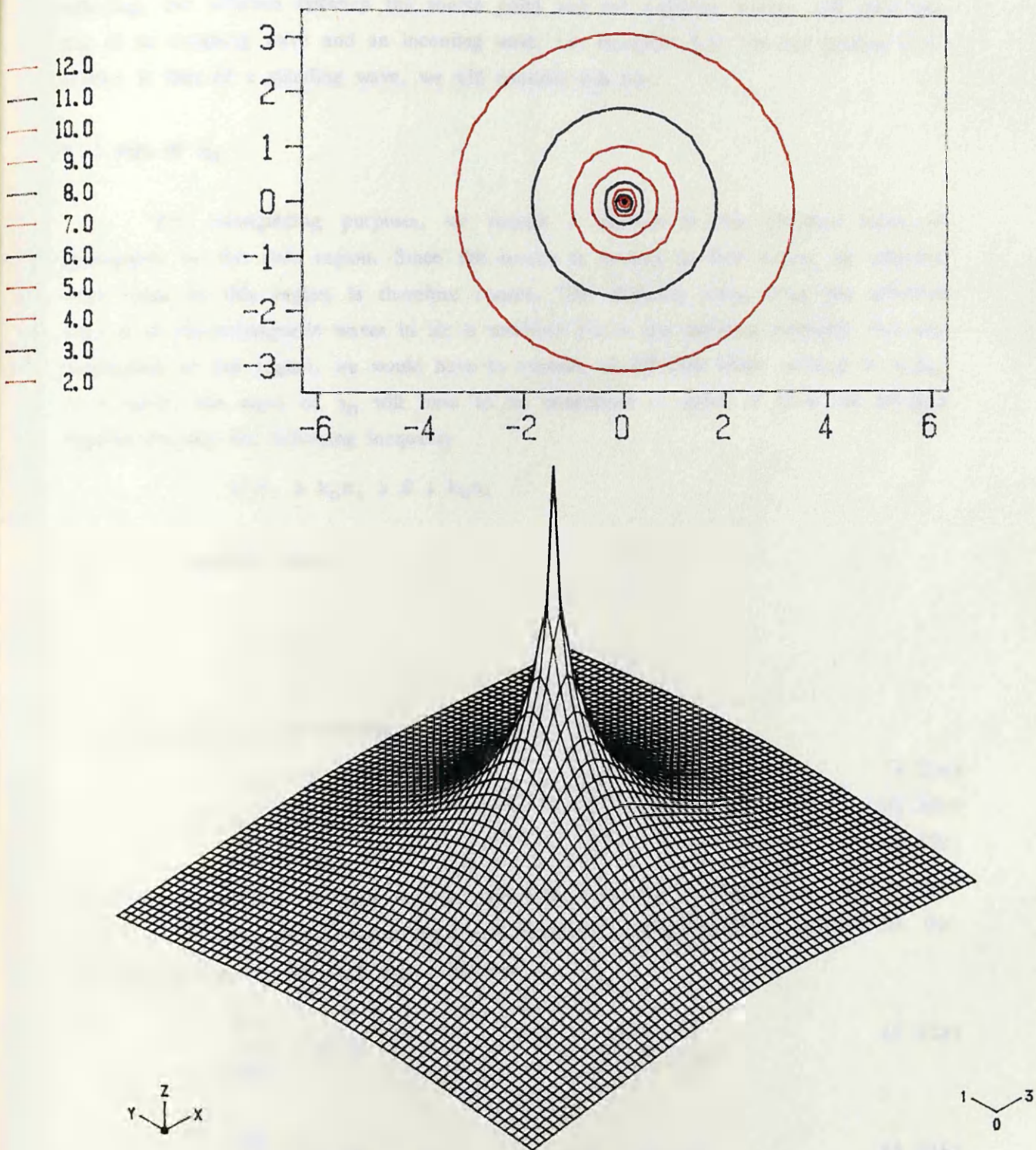


Figure 5.2 2D and 3D plot of free space Green's Function

5.3 DIELECTRIC SLAB GF SOLUTION – SITUATION 1

Figure 5.3a shows the situation where the point source is located in free space in the presence of a dielectric slab. Using the assumptions made earlier in chapter 4, we shall calculate the GF in all three regions. Since the dielectric interface is partially reflecting, our solution between the source point and the dielectric surface will constitute that of an outgoing wave and an incoming wave, i.e. equation (5.9). As the guiding layer solution is that of a standing wave, we will consider this too.

5.3.1 Sign of η_n

For waveguiding purposes, we require a solution to the effective index of propagation in the slab region. Since the source is located in free space, an effective index value in this region is therefore chosen. The difficulty arises since the effective index β of electromagnetic waves in air is unknown (as in the previous problem). For any propagation in this region, we would have to consider an effective index value $\beta > n_1 k_0$. As a result, the signs of η_n will have to be considered in order to have the solution required obeying the following inequality

$$k_0 n_2 \geq k_0 n_3 \geq \beta \geq k_0 n_1$$

Hence from equation (4.3.1)

$$\kappa_1^2 \leq 0$$

$$\kappa_2^2 \geq 0$$

$$\kappa_3^2 \geq 0$$

the following changes of variables are made

$$\eta_1^2 = k_x^2 - \kappa_1^2 \tag{5.20a}$$

$$\eta_2^2 = \kappa_2^2 - k_x^2 \tag{5.20b}$$

$$\eta_3^2 = \kappa_3^2 - k_x^2 \tag{5.20c}$$

The above ensure that the wave equation will yield a solution for the GF in air, and that the GF in the other two dielectric regions is evanescent. Using the above substitutions, the homogeneous equation for each region becomes

$$\frac{\partial^2 G}{\partial y^2} - \eta_1^2 G = 0 \quad \begin{array}{l} y > y' \\ 0 < y < y' \end{array} \tag{5.21a}$$

$$\frac{\partial^2 G}{\partial y^2} + \eta_2^2 G = 0 \quad -d < y < 0 \tag{5.21b}$$

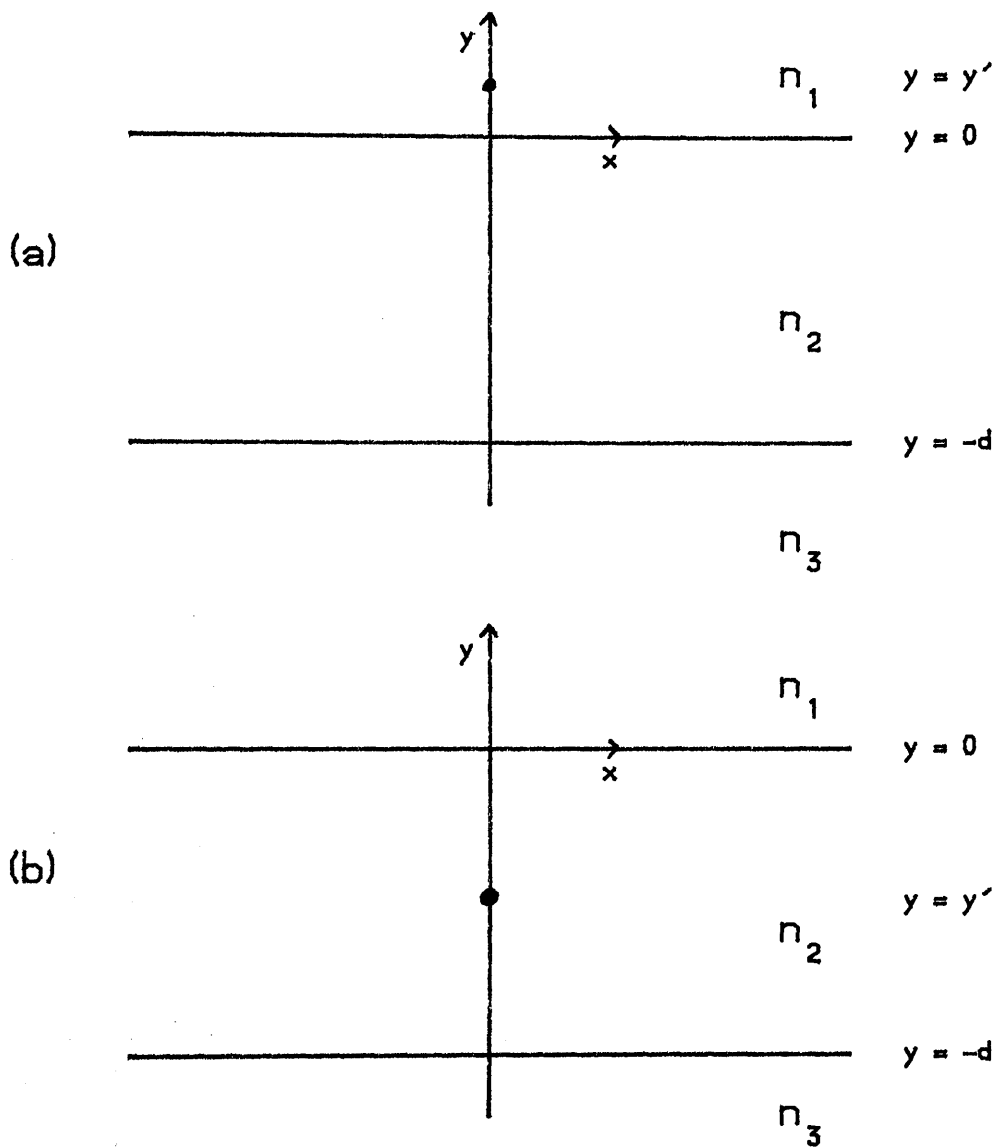


Figure 5.3 Green's Functions Situations

$$\frac{\partial^2 G}{\partial y^2} + \eta_3^2 G = 0 \quad y < -d \quad (5.21c)$$

with general solutions

$$G = Ae^{-\eta_1 y} \quad y > y' \quad (5.22a)$$

$$G = A_1 e^{-\eta_1 y} + B_1 e^{\eta_1 y} \quad 0 < y < y' \quad (5.22b)$$

$$G = A_2 e^{-i\eta_2 y} + B_2 e^{i\eta_2 y} \quad -d < y < 0 \quad (5.22c)$$

$$G = A_3 e^{\eta_3 y} \quad y < -d \quad (5.22d)$$

Note that, as assumed in section 4.1, we have written down a standing wave solution of the GF in the guiding layer using complex exponential notation. The constants A , A_1 , etc. are determined by applying the discontinuity boundary conditions at $y = 0$, $y = -d$, and at the source point y' .

$$y = -d \quad G : \quad A_3 e^{-\eta_3 d} = A_2 e^{i\eta_2 d} + B_2 e^{-i\eta_2 d} \quad (5.23a)$$

$$dG/dy : \quad \eta_3 A_3 e^{-\eta_3 d} = -i\eta_2 A_2 e^{i\eta_2 d} + i\eta_2 B_2 e^{-i\eta_2 d} \quad (5.23b)$$

$$y = 0 \quad G : \quad A_1 + B_1 = A_2 + B_2 \quad (5.23c)$$

$$dG/dy : \quad -\eta_1 A_1 + \eta_1 B_1 = -i\eta_2 A_2 + i\eta_2 B_2 \quad (5.23d)$$

$$y = y' \quad G : \quad Ae^{-\eta_1 y'} = A_1 e^{-\eta_1 y'} + B_1 e^{\eta_1 y'} \quad (5.23e)$$

$$dG/dy : \quad -\eta_1 Ae^{-\eta_1 y'} + \eta_1 A_1 e^{-\eta_1 y'} - \eta_1 B_1 e^{\eta_1 y'} = -1 \quad (5.23f)$$

After some manipulation, the constants are found to be

$$B_1 = \frac{1}{2\eta_1} e^{-\eta_1 y'} \quad (5.24a)$$

$$A_2 = (-\eta_3 + i\eta_2) e^{-\eta_1 y'} e^{-i\eta_2 d} / \text{denom} \quad (5.24b)$$

$$B_2 = (\eta_3 + i\eta_2) e^{\eta_2 d} e^{-\eta_1 y'} / \text{denom} \quad (5.24c)$$

$$A_1 = A_2 + B_2 - B_1 \quad (5.24d)$$

$$A = A_1 + \frac{1}{2\eta_1} e^{\eta_1 y'} \quad (5.24e)$$

$$A_3 = (A_2 e^{-i\eta_2 d} + B_2 e^{i\eta_2 d}) e^{\eta_3 d} \quad (5.24f)$$

$$\text{denom} = 2i\eta_1 \eta_3 \sin(\eta_2 d) + 2i\eta_2 [(\eta_1 + \eta_3) \cos(\eta_2 d) - \eta_2 \sin(\eta_2 d)] \quad (5.24g)$$

5.3.2 Inverse Fourier Transform Solution

The required GF for each region is given by performing the IFT (equation F6 in Appendix F) to equations (5.22a) – (5.22d).

The spatial GF for a point source y' located $0.5\mu\text{m}$ above a dielectric slab of thickness $d = 0.5\mu\text{m}$ and refractive index $n_2 = 3.44$, substrate refractive index $n_3 =$

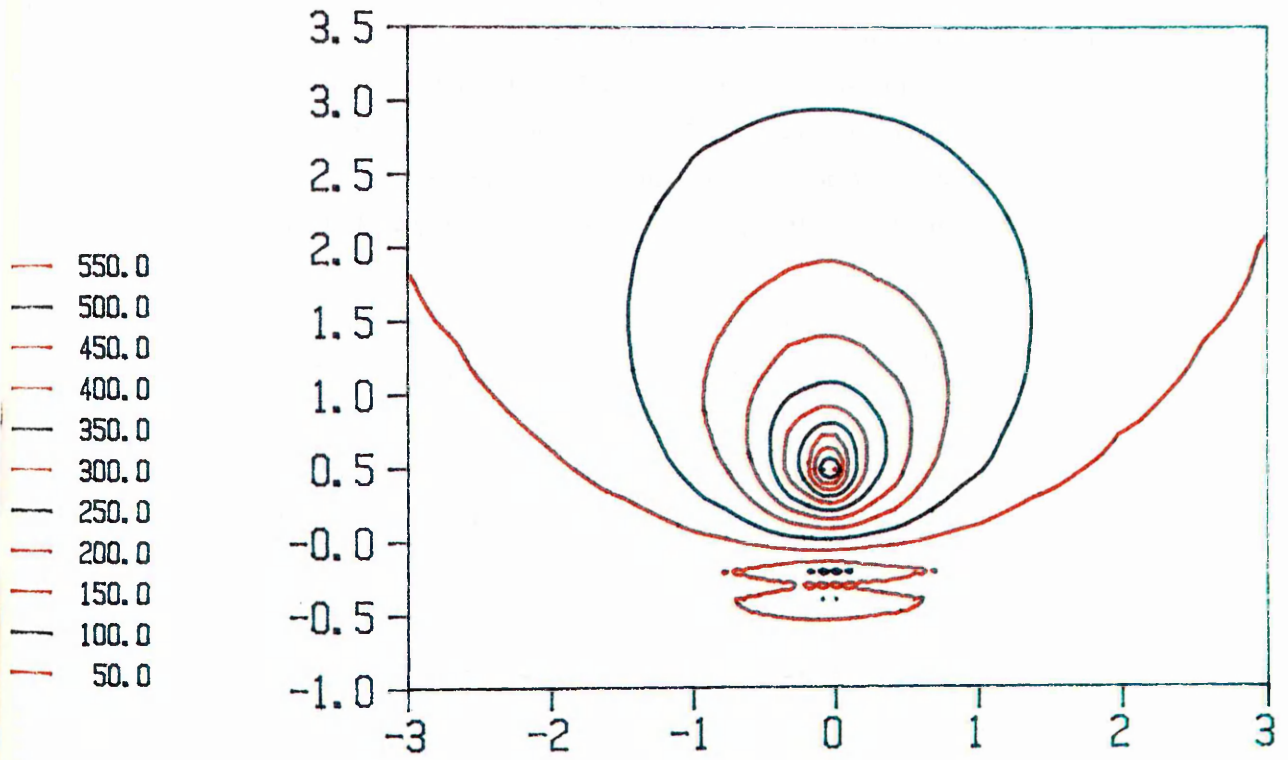


Figure 5.4 2D Contour Plot of Green's Function for Situation 1

3.34 is shown in figure 5.4. Here a Δx resolution of $0.1\mu\text{m}$ was chosen by bandlimiting the forward Fourier transform in the range $-7.75k_0 < k_x < 7.75k_0$. The intermediate points of the spatial GF have been interpolated by the IBM UNIRAS™ graphics routine.

A large singularity is again observed at the source point $(x', y') = (0.0, 0.5)$, and decays radially. Note that the decay is slow for $y > y'$ since an effective index of $n_e = 1.001$ was chosen. At the other side of the source point, the decay is rapid due to reflections from the dielectric boundary surface at $y = 0$.

The Fortran program listing to calculate the above GF is listed in Appendix I.

5.4 DIELECTRIC SLAB GF SOLUTION – SITUATION 2

For many waveguide analyses, the source of excitation is present in a dielectric region enclosed by a cladding and substrate layer. For this situation we would require the delta source point in the n_2 region (figure 5.3b), with the corresponding inhomogeneous GF wave equation (5.3) to solve. Using the guidance inequality described in section 2.1.4 and using equations (5.20) with $\eta_3^2 = k_x^2 - \kappa_3^2$, the wave equations to solve for each dielectric region are

$$\frac{\partial^2 G}{\partial y^2} - \eta_1^2 G = 0 \quad y > 0 \quad (5.26a)$$

$$\frac{\partial^2 G}{\partial y^2} + \eta_2^2 G = 0 \quad y' < y < 0 \quad (5.26b)$$

$$\frac{\partial^2 G}{\partial y^2} + \eta_2^2 G = 0 \quad -d < y < y' \quad (5.26c)$$

$$\frac{\partial^2 G}{\partial y^2} - \eta_3^2 G = 0 \quad y < -d \quad (5.26d)$$

The solutions to these are

$$G = Ae^{-\eta_1 y} \quad y > 0 \quad (5.27a)$$

$$G = A_1 e^{-i\eta_2 y} + B_1 e^{i\eta_2 y} \quad y' < y < 0 \quad (5.27b)$$

$$G = A_2 e^{-i\eta_2 y} + B_2 e^{i\eta_2 y} \quad -d < y < y' \quad (5.27c)$$

$$G = A_3 e^{\eta_3 y} \quad y < -d \quad (5.27d)$$

As before, the coefficients A , A_1 , etc. are determined by applying the discontinuity

boundary conditions at $y = 0$, $y = -d$, and at the source point $y = y'$.

$$y = -d \quad G : \quad A_3 e^{-\eta_3 d} = A_2 e^{i\eta_2 d} + B_2 e^{-i\eta_2 d} \quad (5.28a)$$

$$dG/dy : \quad \eta_3 A_3 e^{-\eta_3 d} = -i\eta_2 A_2 e^{i\eta_2 d} + i\eta_2 B_2 e^{-i\eta_2 d} \quad (5.28b)$$

$$y = 0 \quad G : \quad A = A_1 + B_1 \quad (5.28c)$$

$$dG/dy : \quad -\eta_1 A = -i\eta_2 A_1 + i\eta_2 B_1 \quad (5.28d)$$

$$y = y' \quad G : \quad A_1 e^{-\eta_2 y'} + B_1 e^{\eta_2 y'} = A_2 e^{-\eta_2 y'} + B_2 e^{\eta_2 y'} \quad (5.28e)$$

$$dG/dy : \quad -\eta_2 A_1 e^{-\eta_2 y'} + \eta_2 B_1 e^{\eta_2 y'} + \eta_2 A_2 e^{-\eta_2 y'} - \eta_2 B_2 e^{\eta_2 y'} = -1 \quad (5.28f)$$

After some manipulation, the coefficients are found to be

$$\begin{aligned} B_1 &= \frac{i}{2\eta_2} \left[e^{i\eta_2 y'} e^{i\eta_2 d} + \frac{(i\eta_2 - \eta_3)}{(\eta_3 + i\eta_2)} e^{-i\eta_2 y'} e^{-i\eta_2 d} \right] / \text{denom} \\ A_1 &= -(\eta_1 + i\eta_2) / (\eta_1 - i\eta_2) B_1 \\ B_2 &= \frac{i}{2\eta_2} \left[e^{i\eta_2 y'} e^{i\eta_2 d} - \frac{(\eta_1 + i\eta_2)}{(\eta_1 - i\eta_2)} e^{-i\eta_2 y'} e^{i\eta_2 d} \right] / \text{denom} \\ A_2 &= (-\eta_3 + i\eta_2) / (\eta_3 + i\eta_2) B_2 e^{-2i\eta_2 d} \\ A &= A_1 + B_1 \\ A_3 &= (A_2 e^{i\eta_2 d} + B_2 e^{-i\eta_2 d}) e^{\eta_3 d} \\ \text{denom} &= \left[\frac{(\eta_1 + i\eta_2)}{(\eta_1 - i\eta_2)} e^{i\eta_2 d} + \frac{(i\eta_2 - \eta_3)}{(\eta_3 + i\eta_2)} e^{-i\eta_2 d} \right] \end{aligned} \quad (5.29)$$

5.4.1 Singularity Nature of the Green's Function

Before attempting to derive the required spatial GF via the IFT, some characteristics of the GF with the point source located within the active layer are discussed. Since a numerical IFT is readily applicable here, we have to investigate possible contributions to the final GF by the physical conditions imposed on our GF.

The presence of dielectric boundaries along the x -direction gives rise to simple pole singularities in the GF²⁷. These poles contribute to the modal distribution of the GF. Simple calculus using the method of residues can be implemented as the IFT integral requires avoidance of these poles.

The remaining part of the GF in the Fourier domain (after removal of these poles) can be calculated numerically, thus giving a spatial GF that decays as $|x-x'| \rightarrow \infty$.

Furthermore, as the propagation constant of the waveguide is required, we can derive a transcendental equation from the GF of the guiding layer by manipulating the singularity nature of the GF at the poles. For this case the denominator equation (5.29) is equated to zero. The resulting transcendental equation is simple and can be solved as before and is formulated in the next chapter. The frequency at which the poles occur can also be determined by the same transcendental equation.

5.5 CONCLUSIONS

Starting from the three dimensional homogeneous GF wave equation, we have reduced the problem to a one dimensional equation by exploiting the translational invariance of the slab structure. We have solved this equation for various situations involving the dielectric slab, and using the boundary conditions specified in section 4.4.3, the spatial GF is matched across all discontinuities. The conditions at infinity are explicitly incorporated in the solution, and comparisons with the Hankel function lead to the strong argument that the solution is correct and therefore accurate. At a glance, using the discrete Fourier transform, we can deduce the shape of the spatial GF, observe the singularity at the source point and the decay away from the source point. Such theories given about the GF have been investigated and are concluded to be correct.

Finally for the source point in the guiding layer, we have derived a GF expression whose IFT can be calculated analytically by the method of residues. The singularity nature of the source point will lead to a simple transcendental equation that will be solved for the eigenvalues of the slab. This is now developed in the next chapter.

As the required GF for the slab is to be determined analytically, we will derive the modal contribution of the spatial GF $g_m(x,y)$ via the residue theorem. The determination of the GF in the frequency domain has resulted with the GF having a denominator that can be equated to zero. From this the resulting transcendental equation, which is similar to the TE transcendental equation (2.48), can be solved for the effective index (and frequency of the poles) since it takes account of the depth of the slab d and the surrounding refractive indices. The coordinates of y and y' are not relevant at this stage.

6.1 DERIVATION OF THE GF TRANSCENDENTAL EQUATION

The singularity occurs in the Fourier domain when the denominator of the above GF tends to zero. Consider equation (5.29). The denominator can be transformed into

$$[e^{i\Phi_1} e^{i\eta_2 d} - e^{-i\Phi_3} e^{-i\eta_2 d}] \quad (6.1)$$

where $\Phi_1 = 2 \tan^{-1} [\eta_2 / \eta_1]$ (6.2)

$$\Phi_3 = 2 \tan^{-1} [\eta_2 / \eta_3] \quad (6.3)$$

At the singularity, equation (6.1) is equated to zero, hence

$$e^{i(\Phi_1 + \Phi_3 + 2\eta_2 d)} = 1$$

i.e. $\Phi_1 + \Phi_3 + 2\eta_2 d = 2q\pi \quad q = 1, 2, \dots$ (6.4)

This is the transverse resonance condition equation which can be solved to obtain the eigenvalue β (or effective index n_e) and the poles of the GF.

6.1.1 Solutions to the GF Transcendental Equation

Figure 6.1 shows the above equation plotted for various choices of effective index n_e for waveguide structure 2. The value of the propagation constant can be read off immediately from where the graph intersects the resonance condition at 2π . Here $q = 1$ and therefore the solution obtained is for the fundamental mode ($n_e = 3.409374$). Figure 6.2 shows the transcendental equation plotted for the waveguide 1 slab structure. As this is a two moded structure, we see two solutions of the transcendental equation. The corresponding effective indices for the the two modes are $n_{e_0} = 3.407594$ and $n_{e_1} = 3.319209$.

The GF transcendental equation (6.4) has been solved for the same slab waveguides defined in section 2.3.3. The Fortran computer listing is listed in Appendix J. The results have been tabulated below

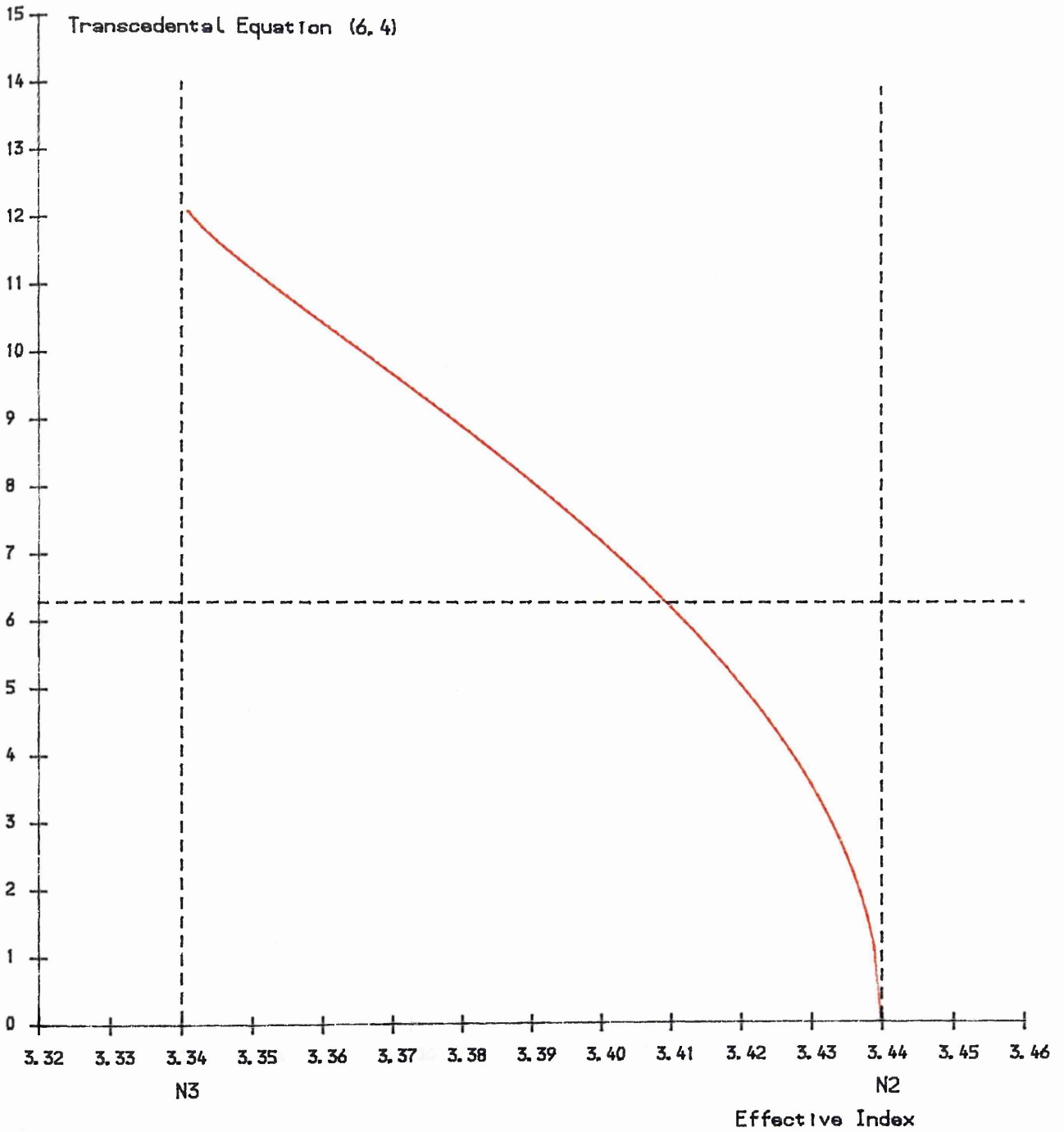


Figure 6.1 Graphical Solution of Transcendental Equation for WG2

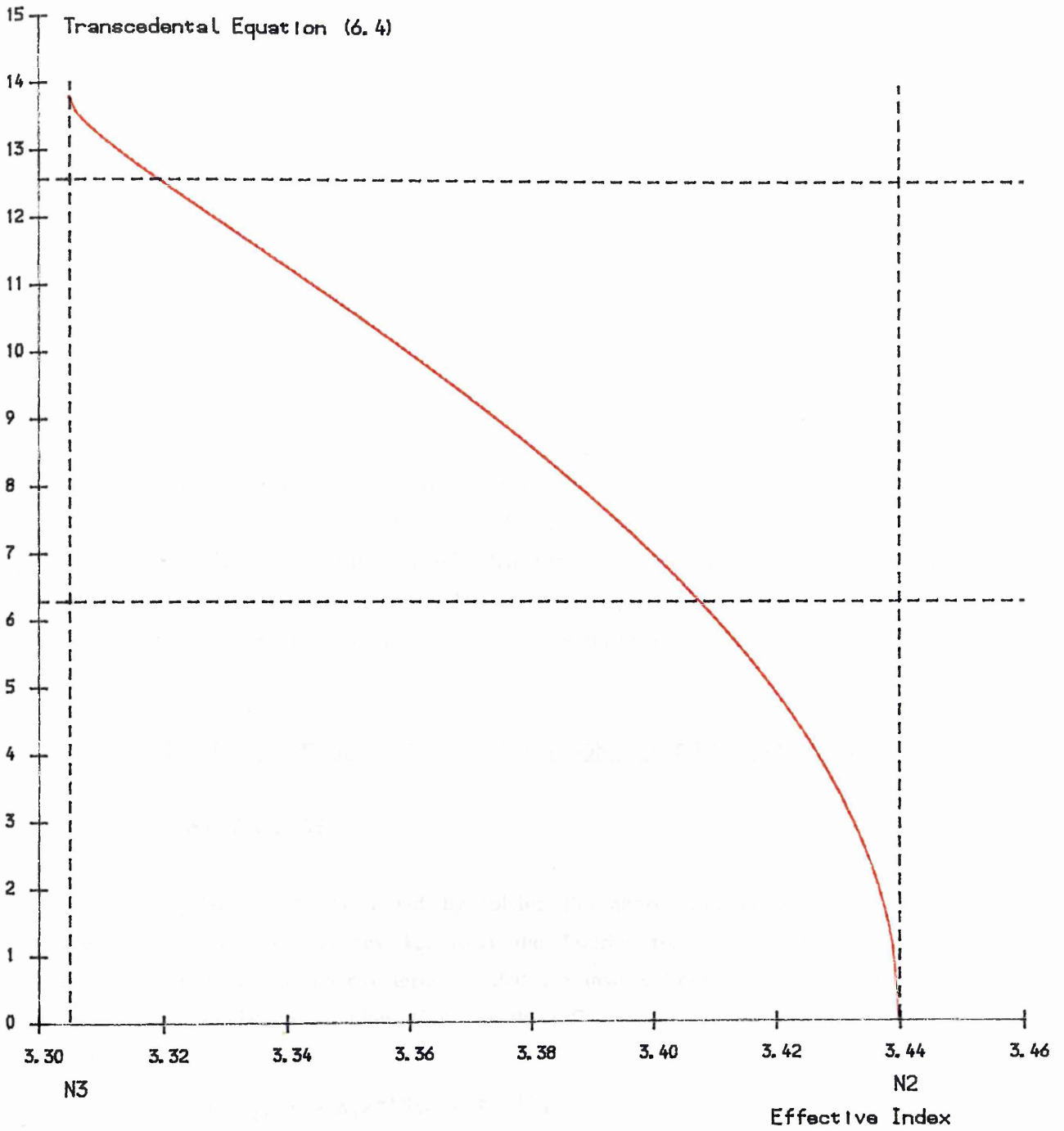


Figure 6.2 Graphical Solution of Transcendental Equation for WG1

Structure	n_3	Fundamental mode		First order mode	
		n_e	(b)	n_e	(b)
1.	3.305	3.407593932	(0.7563)	3.319209968	(0.1034)
2.	3.34	3.409374837	(0.6906)	-	-
3.	3.39	3.414297681	(0.4841)	-	-
4.	3.40	3.416099847	(0.4011)	-	-
5.	3.42	3.422485526	(0.1240)	-	-
6.	3.435	-	-	-	-

Table 6a

The effective index values calculated are in very good agreement with the exact solutions derived in chapter 2. The largest error being $0.7799 \times 10^{-3} \%$ for the waveguide structure 2, and the smallest error being $5.182 \times 10^{-6} \%$ for the first order mode for waveguide 1. From the above results, we can conclude that the GF expressions (5.29) are correct and exact for the three layered slab waveguide. These eigenvalues can therefore be used in the expressions for the spatial GF $g(x,y)$ which are now formulated.

6.2 DERIVATION OF THE MODAL CONTRIBUTION TO THE SPATIAL GF $g_m(x,y)$

6.2.1 Singularities of the GF

The singularities can be found by solving the above transcendental equation as a function of the spatial frequency k_x . Next the Fourier transform of the GF must be modified to extract the singularity term, so that the inverse Fourier transform (IFT) of the GF will yield a modal contribution. Consider the GF equation (5.27b) for the region $y' < y < 0$

$$\begin{aligned}
 G(k_x, y) &= A_1 e^{-i\eta_2 y} + B_1 e^{i\eta_2 y} \\
 &= \left[- \frac{(\eta_1 + i\eta_2)}{(\eta_1 - i\eta_2)} e^{-i\eta_2 y} + e^{i\eta_2 y} \right] B_1 \\
 &= \frac{i}{2\eta_2} \left[\begin{array}{c} \text{"} \\ \text{"} \end{array} \right] \left[e^{i\eta_2 y'} e^{i\eta_2 d} + \frac{(i\eta_2 - \eta_3)}{(\eta_3 + i\eta_2)} e^{-i\eta_2 y'} e^{-i\eta_2 d} \right] \\
 &\quad \underline{\hspace{10cm}} \\
 &\quad \left[e^{i\Phi_1} e^{i\eta_2 d} - e^{-i\Phi_3} e^{-i\eta_2 d} \right]
 \end{aligned}$$

$$= \frac{i/2\eta_2 \Psi(k_x, y) \Psi(k_x, y')}{[e^{i\Phi_1} e^{i\eta_2 d} - e^{-i\Phi_3} e^{-i\eta_2 d}]}$$

Rewriting the above, at $k_x = k_q$

$$G(k_x, y) = \frac{G'(k_x, y, y')}{\{1 - e^{if(k_x)}\}} \quad (6.5)$$

where

$$f(k_x) = \Phi_1 + \Phi_2 + 2\eta_2 d \quad (6.6a)$$

$$G'(k_x, y, y') = i/2\eta_2 \Psi(k_x, y) \Psi(k_x, y') \quad (6.6b)$$

$$\Psi(k_x, y) = \left[-\frac{(\eta_1 + i\eta_2)}{(\eta_1 - i\eta_2)} e^{-i\eta_2 y} + e^{i\eta_2 y} \right] \quad (6.6c)$$

$$\Psi(k_x, y') = \left[e^{i\eta_2 y'} e^{i\eta_2 d} + \frac{(i\eta_2 - \eta_3)}{(\eta_3 + i\eta_2)} e^{-i\eta_2 y'} e^{-i\eta_2 d} \right] \quad (6.6d)$$

6.2.2 Pole Contribution of the Green's Function

Using the Taylor series expansion about the point $(x-a)$

$$f(x) = f(a) + f'(a)(x-a) + f''(a)(x-a)^2/2! + \dots$$

equation (6.6) becomes

$$\begin{aligned} f(k_x) &= f(k_q) + f'(k_q)(k_x - k_q) + f''(k_q)(k_x - k_q)^2/2! + \dots \\ &= 2q\pi + f'(k_q)(k_x - k_q) + \dots \end{aligned}$$

where k_q is the singular point on the real k_x axis. Higher order powers have been omitted. The denominator of equation (6.5) can then be approximated by

$$\begin{aligned} 1 - e^{if(k_x)} &= 1 - e^{i2q\pi} e^{i(f'(k_q)(k_x - k_q) + \dots)} \\ &= 1 - 1 \cdot [1 + if'(k_q)(k_x - k_q) + \dots] \\ &= -if'(k_q)(k_x - k_q) + \dots \end{aligned} \quad (6.7)$$

where the Taylor series for the exponential term is given by²⁸

$$e^z = 1 + z + z^2/2! + z^3/3! + \dots$$

After this expansion, the pole contributions to the GF in equation (6.5) becomes

$$\begin{aligned} G_m(k_x, y) &\approx \frac{1/2\eta_2 \Psi(k_q, y) \Psi(k_q, y')}{-f'(k_q)(k_x - k_q)} & k_x \approx k_q \\ &\approx \frac{1/2\eta_2 \Psi(k_{-q}, y) \Psi(k_{-q}, y')}{-f'(-k_q)(k_x + k_q)} & k_x \approx -k_q \end{aligned}$$

We now introduce the x -coordinate variable by applying the IFT as defined in equation (5.5), i.e.

$$\begin{aligned}
g_m(x,y) &= \frac{1}{2\pi} \int_{-\infty}^{+\infty} \frac{1/2\eta_2 \Psi(k_q,y) \Psi(k_q,y')}{-f'(k_q)(k_x-k_q)} e^{ik_x x} dk_x \\
&+ \frac{1}{2\pi} \int_{-\infty}^{+\infty} \frac{1/2\eta_2 \Psi(-k_q,y) \Psi(-k_q,y')}{-f'(-k_q)(k_x+k_q)} e^{ik_x x} dk_x \quad (6.8)
\end{aligned}$$

The above integral can be implemented using the Cauchy residue theorem²⁹. The integral has been split into two cases. The first case, $x > 0$, the contour of integration is the path of an infinite semicircle in the upper half plane, and the second case, $x < 0$, the contour path is the path enclosing the semicircle in the lower half plane (figure 6.3). The poles at $k_x = \pm k_q$ lie on the real axis. We integrate by displacing the poles by $i\gamma$ and then taking the limit as $\gamma \rightarrow 0$. So for γ positive, contour C_1 encloses the pole at $k_x = k_q + i\gamma$ and the residue at this pole is (for $x > 0$)

$$\text{Residue at } k_x = k_q + i\gamma = \frac{1/2\eta_2 \Psi(k_q + i\gamma, y) \Psi(k_q + i\gamma, y')}{-f'(k_q + i\gamma)} e^{i(k_q + i\gamma)x} \quad (6.9a)$$

Similarly, the residue enclosed by the contour C_2 gives for $x < 0$

$$\text{Residue at } k_x = -(k_q + i\gamma) = \frac{1/2\eta_2 \Psi(-(k_q + i\gamma), y) \Psi(-(k_q + i\gamma), y')}{-f'(-(k_q + i\gamma))} e^{-i(k_q + i\gamma)x} \quad (6.9b)$$

6.2.3 Spatial GF $g_m(x,y)$

Now letting $\gamma \rightarrow 0$, the spatial pole contribution of the GF is given by the residue theorem as

$$\begin{aligned}
g_m(x,y) &= 2\pi i * (\text{sum of residues}) \\
&= \frac{i/2\eta_2 \Psi(k_q, y) \Psi(k_q, y')}{-f'(k_q)} e^{ik_q x} \quad x > 0 \quad (6.10a)
\end{aligned}$$

$$= \frac{i/2\eta_2 \Psi(-k_q, y) \Psi(-k_q, y')}{-f'(-k_q)} e^{-ik_q x} \quad x < 0 \quad (6.10b)$$

The GF $g(x,y)$ can now be calculated for any point (x,y) for a given source point (x',y') . Since we have assumed the source point to lie on the origin, we have let $x' = 0$. Reintroducing this term we simply replace the exponential term by $e^{ik_q(x-x')}$ or $e^{-ik_q(x-x')}$.

The value of $f'(\pm k_q)$ can be determined from the derivative of equation (6.4) i.e.

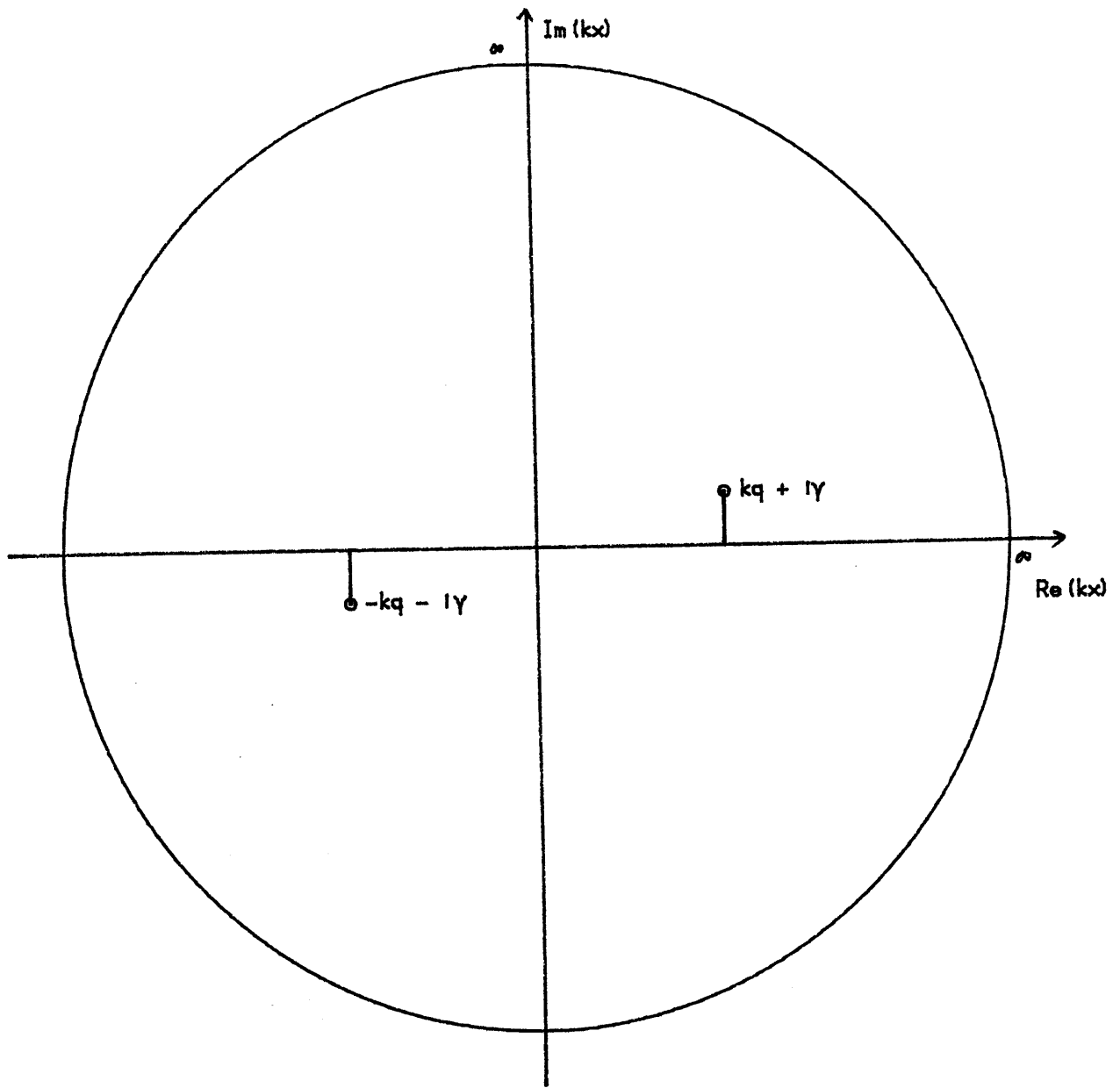


Figure 6.3 Plane of Integration for the Cauchy Integrals

$$f(k_x) = \Phi_1 + \Phi_3 + 2\eta_2 d = 2q\pi$$

$$\begin{aligned} f'(k_x = \pm k_q) &= \frac{\partial}{\partial k_x} \Phi_1 + \frac{\partial}{\partial k_x} \Phi_3 + \frac{\partial}{\partial k_x} 2\eta_2 d \\ &= \frac{\partial}{\partial k_x} \left[2 \tan^{-1} \left[\frac{\eta_2}{\eta_1} \right] \right] \\ &\quad + \frac{\partial}{\partial k_x} \left[2 \tan^{-1} \left[\frac{\eta_2}{\eta_3} \right] \right] + \frac{\partial}{\partial k_x} 2\eta_2 d \end{aligned}$$

After some manipulation, the above equation is simplified to

$$f'(k_q) = -2k_q \left[\frac{\eta_1/\eta_2 + \eta_2/\eta_1}{\eta_2^2 + \eta_1^2} \frac{\eta_3/\eta_2 + \eta_2/\eta_3}{\eta_2^2 + \eta_3^2} + \frac{d}{\eta_2} \right] \quad (6.11)$$

The calculation of the root k_q and the value of $f'(k_q)$ are contained in the Fortran program GFCALCS listed in Appendix J.

6.3 DERIVATION OF THE IFT GREEN'S FUNCTION $g_n(x,y)$

Having completed the modal contribution of the GF, there remains the nonsingular part of the GF. This GF, $g_n(x,y)$, is calculated numerically using the IFT equation defined by (5.5). Thus the complete spatial GF $g(x,y)$ is written as the sum of the two individual components

$$g(x,y) = g_n(x,y) + g_m(x,y)$$

i.e.

$$\begin{aligned} g(x,y) &= \frac{1}{2\pi} \int_{-\infty}^{+\infty} \left[\frac{i/2\eta_2 \Psi(k_x, y) \Psi(k_x, y')}{[e^{i\Phi_1} e^{i\eta_2 d} - e^{-i\Phi_3} e^{-i\eta_2 d}]} \right. \\ &\quad + \left[\frac{i/2\eta_2 \Psi(k_q, y) \Psi(k_q, y')}{-f'(k_q)} e^{ik_q x} \right. \\ &\quad \left. \left. + \frac{i/2\eta_2 \Psi(-k_q, y) \Psi(-k_q, y')}{-f'(-k_q)} e^{-ik_q x} \right] \right] e^{ik_x x} dk_x \\ &\quad + \frac{i/2\eta_2 \Psi(\pm k_q, y) \Psi(\pm k_q, y')}{-f'(\pm k_q)} e^{-ik_q |x|} \quad (6.12) \end{aligned}$$

Similar expressions can be derived for the GF in the other dielectric regions using the solutions given by equations (5.27) and (5.29). These final GF expressions can now be used in the Kirchoff–Huygens line integral. The Fortran computer listings to calculate the modal contribution and the FT GF are listed in appendices K and L respectively. The IFT GF $g_n(x,y)$ can be calculated using the IFT program listed in Appendix H.

The two components of the Green's function $g_m(x,y)$ and $g_n(x,y)$ are shown in figures 6.4 and 6.5 respectively. The modal GF $g_m(x,y)$ dominates, while the numerical GF $g_n(x,y)$ decays exponentially as $x \rightarrow \infty$.

6.4 KIRCHHOFF–HUYGEN'S LINE INTEGRAL

Reproducing the line integral below

$$\psi(r) = \int_C \left[\psi(r') \frac{\partial g}{\partial n} - \frac{\partial \psi(r')}{\partial n} g \right] dl \quad (6.13)$$

where $\psi(r)$ is the electric field within our region of interest. Again as an initial exercise, we will evaluate the above integral for a slab waveguide, the path of the integral is shown in figure 6.6. This has been chosen as the field is at a maximum within the guiding layer, and the solution to the exact field is also known. However we do have the flexibility to enclose any other region of interest. For an initial guess of the field $\psi(r')$, we shall use the FD method solution of the electric field for a slab region.

6.4.1 Matrix Implementation

As a direct consequence of implementing the FD method, the above line integral can be represented in discrete form (rewriting ψ as u , $\delta u/\delta n$ as $u'(x)$ and $\delta g/\delta n$ as $g'(x_n, x_m)$) as,

$$U(x_m) = \sum_{n=0}^{N-1} u(x_n) g'(x_n, x_m) - u'(x_n) g(x_n, x_m) \quad (6.14)$$

or in matrix form

$$\begin{aligned} [u_1 \ u_2 \ \dots \ u_m] &= [u_1 \ u_2 \ \dots \ u_n] \begin{bmatrix} g'_{11} & g'_{12} & \dots & g'_{1m} \\ g'_{21} & g'_{22} & \dots & g'_{2m} \\ \vdots & \vdots & \ddots & \vdots \\ g'_{n1} & g'_{n2} & \dots & g'_{nm} \end{bmatrix} \\ &- [u'_1 \ u'_2 \ \dots \ u'_n] \begin{bmatrix} g_{11} & g_{12} & \dots & g_{1m} \\ g_{21} & g_{22} & \dots & g_{2m} \\ \vdots & \vdots & \ddots & \vdots \\ g_{n1} & g_{n2} & \dots & g_{nm} \end{bmatrix} \end{aligned} \quad (6.15)$$

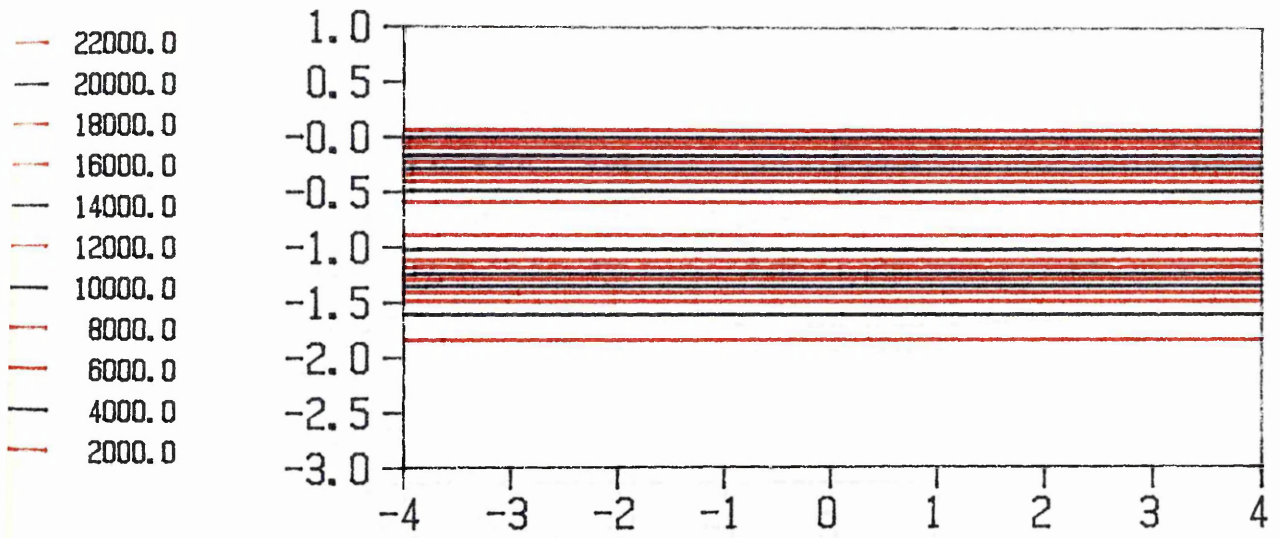


Figure 6.4 Contour Plot of the Modal Green's Function $g_m(x,y)$

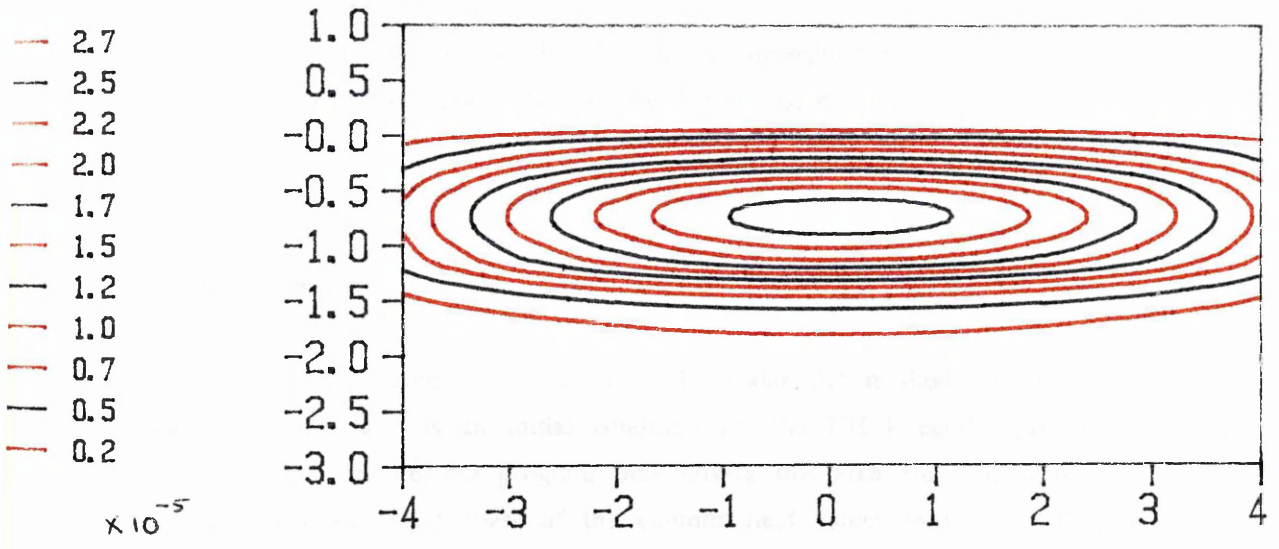


Figure 6.5 Contour Plot of the Numerical Green's Function $g_n(x,y)$

6.4.2 GF Matrix Elements

Figure 6.6 shows the proposed Kirchhoff–Huygens integral path enclosing the dielectric field within the dielectric slab, the maximum of the field placed at the centre of the enclosing 'box'.

Beginning from the top left hand corner, the integral is performed in a clockwise direction, with an interval step of $0.1\mu\text{m}$. This is the suggested step to match the sampling rate in the FD method.

The GF is calculated at every observational point x_n along the contour for every source point x_m . The position of the source point is then incremented to the next sampling point, and the GF again is calculated at each sampling observational point. This is repeated until the last sampling source point is reached.

Thus having completed the elements of the GF and electric field matrices (along with their respective derivatives), the discrete Kirchhoff–Huygens matrix calculation (equation (6.15)) is performed.

The diagonal elements of the GF matrix correspond to the observational point x_n coinciding with the source point x_m . As the GF is not defined at these points (the GF is infinite in this case), the value of the GF here is finite by virtue of the bandlimiting imposed in the inverse Fourier transform.

6.4.3 Iterative Procedure

As an initial exercise, the results of the scalar FD method on the slab waveguide (section 4.6.2) are used as an initial condition for the KH integral equation (6.12). The size of the 'box' for the FD program only covers this area surrounded by this contour. Having calculated an initial guess of the contour field values using the FD program, the GF function is determined as described above. After performing the Kirchhoff–Huygens calculation, the new values of the electric field calculated around the contour are consequently used as an initial condition for the FD program. Overleaf is a flow chart of the process. It is expected that the iteration procedure will converge to give a final result of the effective index and cross sectional field profile of the waveguide structure.

6.5 SLAB WAVEGUIDE RESULTS

The KH integral method was applied to the waveguide 1 structure. For the FD method, an initial field was calculated with a resulting effective index of $n_e = 3.40812758$ ($b = 0.7603$). The modal and numerically calculated GF's $g_m(x,y)$ and $g_n(x,y)$ were determined and the KH integral was performed with these components.

Figure 6.7 shows the electric field around the chosen contour in the slab guiding

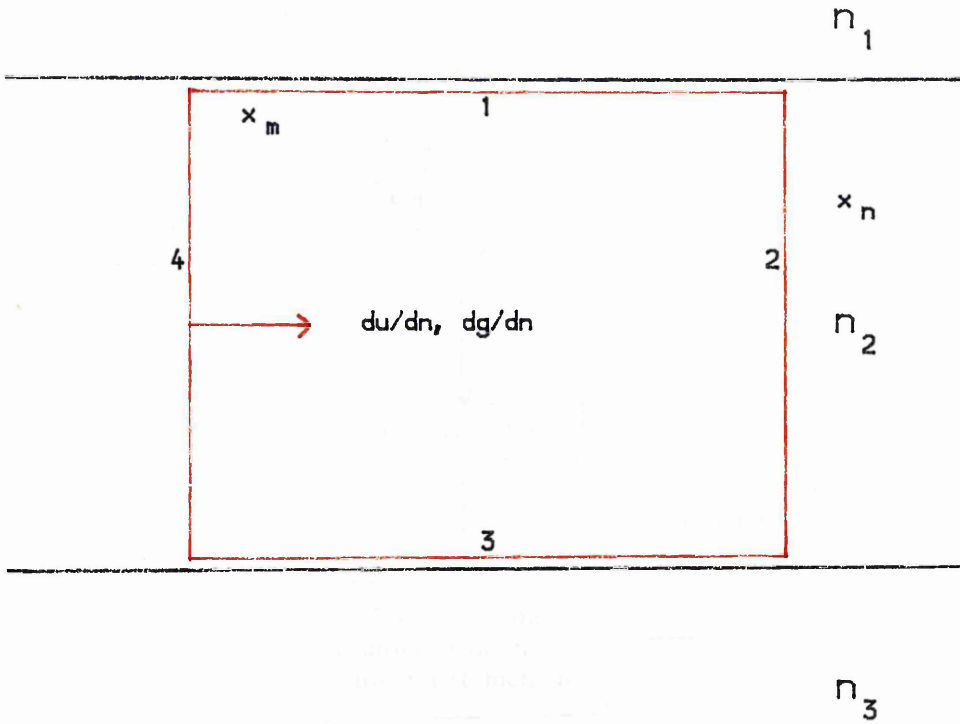
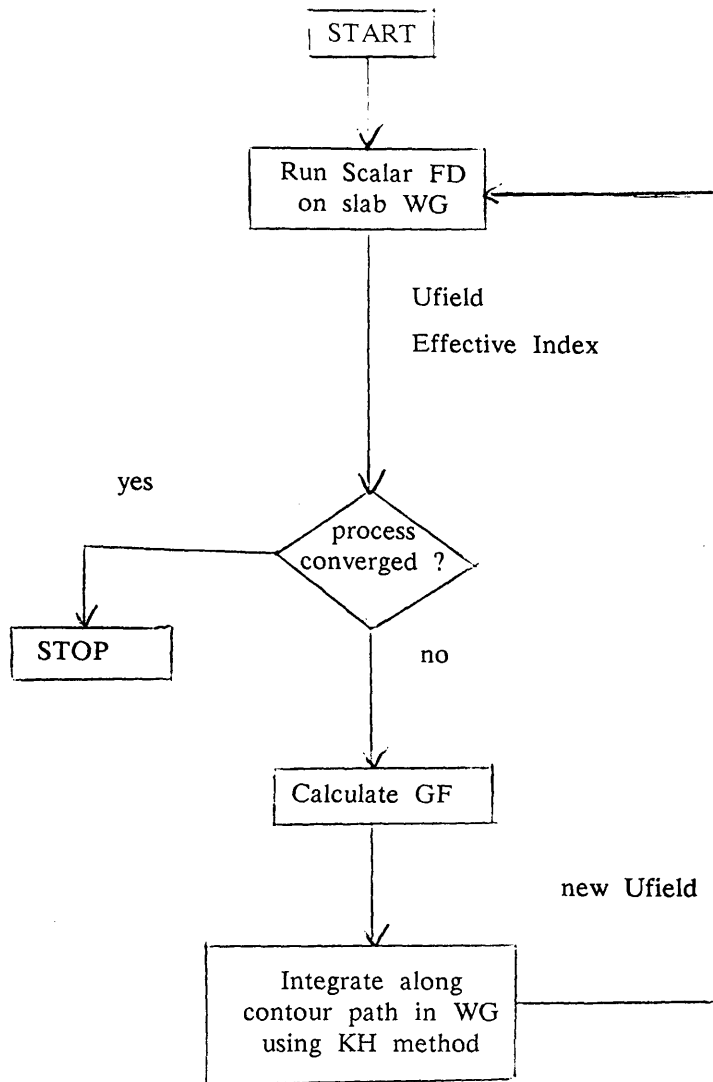


Figure 6.6 Kirchhoff–Huygens Line Integral Path



region. The paths within the contour are labelled 1 – 4. The final electric field after the KH integral shows that the KH method does indeed give an approximation to the electric field around the contour. This is particularly true for the contour paths 2 and 4 where the contour path is vertical with the absence of dielectric boundaries. However the electric field in paths 1 and 3 is poorly represented. This is possibly due to the fact that the effective index chosen for the GF's is when the source point is placed in the centre of the guiding layer. For these contour paths, the source point is very close to the dielectric boundary and the effective index of such a situation is different. This conclusion is drawn from an investigation that was made when the effective index changed using the Rayleigh quotient (equation (3.7)) in the FD method for slab waveguides whenever the focal point of the electric field was displaced from the centre of the slab. As the GF programs assume a particular effective index for a source point located in the centre of the slab, it takes no account if the effective index changes when the position of the source point changes relative to the boundary. To solve this, we would be required to calculate the effective index everytime the source point is moved vertically for both components of the GF.

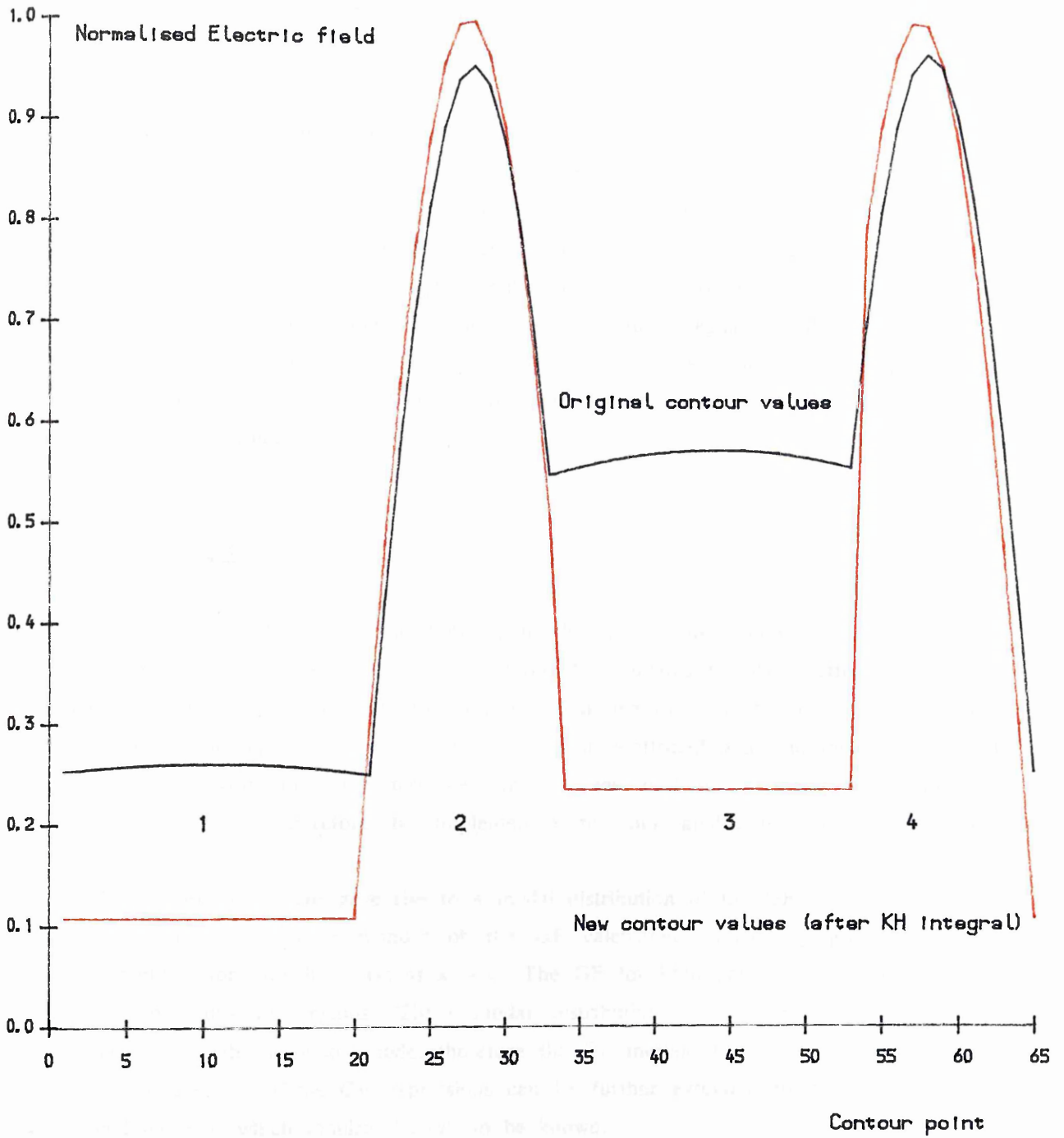


Figure 6.7 Plot of Contour Electric Field Using the KH Integral

6.6 RIB WAVEGUIDE RESULTS

The rib waveguide structure is difficult to manipulate due to the finite width of the rib in the lateral direction. As discussed earlier, approximate techniques are therefore implemented such as treating the structure as three separate slab modes as performed in the Effective Index Method (EIM). It would be possible to calculate the GF in this manner, but the inherent errors that arise from the EIM would be encountered.

The FD technique is useful since the electric field is well represented within the rib structure. The majority of the field is concentrated within the rib, therefore the contour path of the Kirchhoff–Huygens integral would enclose this part. However the GF for the rib is difficult to determine, therefore the GF for a slab waveguide of the same depth as the rib and layer could be used. The result is therefore expected to converge by the iterative method (section 6.4.3). The effective index calculated by the FD program would be used in the calculation of the GF.

6.7 CONCLUSIONS

Determining the GF for a source point located in the guiding region of a three layered slab waveguide has resulted in a method of calculating the exact effective index of propagation and the corresponding modal distribution due to a point source located in the guiding layer. The results of this method have been confirmed with the method described in chapter 2. With this basic test we can conclude that the GF has been correctly determined and can therefore be implemented for our analytical study of the slab waveguide.

The poles of the GF gave rise to a modal distribution of the GF, $g_m(x,y)$, which is the more dominant. The remainder of the GF calculated numerically gives rise to a smaller contribution, which decays as $x \rightarrow \infty$. The GF for both parts decays rapidly in the cladding and substrate regions. These modal distributions are consistent with what is expected for a slab waveguide mode, therefore the GF method has given us many answers about mode profiles. These GF expressions can be further extended to be used for other analytical methods which require the GF to be known.

Discretising the KH integral has led to a simple matrix calculation which can easily be applied to the contour chosen in the structure. Thus the problem has continually been simplified without the loss of the analytical technique. It is expected that the electric field calculated using the Kirchhoff–Huygens line integral will converge on the vertical paths 2 and 4 using the iterative loop, but not for the horizontal paths. Possible solutions to this problem would be to calculate the effective index for different values of source point (i.e. the y' coordinate of the source point) or by choosing a horizontal path that is relatively distant to any horizontal dielectric interfaces.

7.1 WAVEGUIDE STUDY

Our initial investigations of dielectric slab waveguides using Maxwell's equations led us to the determination of the effective index of wave propagation for various structures. As this theory was established as being exact, we have based further numerical study on this. Because the ridge waveguide structure could not be analysed analytically, approximate techniques were implemented.

The EIM proved simple to implement for the ridge structure. However it was accurate if the rib height was small compared to the slab height. If the rib was higher, the result tended to be higher than other methods. Because of this nature, the EIM has been regarded as an upper limit for the effective index⁷.

The FD method has proved very simple and versatile to implement on the ridge waveguide. This is primarily due to the fact that a rectangular mesh is used, and that the FD approximation is easily applicable to the scalar Helmholtz wave equation. The mesh spacing and box size could be chosen very easily. However a difficulty arose since the solution of the fields at a corner dielectric boundary is a singularity, which cannot be accurately modelled by any known technique. The error involved in the FD method is $(\Delta x)^2$, so it was anticipated that this error could be reduced by choosing a smaller mesh. However this results in increased computer time.

Investigations were also made into the size of the enclosing box which surrounded the waveguide structure. As the FD program set the electric field to zero at the box boundary, a smaller box around a waveguide structure resulted in a poor representation of the mode profile, thus an incorrect estimate of the effective index. A larger box would include the decay of the electric field as we moved away from the centre of the structure. Again, because of more elements in the FD matrix, the penalty for this is computer time. Therefore it is important to consider the enclosing box dimensions for the FD method.

In order to save time, full advantage was used with the inclusion of an acceleration parameter to improve convergence, and of the vectorial array processing facility on the mainframe computer, which decreased the time spent running the FD program considerably.

7.2 GREEN'S FUNCTION STUDY

The theory of Green's functions was investigated with the determination of the GF for three different situations. For the free space situation the GF proved to have singularity at the source point and decayed exponentially radially. The GF was also

proved to be continuous across the source point according to boundary condition stated in equation (4.23).

The GF for a point source located above a dielectric slab showed the rapid decay of the GF between the source point and the dielectric layer. This is due to the cause of destructive interference of the outgoing and incoming reflected waves. The decay is slower for the region above the source point.

The GF for the source point located inside the guiding layer proved to have poles at particular frequencies as discussed by Marcuvitz/Felsen²⁷. The determination of this GF resulted in a transcendental equation, which when solved, determined the effective index of propagation for the slab waveguide. This method proved to be as accurate as the exact method using Maxwell's equations, thus confirming that the GF calculated was correct.

As a final check, the GF's were implemented in the Kirchhoff– Huygens line integral method. Because of the omission of calculating the effective index for different point sources of the GF in the slab waveguide, the Kirchhoff– Huygens integral failed to converge at the horizontal dielectric boundaries. However the field is fairly well represented on the vertical paths of the contour.

7.3 IMPROVEMENTS AND FUTURE CONSIDERATIONS

The above investigation has led to the conclusion that the implementation of the Green's function for optical waveguides is feasible, and can be improved. This is particularly true as the Fourier method is advantageous because of the planar stratification of the waveguides, which reduces to the problem to an ordinary differential equation with one coordinate variable.

The problems were tackled using the scalar finite difference technique but full vectorial solutions of the GF are readily available and easy to implement^{21, 23}. This would ensure that both TE and TM polarisations could be investigated. Coupled to this, a vectorial solution of the FD method could be used, one which has been developed in the department³⁰ and by other authors³¹. Therefore, with more time, the simple numerical method of solving the field profile, Green's function and effective index value with the Kirchhoff– Huygens integral can be implemented using vectorial methods.

REFERENCES

1. Marcuvitz, N., "Waveguide Handbook", Peter Peregrinus, 1951.
1. Miller, S. E., "Integrated Optics: An Introduction.", Bell Syst. Tech. Journal, vol. 48, No. 7, pp2059–2070, 1969.
3. Adams, M. J., "Introduction to Optical Fibres", John Wiley & Sons, 1981.
4. Fleming, J. W., "Material Dispersion in Light-guide Glasses", Electronics Letters, vol. 14, pp328–362, 1978.
5. Kao, C. K., "Fibre Optics. Optical Fibre Communication Technology", Electr. Comm. (GB), vol. 54, No. 3, p245, 1979.
6. Marcatili, E. A. J., "Dielectric Rectangular Waveguide and Directional Coupler for Integrated Optics", Bell Syst. Tech. Journal, vol. 48, No. 7, pp2071–2102, 1969.
7. Chaing, K. S., "Dual Effective-index Method for the Analysis of Rectangular Dielectric Waveguides", Applied Optics, vol. 25, pp2169–2174, 1986.
8. Benson, T. M., Buus, J., "Optical guiding in III–V semiconductor rib structures.", IEE 2nd European Conf. on Integrated Optics, 17–18th October, pp17–20, 1983.
9. Fikioris, J. G., Tsalamengas, J. L., "Strongly and Uniformly Convergent Green's Functions Expansions", J. Franklin Inst., vol. 324, No. 1, pp1–17, 1987.
10. Pichot, Ch., "Exact Numerical Solution for the Diffused Channel Waveguide", Optics Communications, vol. 41, No. 3, pp169–173, 1982.
11. Kiang, J. F., Ali, S. M., Kong, J. A., "Integral Equation Solution to the Guidance and Leakage Properties of Coupled Dielectric Strip Waveguides", IEEE Trans. Microwave Theory and Techniques, vol. 38, No. 2, pp193–203, 1990.
12. Working Group I, COST 216, "Comparison of Different Modelling Techniques for Longitudinally Invariant Integrated Optical Waveguides.", IEE Proc. (J) Optoelectronics, vol. 136, No. 5, pp273–280, 1989.
13. Robertson, M.J., Ritchie, S., Dayan, P., "Semiconductor Waveguides: Analysis of

Optical Propagation in Single Rib Structures and Directional Couplers.", IEE Proc. (J) Optoelectronics, vol. 132, No. , pp336– 342, 1985.

14. Stern, M. S., "Semivectorial Polarised Finite Difference Method for Optical Waveguides with Arbitrary Index Profiles", IEE Proc. (J) Optoelectronics, vo. 135, No. 1, pp56– 63, 1988.

15. Stern, M. S., Kendall, P. C., McIlroy, P. W. A., "Analysis of the Spectral Index Method for Vector Modes of Rib Waveguides", IEE Proc. (J), Optoelectronics, vol. 137, No. 1, pp21– 26, 1990.

16. Vassallo, C., Wang, Y. H., "A New Semivigorous Analysis of Rib Waveguides", Journal of Lightwave Tech., vol.8, No. 1, pp56– 65, 1990.

17. Kogelnick, H, "Theory of Optical Waveguides", Chapter 2, in Tamir, T. (Ed.) "Guided– Wave Optoelectronics", Springer– Verlag, 1990.

18. Bhumbra, B. S., "Analysis of Nonlinear Waveguides in GaAs/AlGaAs", PhD Thesis, Glasgow University, 1990.

19. Morse, P.M., Feshbach, H., "Methods of Theoretical Physics", vol. I, McGraw Hill, 1953.

20. Pralong, M. L. M., "Evanescent Field Coupling Theory of a D– fibre", MScThesis, Glasgow University, 1989.

21. Stevenson, R. C., "Green's Function for the Helmholtz Equation of a Scalar Wave in an Anisotropic Halfspace", SIAM Journal Applied Math., vol. 50, No. 1, pp199– 215, 1990.

22. Spicopoulos, T., Teodoridis, V., Gardiol, F. E., "Dyadic Green's Function for the Electromagnetic Field in Multilayered Isotropic Media: An Operator Approach", Proc. Inst. Elec. Eng., vol. 132, pt H, No. 5, pp329– 334, 1985.

23. Kolk, E. W., Baken, H. G., Blok, H., "Domain Integral Equation Analysis of Integrated Optical Channel and Ridge Waveguides in Stratified Media", IEEE Trans. Micro. Theory Tech., vol 38, No. 1, pp77– 85, 1990.

24. Su, C. C., "A Simple Evaluation of some Principle Value Integrals for Dyadic Green's Functions Using Symmetry Property", IEEE Trans. Ant. Propgn., vol. 35, No. 11,

pp1306–1307, 1987.

25. NAG Fortran Library Manual, Mark 12, vol. 1, pp contents–D025, 1987
26. Ramo, S., van Duzer, T., Whinnery, J. R., "Fields and Waves in Communication Electronics", Wiley, 1984.
27. Felsen, L. B., Marcuvitz, N., "Radiation and Scattering of Waves", Prentice Hall, 1973.
28. Kreysig, E., "Advanced Engineering Mathematics", John Wiley & Sons, 1972.
29. Arfken, G., "Mathematical Methods for Physicists", Academic Press, 1985.
30. Taylor, M. R. S., Dept. of Electronics, Glasgow University, Private communication.
31. Stern, M. S., "Semivectorial Polarised H Field Solutions for Dielectric Waveguides with Arbitrary Index Profiles", IEE Proc. (J) Optoelectronics, vol. 135, No. 5, pp333–336, 1988.
32. Smith, G. D., "Numerical Solution of Partial Differential Equations: Finite Difference Methods", Clarendon Press, 1978.
33. Bracewell, R., "The Fourier Transform and its Applications", McGraw Hill, 1986.

APPENDIX A Transcendental Equation Program

PROGRAM TRANSCENDENTAL

C This program will calculate the root of the transcendental
C equation (2.48) for TE polarisation. The value is calculated
C using progressively smaller error EPS as used by the NAG
C routine C05AJF.

COMMON/WORK/ D, K0, N1, N2, N3, PI, Q

DOUBLE PRECISION B, NE, K0, KQ, PI
DOUBLE PRECISION D, LAMBDA, N1, N2, N3
DOUBLE PRECISION EPS, ETA
INTEGER IFAIL, K, NFMAX, Q
EXTERNAL TENE

WRITE(6,*) 'Input the depth of the slab (um)'
READ (5,*) D
WRITE(6,*) 'Enter N1, N2, N3'
READ (5,*) N1, N2, N3
WRITE(6,*) 'Input the operating wavelength (um)'
READ (5,*) LAMBDA
WRITE(6,*) 'Input the mode number q'
READ (5,*) Q

D = D * 1D-6
LAMBDA = LAMBDA * 1D-6
PI = 4*ATAN(1.0D0)
K0 = 2.0D0*PI/LAMBDA

C This part will find the root (or eigenvalue ne).

DO 10 K = 1, 10
 EPS = 10.0D0**(-K)
 NE = N3 + 0.01D0
 ETA = 0.0D0
 NFMAX = 500
 IFAIL = 0
 CALL C05AJF (NE, EPS, ETA, TENE, NFMAX, IFAIL)
 B = (NE**2 - N3**2)/(N2**2 - N3**2)
 WRITE(6,97) 'Ne = ', NE, 'b = ', B

10 CONTINUE

97 FORMAT(A6, F15.9, A6, F10.4)

STOP
END

REAL FUNCTION TENE(NE)

C This function calculates the value of the transcendental eqn.
C for a given value of the effective index (Ne). The eqn is
C

$$\text{PHI1} + \text{PHI2} + 2 * \text{ETA}^2 * \text{D} = (2q) * \text{PI}.$$

C

COMMON/WORK/ D, K0, N1, N2, N3, PI, Q

DOUBLE PRECISION BETA, KX, K0, NE, PI, PHI1, PHI2
DOUBLE PRECISION D, LAMBDA, N1, N2, N3
DOUBLE PRECISION ETA1, ETA2, ETA3
INTEGER Q

KX = 0.0D0

CALL ETA_KAPPA (NE, KX, ETA1, ETA2, ETA3)

PHI1 = 2.0D0 * ATAN(ETA2/ETA1)

PHI2 = 2.0D0 * ATAN(ETA2/ETA3)

TENE = -PHI1 -PHI2 + 2.0D0*ETA2*D - 2*DFLOAT(Q)*PI

END

SUBROUTINE ETA_KAPPA (NE, KX, ETA1, ETA2, ETA3)

COMMON/WORK/ D, K0, N1, N2, N3, PI, Q

DOUBLE PRECISION BETA, K0, KX, NE, N1, N2, N3
DOUBLE PRECISION KAPPA1, KAPPA2, KAPPA3
DOUBLE PRECISION ETA1, ETA2, ETA3
DOUBLE PRECISION D, PI
INTEGER Q

BETA = NE*K0

KAPPA1 = (N1 * K0)**2 - BETA**2

KAPPA2 = (N2 * K0)**2 - BETA**2

KAPPA3 = (N3 * K0)**2 - BETA**2

C N2 > Ne > N3 > N1 Situation.

ETA1 = DSQRT(KX**2 - KAPPA1)

ETA2 = DSQRT(KAPPA2 - KX**2)

ETA3 = DSQRT(KX**2 - KAPPA3)

END

NE2 = SIMING, NO, NS, NS, A, Q, ID, LAMBDA, PI

THE PART OF STRUCTURE

NE2 = SIMING, NO, NS, NS, D, A, ID, LAMBDA, PI

THE PART OF STRUCTURE

APPENDIX B Effective Index Method Program

PROGRAM RIB_EIM

C This program calculates the effective index of a rib waveguide
 C using the Effective Index Method of slab guides. The variable
 C used are

C A Height of rib (in microns).
 C D Depth of slab (in microns).
 C W Width of rib (in microns).
 C NC Refractive index of the cladding.
 C NG Refractive index of the guiding layer.
 C NS Refractive index of the substrate layer.
 C NE1 Effective index value of rib.
 C NE2 Effective index value of slab.
 C NE Effective index value of mode.
 C LAMBDA Operating wavelength.
 C EIM Subroutine to calculate the effective index
 C of a given slab structure.
 C FNEFF Subroutine to calculate the transcendental eqn.

DOUBLE PRECISION A, D, W, LAMBDA
 DOUBLE PRECISION NC, NG, NS, NE1, NE2, NE
 EXTERNAL EIM, FNEFF

WRITE(6,*) 'Type in the height of the rib (um)'
 READ (5,*) A
 WRITE(6,*) 'Type in the height of the guiding layer (um)'
 READ (5,*) D
 WRITE(6,*) 'Type in the width of the rib'
 READ (5,*) W
 WRITE(6,*) 'Type in N1, N2, N3'
 READ (5,*) NC, NG, NS
 WRITE(6,*) 'Type in the operating wavelength (um)'
 READ (5,*) LAMBDA

LAMBDA = LAMBDA * 1D-6
 A = A * 1D-6
 D = D * 1D-6
 W = W * 1D-6

C THICK PART OF STRUCTURE

NE1 = EIM(NC, NG, NS, NS, A, 0.0D0, LAMBDA, 'TE', 0)

C THIN PART OF STRUCTURE

NE2 = EIM(NC, NG, NS, NS, D, 0.0D0, LAMBDA, 'TE', 0)

C TOP PART OF STRUCTURE

NE = EIM(NE2, NE1, NE2, NE2, W, 0.0D0, LAMBDA, 'TE', 0)

WRITE(6,97) 'NE1 =', NE1

```

WRITE(6,97) 'NE2 =', NE2
WRITE(6,98) 'Effective index of structure = ', NE
WRITE(6,99) 'Normalised index b = ', (NE**2 - NS**2)/(NG**2-NS
97 FORMAT(A6,F15.9)
98 FORMAT(A32,F15.9)
99 FORMAT(A22,F15.9)

```

```

STOP
END

```

```

DOUBLE PRECISION FUNCTION EIM (N1, N2, N3, N4, D2, D3, LAMBDA,
1 POLRSN, MODE)

```

```

C This program calculates the effective index for a 4 layer prob
C using the effective index method. For the 3 layer, let N3=N4 a
C D3 = 0.0.

```

```

COMMON/WORK/ K0, PI, ETA1, ETA2, ETA3, ETA4

```

```

DOUBLE PRECISION N1, N2, N3, N4, FERROR, LAMBDA, D2, D3
DOUBLE PRECISION K0, PI, ETA1, ETA2, ETA3, ETA4
DOUBLE PRECISION NEFFMIN, NEFFMID, NEFFMAX, FMIN, FMID, FMAX
INTEGER MODE
CHARACTER*2 POLRSN

```

```

PI = 4*DATAN(1.0D0)
K0 = 2.0D0 * PI / LAMBDA
FERROR = 1D-7

```

```

IF (POLRSN .EQ. 'TM') THEN
  ETA1 = 1.0D0/N1**2
  ETA2 = 1.0D0/N2**2
  ETA3 = 1.0D0/N3**2
  ETA4 = 1.0D0/N4**2

```

```

ELSE
  ETA1 = 1.0D0
  ETA2 = 1.0D0
  ETA3 = 1.0D0
  ETA4 = 1.0D0

```

```

ENDIF

```

```

WRITE(6,*) 'Calculating ...'

```

```

IF (N1 .GT. N3) THEN
  NEFFMIN = N1 + 1D-10

```

```

ELSE
  NEFFMIN = N3 + 1D-10

```

```

ENDIF

```

```

NEFFMAX = N2 - 1D-10
FMAX = FNEFF(NEFFMAX, N1, N2, N3, N4, D2, D3, MODE)
FMIN = FNEFF(NEFFMIN, N1, N2, N3, N4, D2, D3, MODE)

```

```

IF (((FMAX .GT. 0.0D0) .AND. (FMIN .GT. 0.0D0)) .OR.
1 ((FMAX .LT. 0.0D0) .AND. (FMIN .LT. 0.0D0))) THEN

```

```

  WRITE(6,*) 'Mode not propagating'
  EIM = 1.0D0
  GOTO 300

```

```

ENDIF

```

```

100  NEFFMID = (NEFFMAX + NEFFMIN)/2.0D0

      FMAX   = FNEFF(NEFFMAX, N1, N2, N3, N4, D2, D3, MODE)
      FMID   = FNEFF(NEFFMID, N1, N2, N3, N4, D2, D3, MODE)
      FMIN   = FNEFF(NEFFMIN, N1, N2, N3, N4, D2, D3, MODE)

      IF (FMID .GT. 0.0D0) THEN
          NEFFMIN = NEFFMID
      ENDIF

      IF (FMID .LT. 0.0D0) THEN
          NEFFMAX = NEFFMID
      ENDIF

      IF (ABS(NEFFMAX - NEFFMIN) .LT. FERROR) GOTO 200

      GOTO 100

200  EIM = NEFFMID

300  END

      DOUBLE PRECISION FUNCTION FNEFF(NEFF, N1, N2, N3, N4, D2, D3,
1      MODE)

      COMMON/WORK/ K0, PI, ETA1, ETA2, ETA3, ETA4

      DOUBLE PRECISION NEFF, N1, N2, N3, N4, D2, D3
      DOUBLE PRECISION K0, PI, ETA1, ETA2, ETA3, ETA4
      DOUBLE PRECISION K1, K2, K3, K4, S1, S2, S3, S4
      INTEGER MODE

      K1 = K0*DSQRT(NEFF**2 - N1**2)
      K2 = K0*DSQRT(N2**2 - NEFF**2)
      K3 = K0*DSQRT(NEFF**2 - N3**2)
      K4 = K0*DSQRT(NEFF**2 - N4**2)
      S3 = DEXP(K3*D3) * (ETA3*K3 + ETA4*K4)
      S4 = DEXP(-K3*D3) * (ETA3*K3 - ETA4*K4)
      S1 = ETA3*K3 * (S3-S4)
      S2 = ETA2*K2 * (S3+S4)
      S2 = S1/S2
      S1 = ETA1*K1 / (ETA2*K2)
      FNEFF = K2*D2 - DATAN(S1) - DATAN(S2) - DFLOAT(MODE) * PI

      END

```


C Calculation constants:
 REAL H1, H2, WIDTH, N1, N2, N3
 REAL MESHSIZE, XDIM, YDIM, EPEAK
 DOUBLE PRECISION CONSTANT1, CONSTANT2
 DOUBLE PRECISION LAMBDA, PI, NEFF

C Counters:

INTEGER COUNTER1, COUNTER2, COUNTER3
 INTEGER COORD1, COORD2

LOGICAL CONV
 CHARACTER*1 MODE

PI = 4*ATAN(1.0D0)

WRITE(6,*) ' Input height of the rib'
 READ(5,*) H1
 WRITE(6,*) ' Input height of layer'
 READ(5,*) H2
 WRITE(6,*) ' Input width of waveguide'
 READ(5,*) WIDTH
 WRITE(6,*) ' Input refractive index of guide'
 READ(5,*) N1
 WRITE(6,*) ' Input refractive index of substrate'
 READ(5,*) N2
 WRITE(6,*) ' Input refractive index of air'
 READ(5,*) N3
 WRITE(6,*) ' Input mesh spacings in microns (0.1, 0.05, 0.01)'
 READ(5,*) MESHSIZE
 WRITE(6,*) ' Input box dimensions (in microns)'
 READ(5,*) XDIM, YDIM
 WRITE(6,*) ' Input effective index estimate'
 READ(5,*) NEFF
 WRITE(6,*) ' Input wavelength in microns'
 READ(5,*) LAMBDA
 WRITE(6,*) ' Fundamental (F) or 1st order (1) mode ?'
 READ(5,97) MODE
 97 FORMAT (A1)

CONSTANT2 = NEFF**2
 CONSTANT1 = (MESHSIZE*2*PI/LAMBDA)**2

CALL FILLMATX (H1, H2, WIDTH, N1, N2, N3, MODE)

C Calculate the start and end values of the matrix in which
 C the mesh box is to be used.

XSTART = 250 - XDIM/(2*MESHSIZE) + 0.1
 XEND = 250 + XDIM/(2*MESHSIZE) + 0.1
 YSTART = 250 - YDIM/(2*MESHSIZE) + 0.1
 YEND = 250 + YDIM/(2*MESHSIZE) + 0.1

IF (MODE .EQ. '1') THEN
 XSTART = 250
 ENDIF

WRITE(6,*) 'XSTART =', XSTART, ' XEND =', XEND
 WRITE(6,*) 'YSTART =', YSTART, ' YEND =', YEND
 WRITE(6,*) 'ARRAY SIZE IS', XEND-XSTART, YEND-YSTART

```

DO 320 COUNTER1 = 1,5
  WRITE(6,*) 'FIRST LOOP COUNTER =', COUNTER1
  CALL RELAX(1.0,XSTART,XEND,1,YSTART,YEND,1)
  CALL RELAX(1.0,XSTART,XEND,1,YEND,YSTART,-1)
  CALL RELAX(1.0,XEND,XSTART,-1,YEND,YSTART,-1)
  CALL RELAX(1.0,XEND,XSTART,-1,YSTART,YEND,1)
320 CONTINUE

C Iterate with relaxation factor of 1.600 until there is no
C significant change in the ratio of the two fields

COUNTER1 = 1

DO 250 COUNTER2 = 1,20
  WRITE(6,*) 'SECOND LOOP COUNTER =', COUNTER2
  CALL INDEXFIND(XSTART, XEND, YSTART, YEND)

  DO 250 COUNTER1 = 0,2
    CALL RELAX(1.600,XSTART,XEND,1,YSTART,YEND,1)
    CALL RELAX(1.600,XSTART,XEND,1,YEND,YSTART,-1)
    CALL RELAX(1.600,XEND,XSTART,-1,YEND,YSTART,-1)
    CALL RELAX(1.600,XEND,XSTART,-1,YSTART,YEND,1)
250 CONTINUE

C Iterate with a relaxation factor of 1 to smooth result and
C calculate final value of effective index.

COUNTER1 = 1

DO 280 COUNTER3 = 1,20
  WRITE(6,*) 'THIRD LOOP COUNTER =', COUNTER3
  CALL INDEXFIND(XSTART, XEND, YSTART, YEND)

  DO 280 COUNTER1 = 0,4
    CALL RELAX(1.0,XSTART,XEND,1,YSTART,YEND,1)
    CALL RELAX(1.0,XSTART,XEND,1,YEND,YSTART,-1)
    CALL RELAX(1.0,XEND,XSTART,-1,YEND,YSTART,-1)
    CALL RELAX(1.0,XEND,XSTART,-1,YSTART,YEND,1)
280 CONTINUE

CALL INDEXFIND(XSTART, XEND, YSTART, YEND)

WRITE(6,1) 'b =', (CONSTANT2 - N2**2)/(N1**2 - N2**2)
1 FORMAT (A4, F8.4)

EPEAK = PEAKFIND(EFIELD, XSTART, XEND, YSTART, YEND,COORD1,COORD2)
WRITE(6,*) 'EPEAK IS', EPEAK, 'AT', COORD1, COORD2

CALL PLOT (EFIELD, XSTART, XEND, YSTART, YEND, MESH SIZE, EPEAK)

STOP
END

C ***** SUBROUTINES *****
C Subroutine to fill matrices.

SUBROUTINE FILLMATX (H1, H2, WIDTH, N1, N2, N3, MODE)

COMMON/WORK1/ EPSILON(0:500,0:500), CONV, MESH SIZE

```

COMMON/WORK2/ EFIELD (0:500,0:500), CONSTANT1, CONSTANT2

INTEGER X,Y, CENTRE, IOFFSET
REAL EPSILON, H1, H2, WIDTH, MESHSIZE, N1, N2, N3
REAL LENGTH, HEIGHT, OFFSET
DOUBLE PRECISION EFIELD, CONSTANT1, CONSTANT2, PI
LOGICAL CONV
CHARACTER*1 MODE

C Fill refractive index matrix and zero field matrices.

PI = 4*ATAN(1.0D0)

DO 10 X = 0,500
DO 15 Y = 0,250
EPSILON(X,Y) = N3**2
EFIELD(X,Y) = 0.0D0
15 CONTINUE

DO 20 Y = 251, (250 + H2/MESHSIZE) + 0.1
EPSILON(X,Y) = N1**2
EFIELD(X,Y) = 0.0D0
20 CONTINUE

DO 10 Y = (251+H2/MESHSIZE) + 0.1, 500
EPSILON(X,Y) = N2**2
EFIELD(X,Y) = 0.0D0
10 CONTINUE

DO 30 X = 250-WIDTH/(2*MESHSIZE) + 0.1, 249+WIDTH/(2*MESHSIZE)+0.1
DO 30 Y = 251-H1/MESHSIZE + 0.1, 250
EPSILON(X,Y) = N1**2
EFIELD(X,Y) = 0.0D0
30 CONTINUE

LENGTH = WIDTH/MESHSIZE
HEIGHT = (H1 + H2)/MESHSIZE

X1 = 250 - WIDTH/(2*MESHSIZE) - 0.9
Y1 = 250 - H1/MESHSIZE + 0.1

WRITE(6,*)'Input offset for the FIELD'
READ(5,*) OFFSET

IOFFSET = OFFSET/MESHSIZE + 0.1
IOFFSET = 250 + H2/MESHSIZE + 0.1 - IOFFSET
CENTRE = HEIGHT/2 + 1.1
CENTRE = 250 - H1/MESHSIZE + 0.1 + CENTRE
IOFFSET = IOFFSET - CENTRE

WRITE(6,*)'CENTRE',CENTRE,'IOFFSET',IOFFSET

IF (MODE .EQ. 'F') THEN
DO 40 X = 250-WIDTH/(2*MESHSIZE) + 0.1, 249+WIDTH/(2*MESHSIZE)+0.1
DO 40 Y = 251-H1/MESHSIZE + 0.1, 250+H2/MESHSIZE + 0.1
EFIELD(X,Y+IOFFSET) = SIN(PI*(Y-Y1)/HEIGHT)*SIN(PI*(X-X1)/LENGTH)
40 CONTINUE

ELSE

```

C      DO 41 X = 249, 249+WIDTH/(2*MESH SIZE)+0.1
C      DO 41 Y = 251-H1/MESH SIZE + 0.1, 250+H2/MESH SIZE + 0.1
C      EFIELD(X,Y+IOFFSET) = SIN(PI*(Y-Y1)/HEIGHT)*SIN(PI*(X-X1)/LENGTH
      EFIELD(253, 250) = 1.0D0
C1     CONTINUE
      ENDIF

      RETURN
      END

```

C Subroutine to perform relaxation on E-field.

```

SUBROUTINE RELAX(RFACTOR, XSTART, XEND, XINC, YSTART, YEND, YINC)

```

```

COMMON/WORK1/ EPSILON(0:500,0:500), CONV, MESH SIZE
COMMON/WORK2/ EFIELD(0:500, 0:500), CONSTANT1, CONSTANT2

```

```

INTEGER X, Y, XSTART, XEND, XINC, YSTART, YEND, YINC
REAL EPSILON
DOUBLE PRECISION EFIELD, CONSTANT1, CONSTANT2
REAL RFACTOR, UFACTOR
LOGICAL CONV

```

```

UFACTOR = RFACTOR - 1

```

C Main iteration routine.

```

DO 10 Y = YSTART, YEND, YINC
  DO 20 X = XSTART, XEND, XINC

```

```

    EFIELD(X,Y) = RFACTOR*(EFIELD(X+1,Y) + EFIELD(X-1,Y) +
1      EFIELD(X,Y+1) + EFIELD(X,Y-1) ) /
1 (4 - CONSTANT1*(EPSILON(X,Y) - CONSTANT2))
1 - UFACTOR * EFIELD(X,Y)

```

```

    IF (EFIELD(X,Y) .LT. 0.1D-20) THEN
      EFIELD(X,Y) = 0.0D0

```

```

    ENDIF
20  CONTINUE

```

```

10  CONTINUE

```

```

      RETURN
      END

```

C Subroutine to update effective index.

```

SUBROUTINE INDEXFIND (XSTART, XEND, YSTART, YEND)

```

```

COMMON/WORK1/ EPSILON(0:500,0:500), CONV, MESH SIZE
COMMON/WORK2/ EFIELD(0:500,0:500), CONSTANT1, CONSTANT2

```

```

INTEGER X, Y, XSTART, XEND, YSTART, YEND
REAL EPSILON, MESH SIZE
DOUBLE PRECISION EFIELD, CONSTANT1, CONSTANT2
DOUBLE PRECISION TOPSUM, BOTSUM, CONST
LOGICAL CONV

```

```
TOPSUM = 0.0D0
BOTSUM = 0.0D0
CONV = .FALSE.
```

C Sum the upper and lower functions

```
DO 10 Y = YSTART, YEND
  DO 10 X = XSTART, XEND
```

```
    TOPSUM = TOPSUM + EFIELD(X,Y) * (EFIELD(X+1,Y) + EFIELD(X-1,Y)
1    + EFIELD(X,Y+1) + EFIELD(X,Y-1) - 4 * EFIELD(X,Y)
1    + EFIELD(X,Y) * EPSILON(X,Y) * CONSTANT1)
    BOTSUM = BOTSUM + EFIELD(X,Y) * EFIELD(X,Y)
```

10 CONTINUE

C Recalculate the effective index

```
CONST = TOPSUM / (BOTSUM*CONSTANT1)
```

C IF ((CONST - CONSTANT2)/CONST .LT. 0.01D0) THEN

C CONV = .TRUE.

C ENDDIF

```
CONSTANT2 = CONST
```

```
WRITE(6,98) ' Effective index =', SQRT(CONSTANT2)
```

98 FORMAT(A20, F15.8)

```
RETURN
```

```
END
```

C Subroutine to find the maximum field value.

```
REAL FUNCTION PEAKFIND (FIELD, XSTART, XEND, YSTART, YEND, COORD1,
1 COORD2)
```

```
DOUBLE PRECISION FIELD (0:500, 0:500)
```

```
INTEGER XSTART, XEND, YSTART, YEND, X, Y, COORD1, COORD2
```

```
PEAKFIND = 0.1E-50
```

```
DO 10 X = XSTART, XEND
```

```
  DO 10 Y = YSTART, YEND
```

```
    IF ( FIELD(X,Y) .GT. PEAKFIND ) THEN
```

```
      PEAKFIND = FIELD(X,Y)
```

```
      COORD1 = X
```

```
      COORD2 = Y
```

```
    ENDDIF
```

10 CONTINUE

```
RETURN
```

```
END
```

C Subroutine to print the EFIELD values.

```
SUBROUTINE PLOT (FIELD, XSTART, XEND, YSTART, YEND, MESH SIZE,
1 EPEAK)
```

```
DOUBLE PRECISION FIELD (0:500, 0:500)
```

```
INTEGER XSTART, XEND, YSTART, YEND, X, Y
```

```
REAL MESH SIZE, EPEAK
```

OPEN(2,FILE='/FIELD UMPDATA', FORM='FORMATTED')

DO 10 X = XSTART, XEND

DO 10 Y = YSTART, YEND

'WRITE (2,99) (X-250)*MESH SIZE, (250-Y)*MESH SIZE, FIELD(X,Y)

1 / EPEAK

10 CONTINUE

99 FORMAT(2F10.2, F20.8)

RETURN

END

APPENDIX D Finite Difference Approximation

D1. Finite Difference Approximation to Derivatives

When a function $u = u(x)$ and its derivatives are single-valued, finite and continuous functions of x , then expanding u about the points $(x+h)$ and $(x-h)$ via Taylor's theorem

$$u(x+h) = u(x) + hu'(x) + \frac{1}{2}h^2u''(x) + \frac{1}{6}h^3u'''(x) + \dots \quad (D1)$$

and

$$u(x-h) = u(x) - hu'(x) + \frac{1}{2}h^2u''(x) - \frac{1}{6}h^3u'''(x) + \dots \quad (D2)$$

Addition of these expansions gives

$$u(x+h) + u(x-h) = 2u(x) + h^2u''(x) + O(h^4)$$

where $O(h^4)$ denotes terms containing fourth and higher order powers of h . Assuming these are negligible in comparison with lower powers of h it follows that

$$u''(x) = \left[\frac{\partial^2 u}{\partial x^2} \right] = \frac{1}{h^2} \left[u(x+h) + u(x-h) - 2u \right] \quad (D3)$$

with a leading error on the right hand side of h^2 .

Subtracting equation (D2) from (D1) and neglecting h^3 terms

$$u(x+h) - u(x-h) = 2hu'(x)$$

i.e.

$$u'(x) = \left[\frac{\partial u}{\partial x} \right] = \frac{1}{2h} \left[u(x+h) - u(x-h) \right] \quad (D4)$$

with a leading error of order h^2 . Equation (D4) approximates the slope of the tangent at P (figure D.1) by the slope of the chord AB. This is known as the *central-difference* approximation. We can also approximate the slope of the tangent at P by either the slope of the chord PB, giving the *forward-difference* formula

$$u'(x) \approx \frac{1}{h} \left[u(x+h) - u(x) \right] \quad (D5)$$

or the slope of the chord AP giving the *backward-difference* formula

$$u'(x) = \frac{1}{h} \left[u(x) - u(x-h) \right] \quad (D6)$$

D2. Finite Difference Notation For Two Variables

Assume u is a function of the independent variables x and y i.e. $u = u(x,y)$. Subdivide

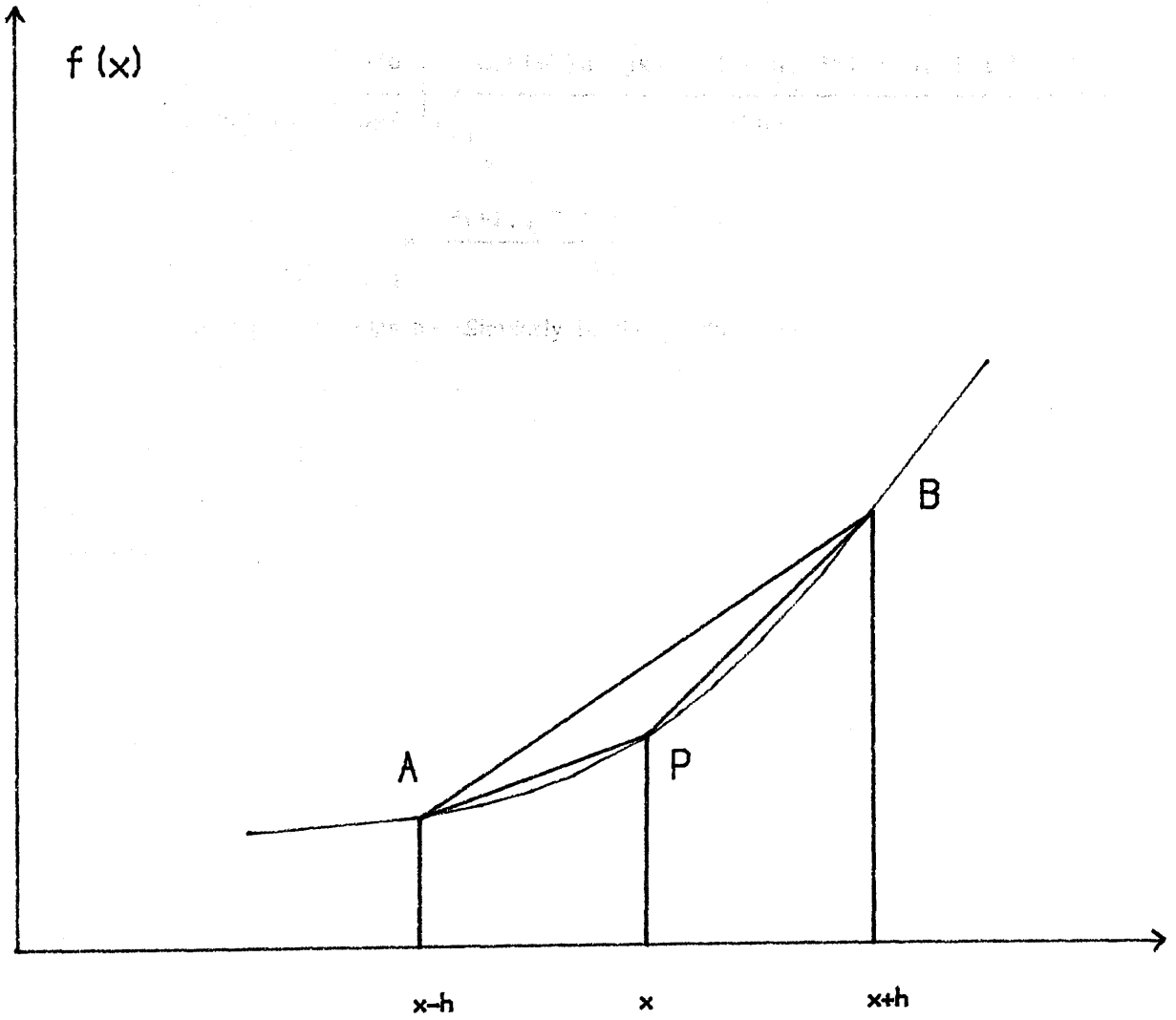


Figure D.1. FD Approximation of the Tangent of a Curve

the x - y plane into a grid with sides $\delta x = h$, $\delta y = k$ as shown in figure D.2. Let the coordinates (x,y) of the representative mesh point P be

$$x = ih; \quad y = jk$$

where i and j are integers. Denote the value of u at P by

$$u_P = u(ih, jk) = u_{i,j}$$

Then by equation (D3)

$$\left[\frac{\partial^2 u}{\partial x^2} \right]_P = \left[\frac{\partial^2 u}{\partial x^2} \right]_{i,j} \approx \frac{u((i+1)h, jk) - 2u(ih, jk) + u((i-1)h, jk)}{h^2}$$

i.e.

$$\left[\frac{\partial^2 u}{\partial x^2} \right]_{i,j} \approx \frac{u_{i+1,j} - 2u_{i,j} + u_{i-1,j}}{h^2} \tag{D7}$$

with a leading error of order h^2 . Similarly in the y -direction

$$\left[\frac{\partial^2 u}{\partial y^2} \right]_{i,j} \approx \frac{u_{i,j+1} - 2u_{i,j} + u_{i,j-1}}{k^2} \tag{D8}$$

with a leading error of order k^2 . With this notation the forward difference approximation for $\partial u/\partial y$ at P is

$$\frac{\partial u}{\partial y} \approx \frac{u_{i,j+1} - u_{i,j}}{k} \tag{D9}$$

with a leading error of $O(k)$.

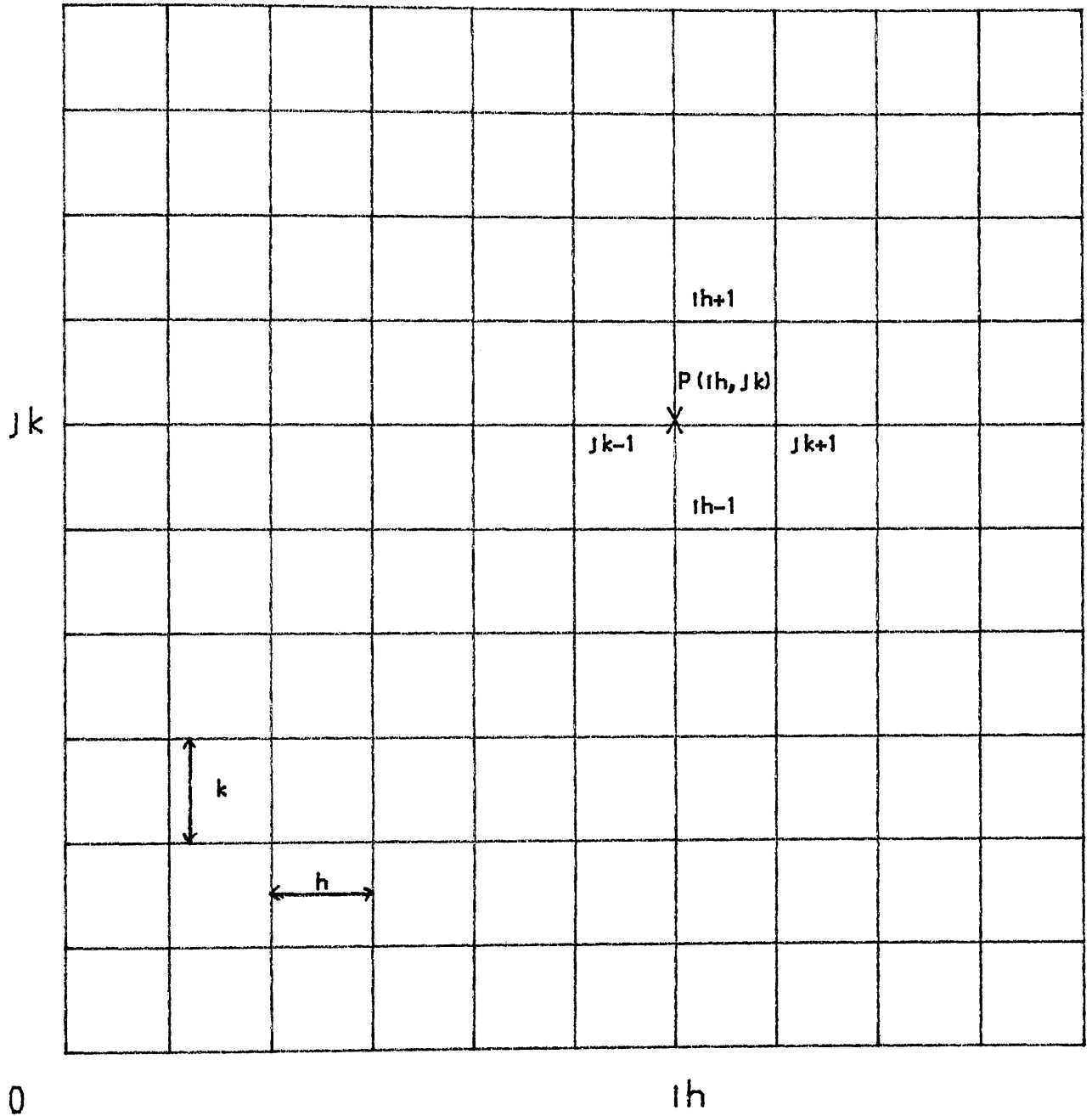


Figure D.2 Finite Difference Grid

E1. Iterative Method For Solving Large Linear Systems of Algebraic Equations

An iterative procedure can be implemented to solve a matrix given that the matrix is sparse and well-conditioned. Such an iterative procedure would be used if a direct method involved more computer memory than can be allowed. The iterative method for solving equations is one in which a first approximation is used to calculate a second approximation which in turn is used to calculate a third and so on. The iterative procedure is said to be convergent when the differences between the exact solution and the successive approximations tend to zero as the number of iterations increase. Consider the matrix equation below

$$Ax = B$$

i.e.

$$\begin{bmatrix} a_{11} & a_{12} & a_{13} & a_{14} \\ a_{21} & a_{22} & a_{23} & a_{24} \\ a_{31} & a_{32} & a_{33} & a_{34} \\ a_{41} & a_{42} & a_{43} & a_{44} \end{bmatrix} \begin{bmatrix} x_1 \\ x_2 \\ x_3 \\ x_4 \end{bmatrix} = \begin{bmatrix} b_1 \\ b_2 \\ b_3 \\ b_4 \end{bmatrix} \tag{E1}$$

Expanding this

$$\begin{aligned} a_{11}x_1 + a_{12}x_2 + a_{13}x_3 + a_{14}x_4 &= b_1 \\ a_{21}x_1 + a_{22}x_2 + a_{23}x_3 + a_{24}x_4 &= b_2 \\ a_{31}x_1 + a_{32}x_2 + a_{33}x_3 + a_{34}x_4 &= b_3 \\ a_{41}x_1 + a_{42}x_2 + a_{43}x_3 + a_{44}x_4 &= b_4 \end{aligned} \tag{E2}$$

Assuming $a_{ii} \neq 0$, these equations may be written as

$$\begin{aligned} x_1 &= \frac{1}{a_{11}} \left[b_1 - a_{12}x_2 - a_{13}x_3 - a_{14}x_4 \right] \\ x_2 &= \frac{1}{a_{22}} \left[b_2 - a_{21}x_1 - a_{23}x_3 - a_{24}x_4 \right] \\ x_3 &= \frac{1}{a_{33}} \left[b_3 - a_{31}x_1 - a_{32}x_2 - a_{34}x_4 \right] \\ x_4 &= \frac{1}{a_{44}} \left[b_4 - a_{41}x_1 - a_{42}x_2 - a_{43}x_3 \right] \end{aligned} \tag{E3}$$

E2. Gauss-Seidel Method

In this method the $(n+1)$ th iterative values are used as soon as they are available and the iteration corresponding to equations (E3) is defined by

$$\begin{aligned}
 x_1^{(n+1)} &= \frac{1}{a_{11}} \left[b_1 - a_{12}x_2^{(n)} - a_{13}x_3^{(n)} - a_{14}x_4^{(n)} \right] \\
 x_2^{(n+1)} &= \frac{1}{a_{22}} \left[b_2 - a_{21}x_1^{(n+1)} - a_{23}x_3^{(n)} - a_{24}x_4^{(n)} \right] \\
 x_3^{(n+1)} &= \frac{1}{a_{33}} \left[b_3 - a_{31}x_1^{(n+1)} - a_{32}x_2^{(n+1)} - a_{34}x_4^{(n)} \right] \\
 x_4^{(n+1)} &= \frac{1}{a_{44}} \left[b_4 - a_{41}x_1^{(n+1)} - a_{42}x_2^{(n+1)} - a_{43}x_3^{(n+1)} \right]
 \end{aligned} \tag{E4}$$

In the general case for m equations

$$x_i^{(n+1)} = \frac{1}{a_{ii}} \left[b_i - \sum_{j=1}^{i-1} a_{ij} x_j^{(n+1)} - \sum_{j=i+1}^m a_{ij} x_j^{(n)} \right] \tag{E5}$$

E3. Successive Over-Relaxation Method

If the Gauss-Seidel iteration equations are written as

$$\begin{aligned}
 x_1^{(n+1)} &= x_1^{(n)} + \frac{1}{a_{11}} \left[b_1 - a_{11}x_1^{(n)} - a_{12}x_2^{(n)} - a_{13}x_3^{(n)} - a_{14}x_4^{(n)} \right] \\
 x_2^{(n+1)} &= x_2^{(n)} + \frac{1}{a_{22}} \left[b_2 - a_{21}x_1^{(n+1)} - a_{22}x_2^{(n)} - a_{23}x_3^{(n)} - a_{24}x_4^{(n)} \right] \\
 x_3^{(n+1)} &= x_3^{(n)} + \frac{1}{a_{33}} \left[b_3 - a_{31}x_1^{(n+1)} - a_{32}x_2^{(n+1)} - a_{33}x_3^{(n)} \right. \\
 &\quad \left. - a_{34}x_4^{(n)} \right] \\
 x_4^{(n+1)} &= x_4^{(n)} + \frac{1}{a_{44}} \left[b_4 - a_{41}x_1^{(n+1)} - a_{42}x_2^{(n+1)} - a_{43}x_3^{(n+1)} \right. \\
 &\quad \left. - a_{44}x_4^{(n)} \right]
 \end{aligned} \tag{E6}$$

it is seen that the expressions in the square brackets are the corrections or changes made to $x_i^{(n)}$ by one Gauss-Seidel iteration. If successive corrections are all one-signed it would be reasonable to expect convergence to be accelerated if each equation of (E6) was given a larger correction term than is defined by equation (E6). This idea leads to the successive over-relaxation or SOR iteration which is defined by the equations

$$\begin{aligned}
x_1^{(n+1)} &= x_1^{(n)} + \frac{\omega}{a_{11}} \left[b_1 - a_{11}x_1^{(n)} - a_{12}x_2^{(n)} - a_{13}x_3^{(n)} - a_{14}x_4^{(n)} \right] \\
x_2^{(n+1)} &= x_2^{(n)} + \frac{\omega}{a_{22}} \left[b_2 - a_{21}x_1^{(n+1)} - a_{22}x_2^{(n)} - a_{23}x_3^{(n)} - a_{24}x_4^{(n)} \right] \\
x_3^{(n+1)} &= x_3^{(n)} + \frac{\omega}{a_{33}} \left[b_3 - a_{31}x_1^{(n+1)} - a_{32}x_2^{(n+1)} - a_{33}x_3^{(n)} - a_{34}x_4^{(n)} \right] \\
x_4^{(n+1)} &= x_4^{(n)} + \frac{\omega}{a_{44}} \left[b_4 - a_{41}x_1^{(n+1)} - a_{42}x_2^{(n+1)} - a_{43}x_3^{(n+1)} - a_{44}x_4^{(n)} \right] \quad (E7)
\end{aligned}$$

The factor ω is called the acceleration parameter or relaxation parameter. So for the general case for m equations the SOR iteration is defined by

$$x_i^{(n+1)} = x_i^{(n)} + \frac{\omega}{a_{ii}} \left[b_i - \sum_{j=1}^{i-1} a_{ij} x_j^{(n+1)} - \sum_{j=i+1}^m a_{ij} x_j^{(n)} \right] \quad (E8)$$

or rewriting as

$$\begin{aligned}
x_i^{(n+1)} &= \frac{\omega}{a_{ii}} \left[b_i - \sum_{j=1}^{i-1} a_{ij} x_j^{(n+1)} - \sum_{j=i+1}^m a_{ij} x_j^{(n)} \right] \\
&\quad - (\omega - 1)x_i^{(n)} \\
&= \omega \text{ (R.H.S. of Gauss-Seidel iteration equations)} \\
&\quad - (\omega - 1)x_i^{(n)} \quad (E9)
\end{aligned}$$

F1. Inverse Fourier Transform

The inverse Fourier transform of a function $F(k_x, y)$ is defined as

$$f(x, y) = \frac{1}{2\pi} \int_{-\infty}^{+\infty} F(k_x, y) e^{ik_x x} dk_x \tag{F1}$$

Rewriting this for a band-limited integral between the range $-Mk_0 < k_x < Mk_0$, where M is a real number and $k_0 = 2\pi/\lambda_0$ is the free space wave number,

$$f(x, y) = \frac{1}{2\pi} \int_{-Mk_0}^{Mk_0} F(k_x, y) e^{ik_x x} dk_x \tag{F2}$$

F2. Shift Property

Making the substitution $k' = k_x + Mk_0$, equation (F2) becomes

$$f(x, y) = \frac{1}{2\pi} \int_0^{2Mk_0} F(k_x, y) e^{ik'x} dk' e^{-iMk_0 x} \tag{F3}$$

Now let $k = 2\pi s$, $dk = 2\pi ds$, so

$$f(x, y) = \int_0^{4\pi Mk_0} F(2\pi s, y) e^{i2\pi s'x} ds' e^{-i2\pi Ms_0 x} \tag{F4}$$

or in discrete form [NAG notes]

$$f_j = \frac{T}{N} \sum_{k=0}^{N-1} F_k e^{ijk2\pi/N} e^{-i2\pi Ms_0 x} \quad j = 0, 1, \dots, N-1 \tag{F5}$$

for $f(x, y)$ in some finite range $(0, T)$ divided into N equal intervals. Now $x = j/4\pi Ms_0$, so equation (F5) reduces to the inverse discrete Fourier transform representation

$$f_j = \frac{T}{N} \sum_{k=0}^{N-1} F_k e^{ijk2\pi/N} e^{-ij/2} \quad j = 0, 1, \dots, N-1 \tag{F6}$$

Hence the inverse Fourier transform has to be post-multiplied by the factor $e^{-ij/2}$.

APPENDIX G Free Space Green's Function Program

PROGRAM GREEN

C PROGRAM TO COMPUTE THE GREEN'S FUNCTION FOR A FREE
C SPACE SITUATION.

REAL Y, YDASH
DOUBLE PRECISION AETA1, BETA, KX, K0, KAPPA1, LAMBDA, N1
1 NEFF, INC, M, PI

COMPLEX*16 ETA1, G

OPEN(1, FILE='/FREE OUTPUT', FORM='FORMATTED')

WRITE(6,*) 'Input source point coord (YDASH)'

READ (5,*) YDASH

WRITE(6,*) 'Input N1'

READ (5,*) N1

WRITE(6,*) 'Input effective index estimate'

READ (5,*) NEFF

WRITE(6,*) 'Input the operating wavelength (um)'

READ (5,*) LAMBDA

WRITE(6,*) 'Input number of intervals (N = power of 2)'

READ(5,*) N

WRITE(6,*) 'Input freq. range of FT (eg 4 = -4ko to 4ko)'

READ(5,*) M

WRITE(1,*) N, M, LAMBDA

YDASH = YDASH * 1E-6

LAMBDA = LAMBDA * 1D-6

PI = 4*ATAN(1.0D0)

K0 = 2*PI/LAMBDA

BETA = NEFF*K0

KAPPA1 = (N1 * K0)**2 - BETA**2

INC = 2*M*K0/N

500 WRITE(6,*) 'Input observation coord (Y)'

READ (5,*) Y

IF (Y .LT. -10.0) GOTO 2000

Y = Y * 1E-6

DO 1000 J = 0, N-1

KX = -M*K0 + J*INC

C Case of Neff > N1

AETA1 = KX**2 - KAPPA1

ETA1 = DCMLPX(AETA1, 0.0D0)

ETA1 = CDSQRT(ETA1)

```
IF (Y .GE. YDASH) THEN  
  G = (0.5D0/ETA1)* CDEXP(-ETA1*Y)  
ENDIF
```

```
IF (Y .LT. YDASH) THEN  
  G = (0.5D0/ETA1)* CDEXP(ETA1*Y)  
ENDIF
```

```
WRITE(1,*) KX, Y, G
```

```
1000 CONTINUE
```

```
WRITE(1,*) ' '  
GOTO 500
```

```
2000 STOP  
END
```

APPENDIX H GF Inverse Fourier Transform Program

PROGRAM IFFT_GREEN

```

C Program to calculate the inverse Fourier transform
C of the Green's function (GF) obtained for the three
C layered dielectric slab structure.

C THE VARIABLES USED ARE:

C KX      : Delta kx values.
C GREEN   : Value of the complex Fourier Transform for the
C           three layered structure.
C XCOORD  : 1xN array of the x coordinates calculated after
C           the Inverse Fourier Transform (ie kx --> x).
C DELTAX  : Discrete increment of the x coordinate.
C N       : Number of intervals in the FT (power of 2).
C M       : Freq. range of FT (ie  $4 = -4k_0 < k_x < 4k_0$ ).

INTEGER N, NY, X, Y
DOUBLE PRECISION M, SCALE, YCOORD
DOUBLE PRECISION DELTAX, LAMBDA, K0, KX, PI
DOUBLE PRECISION XCOORD(0:511), R(0:511), IM(0:511), WORK(0:511)
COMPLEX*16 GREEN, I

OPEN(1, FILE='/FREE OUTPUT', FORM='FORMATTED')
OPEN(4, FILE='/FREE UMPDATA', FORM='FORMATTED')

C Read N (no. of intervals in the FT), FT freq. range and wavelength

READ (1,*) N, M, LAMBDA
WRITE(4,*) N, LAMBDA

LAMBDA = LAMBDA*1D-6
PI = 4*ATAN(1.0D0)
K0 = 2.0*PI/LAMBDA
DELTAX = LAMBDA/(2.0*M)

C Calculate step coordinates in x-direction.

DO 5 J = 1, N
  XCOORD(J-1) = -DELTAX*N/2.0D0 + J*DELTAX
5 CONTINUE

WRITE(6,*) 'How many values of observation points (y) ?'
READ(5,*) NY
MID = N/2 - 1
I = (0.0D0, 1.0D0)
SCALE = N/SQRT(DFLOAT(N))

DO 10 L = 1, NY-2
C WRITE(4,*) 'YDASH =', -DFLOAT(L)/10
DO 10 Y = 1, NY
  DO 15 X = 0, N-1
    READ (1,*) KX, YCOORD, GREEN
    R(X) = DREAL(GREEN)
  
```

```

15      IM(X) = DIMAG(GREEN)
      CONTINUE

      IFAIL = 0
      CALL C06GCF(IM, N, IFAIL)
      CALL C06FCF(R, IM, N, WORK, IFAIL)
      CALL C06GCF(IM, N, IFAIL)

C      Multiply the IFT by the phase factor exp(-j/2) and by
C      scale factor T/SQRT(N).

      DO 21 J = 0, N-1
          GREEN = DCMLPX(R(J), IM(J))
          GREEN = SCALE * GREEN * CDEXP(DCMLPX(0.0D0, -DFLOAT(J)/2.0D0))
          R(J) = DREAL(GREEN)
          IM(J) = DIMAG(GREEN)
21      CONTINUE

      DO 25 X = 0, N-1
          GREEN = DCMLPX(R(X), IM(X))
          WRITE (4,*) XCOORD(X)*1D6, YCOORD*1D6, GREEN
25      CONTINUE

      WRITE (4,*) ' '
10      CONTINUE

      CLOSE (1)
      CLOSE (4)

      STOP
      END

```

APPENDIX I GF Program - Situation 1

PROGRAM GREEN_FUNCTION

C PROGRAM TO COMPUTE THE GREEN'S FUNCTION FOR A THREE
C LAYERED MEDIUM.

C SITUATION 1. SOURCE POINT IN AIR (N1 LAYER).

DOUBLE PRECISION Y, YDASH, D, M
DOUBLE PRECISION AETA1, AETA2, AETA3, NEFF
DOUBLE PRECISION N1, N2, N3
DOUBLE PRECISION KAPPA1, KAPPA2, KAPPA3
DOUBLE PRECISION BETA, LAMBDA, INC, K0, KX, PI

COMPLEX*16 A, A1, B1, A2, B2, A3, G
COMPLEX*16 ETA1, ETA2, ETA3, I, IETA2, IETA2D
COMPLEX*16 AA1, AA2, CA1, CA2, DENOM

CHARACTER*1 ANSWER

WRITE(6,*) 'Input depth of N2 layer (d)'

READ (5,*) D

WRITE(6,*) 'Input N1, N2, N3'

READ (5,*) N1, N2, N3

WRITE(6,*) 'Input effective index estimate'

READ (5,*) NEFF

WRITE(6,*) 'Input the operating wavelength (um)'

READ (5,*) LAMBDA

WRITE(6,*) 'Input number of intervals (N = power of 2)'

READ (5,*) N

WRITE(6,*) 'Input freq. range of FT (eg 4 = -4ko to 4ko)'

READ (5,*) M

OPEN(1,FILE='/FTGREEN1 OUTPUT', FORM='FORMATTED')

WRITE(1,*) N, M, LAMBDA

D = D * 1D-6

LAMBDA = LAMBDA * 1D-6

PI = 4*ATAN(1.0D0)

K0 = 2*PI/LAMBDA

BETA = NEFF*K0

KAPPA1 = (N1 * K0)**2 - BETA**2

KAPPA2 = (N2 * K0)**2 - BETA**2

KAPPA3 = (N3 * K0)**2 - BETA**2

WRITE(6,*) 'KAPPA1 =', KAPPA1

WRITE(6,*) 'KAPPA2 =', KAPPA2

WRITE(6,*) 'KAPPA3 =', KAPPA3

WRITE(6,*) ' '

I = DCMLPX(0.0D0, 1.0D0)

INC = 2*M*K0/N

```

2000 WRITE(6,*) 'Input source point coord (YDASH)'
      READ (5,*) YDASH
      YDASH = YDASH * 1D-6

500  WRITE(6,*) 'Input observation coord (Y)'
      READ (5,*) Y
      IF (Y .LT. -10) GOTO 3000

      Y = Y * 1D-6

      DO 1000 J = 0, N-1

          KX = -M*K0 + J*INC

C          N2 > NE > N3 > N1  Situation.

          AETA1 = KX**2 + KAPPA1
          AETA2 = KAPPA2 - KX**2
          AETA3 = KAPPA3 - KX**2

          ETA1 = DCMLPX(AETA1, 0.0D0)
          ETA2 = DCMLPX(AETA2, 0.0D0)
          ETA3 = DCMLPX(AETA3, 0.0D0)

          ETA1 = CDSQRT(ETA1)
          ETA2 = CDSQRT(ETA2)
          ETA3 = CDSQRT(ETA3)

          IETA2 = I*ETA2
          IETA2D = I*ETA2*D
          CA1 = IETA2 + ETA3
          CA2 = IETA2 - ETA3

          AA1 = ETA1*ETA3*CDSIN(ETA2*D)
          AA2 = AA1 + ETA2*(-ETA2*CDSIN(ETA2*D)
1          + (ETA1+ETA3)*CDCOS(ETA2*D))
          DENOM = 2*I*AA2

          B2 = CA1 * CDEXP(-ETA1*YDASH) * CDEXP(IETA2D)
          A2 = CA2 * CDEXP(-ETA1*YDASH) * CDEXP(-IETA2D)
          A2 = A2/DENOM
          B2 = B2/DENOM

          B1 = CDEXP(-ETA1*YDASH)/(2*ETA1)
          A1 = A2 + B2 - B1

          A3 = (A2*CDEXP(IETA2D) + B2*CDEXP(-IETA2D)) * CDEXP(ETA3*D)
          A = A1 + (CDEXP(ETA1*YDASH))/(2*ETA1)

C  Now calculate the GF for each region.

      IF (Y .GE. YDASH) THEN
          G = A * CDEXP(-ETA1*Y)
      ENDIF

      IF ((Y .LT. YDASH) .AND. (Y .GE. 0.0D0)) THEN
          G = A1 * CDEXP(-ETA1*Y) + B1 * CDEXP(ETA1*Y)
      ENDIF

      IF ((Y .LT. 0.0D0) .AND. (Y .GE. -D)) THEN
          G = A2 * CDEXP(-IETA2*Y) + B2 * CDEXP(IETA2*Y)

```


APPENDIX J GF Transcendental Equation Program

PROGRAM GF_CALCULATIONS

C This program will calculate all the necessary values required
C for the Green's Function for a slab waveguide. The constants
C calculated are:

- C 1. Effective Index Ne
C 2. Root of the transcendenatl eqn. Kq
C 3. Derivative f'(kq) used in the Taylor series expansion.
C

COMMON/WORK/ D, K0, N1, N2, N3, PI, NEFF, Q

DOUBLE PRECISION B, NE, K0, KQ, PI, NEFF
DOUBLE PRECISION D, LAMBDA, N1, N2, N3
DOUBLE PRECISION EPS, ETA
INTEGER IFAIL, K, NFMAX, Q
EXTERNAL TENE, TEKQ

DOUBLE PRECISION ETA1, ETA2, ETA3
DOUBLE PRECISION AA1, AA2, DENOM1, DENOM2, FDASH

OPEN (5, FILE='/GFCALCS INPUT', FORM='FORMATTED')
OPEN (2, FILE='/GFCALCS OUTPUT', FORM='FORMATTED')

WRITE(6,*) 'Input the depth of the slab (um)'
READ (5,*) D
WRITE(6,*) 'Enter N1, N2, N3'
READ (5,*) N1, N2, N3
WRITE(6,*) 'Input the operating wavelength (um)'
READ (5,*) LAMBDA
WRITE(6,*) 'Input the mode number q'
READ (5,*) Q

Q = Q + 1
D = D * 1D-6
LAMBDA = LAMBDA * 1D-6
PI = 4*ATAN(1.0D0)
K0 = 2.0D0*PI/LAMBDA

C This part will find the root (or eigenvalue ne).

DO 10 K = 1, 10
 EPS = 10.0D0**(-K)
 NE = N3 + 0.01D0
 ETA = 0.0D0
 NFMAX = 500
 IFAIL = 0
 CALL C05AJF (NE, EPS, ETA, TENE, NFMAX, IFAIL)
 B = (NE**2 - N3**2)/(N2**2 - N3**2)
 WRITE(6,97) 'Ne = ', NE, 'b = ', B

10 CONTINUE

97 FORMAT(A6, F15.9, A6, F10.4)

```
WRITE(6,*) ' '
```

```
C This part will find the root (or eigenvalue) Kq.
```

```
NEFF = NE
```

```
DO 20 K = 1, 10
```

```
  EPS = 10.0D0**(-K)
```

```
  KQ = 100.0D0
```

```
  ETA = 0.0D0
```

```
  NFMAX = 500
```

```
  IFAIL = 0
```

```
  CALL C05AJF (KQ, EPS, ETA, TEKQ, NFMAX, IFAIL)
```

```
  WRITE(6,98) 'Kq = ', KQ
```

```
20 CONTINUE
```

```
98 FORMAT(A6, F10.2)
```

```
WRITE(6,*) ' '
```

```
C This part will calculate the derivative f'(kq).
```

```
  CALL ETA_KAPPA (NE, KQ, ETA1, ETA2, ETA3)
```

```
C Now calculate the derivative f'(kq)
```

```
  AA1 = (ETA1/ETA2) + (ETA2/ETA1)
```

```
  DENOM1 = ETA1**2 + ETA2**2
```

```
  AA2 = (ETA3/ETA2) + (ETA2/ETA3)
```

```
  DENOM2 = ETA3**2 + ETA2**2
```

```
  FDASH = -2.0D0 * KQ * (AA1/DENOM1 + AA2/DENOM2 + D/ETA2)
```

```
  WRITE (6,*) 'FDASH @ Kq = ',KQ,' = ', FDASH
```

```
  WRITE (2,*) NE, 'b = ',B
```

```
  WRITE (2,*) KQ, FDASH
```

```
STOP
```

```
END
```

```
C ***** FUNCTIONS *****
```

```
REAL FUNCTION TENE(NE)
```

```
C This function calculates the value of the transcendental eqn.  
C for a given value of the effective index (Ne). The eqn is
```

```
C 
$$\text{PHI1} + \text{PHI2} + 2 * \text{ETA2} * \text{D} = (2q) * \text{PI}.$$

```

```
COMMON/WORK/ D, K0, N1, N2, N3, PI, NEFF, Q
```

```
DOUBLE PRECISION BETA, KX, K0, NE, PI, PHI1, PHI2, NEFF
```

```
DOUBLE PRECISION D, LAMBDA, N1, N2, N3
```

```
DOUBLE PRECISION ETA1, ETA2, ETA3
```

```
INTEGER Q
```

```
  KX = 0.0D0
```

```
  CALL ETA_KAPPA (NE, KX, ETA1, ETA2, ETA3)
```

```
  PHI1 = 2.0D0 * ATAN(ETA2/ETA1)
```

PHI2 = 2.0D0 * ATAN(ETA2/ETA3)

TENE = PHI1 + PHI2 + 2.0D0*ETA2*D - 2*DFLOAT(Q)*PI

END

REAL FUNCTION TEKQ(KX)

C This function calculates the value of the transcendental eqn.
C for a given value of the effective index (Ne). The eqn is
C

PHI1 + PHI2 + 2*ETA2*D = (2q)*PI.

COMMON/WORK/ D, K0, N1, N2, N3, PI, NEFF, Q

DOUBLE PRECISION KX, K0, PI, PHI1, PHI2, NEFF

DOUBLE PRECISION D, LAMBDA, N1, N2, N3

DOUBLE PRECISION ETA1, ETA2, ETA3

INTEGER Q

CALL ETA_KAPPA (NEFF, KX, ETA1, ETA2, ETA3)

PHI1 = 2.0D0 * ATAN(ETA2/ETA1)

PHI2 = 2.0D0 * ATAN(ETA2/ETA3)

TEKQ = PHI1 + PHI2 + 2.0D0*ETA2*D - 2*DFLOAT(Q)*PI

END

SUBROUTINE ETA_KAPPA (NE, KX, ETA1, ETA2, ETA3)

COMMON/WORK/ D, K0, N1, N2, N3, PI, NEFF, Q

DOUBLE PRECISION BETA, K0, KX, NE, N1, N2, N3

DOUBLE PRECISION KAPPA1, KAPPA2, KAPPA3

DOUBLE PRECISION ETA1, ETA2, ETA3

DOUBLE PRECISION D, PI, NEFF

INTEGER Q

BETA = NE*K0

KAPPA1 = (N1 * K0)**2 - BETA**2

KAPPA2 = (N2 * K0)**2 - BETA**2

KAPPA3 = (N3 * K0)**2 - BETA**2

C N2 > Ne > N3 > N1 Situation.

ETA1 = DSQRT(KX**2 - KAPPA1)

ETA2 = DSQRT(KAPPA2 - KX**2)

ETA3 = DSQRT(KX**2 - KAPPA3)

END

APPENDIX K GF Program – Situation 2 – Modal Contribution

PROGRAM MODAL_GREEN_FUNCTION

C Program to compute the pole contribution of the Green's
 C function. Solution is in the cartesian X-Y domain.

C Situation 2. Source point in N2 guiding layer.

```
DOUBLE PRECISION FDASH, Y, YDASH, D, M
DOUBLE PRECISION N1, N2, N3, NE, B
DOUBLE PRECISION AETA1, AETA2, AETA3
DOUBLE PRECISION KAPPA1, KAPPA2, KAPPA3
DOUBLE PRECISION BETA, LAMBDA, K0, KQ, KX, PI
CHARACTER*1 ANSWER
```

```
COMPLEX*16 ETA2
DOUBLE PRECISION ETA1, ETA3
COMPLEX*16 PHIA1, PHIA2, PHIB2, PHIA2D, PHIB2D, PHIA3
COMPLEX*16 DENOM, IETA2D, IETA2YD
COMPLEX*16 G, GG, I, CA1, CA2, CA3, CA4, CA5, CA6
INTEGER X
```

```
OPEN(5, FILE='/NEWG2 INPUT', FORM='FORMATTED')
OPEN(1, FILE='/GF2 UMPDATA', FORM='FORMATTED')
```

```
WRITE(6,*) 'Input depth of N2 layer (d)'
READ (5,*) D
WRITE(6,*) 'Input N1, N2, N3'
READ (5,*) N1, N2, N3
WRITE(6,*) 'Input effective index estimate'
READ (5,*) NE
WRITE(6,*) 'Input the operating wavelength (um)'
READ (5,*) LAMBDA
WRITE(6,*) 'Input number of intervals (N = power of 2)'
READ (5,*) N
WRITE(6,*) 'Input root Kq'
READ (5,*) KQ
WRITE(6,*) 'Input derivative of f(kq) graph'
READ (5,*) FDASH
```

```
FDASH = DABS(FDASH)
D = D * 1D-6
LAMBDA = LAMBDA * 1D-6
```

```
I = DCMPLX (0.0D0,1.0D0)
PI = 4*ATAN(1.0D0)
K0 = 2.0D0*PI/LAMBDA
KX = KQ
```

C Calculate the respective wavenumbers for each dielectric region.

```
BETA = NE*K0
KAPPA1 = (N1 * K0)**2 - BETA**2
KAPPA2 = (N2 * K0)**2 - BETA**2
KAPPA3 = (N3 * K0)**2 - BETA**2
```

```

C      N2 > Ne > N3 > N1 Situation.

      AETA1 = KX**2 - KAPPA1
      AETA2 = KAPPA2 - KX**2
      AETA3 = KX**2 - KAPPA3

      ETA2 = DCMLPX(AETA2, 0.0D0)

      ETA1 = DSQRT(AETA1)
      ETA2 = CDSQRT(ETA2)
      ETA3 = DSQRT(AETA3)

2000  WRITE(6,*) 'Input source point coord (YDASH)'
      READ (5,*) YDASH
      YDASH = YDASH * 1D-6
C      WRITE(1,*) 'YDASH =', YDASH

C      Calculate some constants to be used in the Green's function G.

      IETA2D = I * ETA2*D
      IETA2YD = I * ETA2*YDASH

      CA1 = ETA1 + I*ETA2
      CA2 = ETA1 - I*ETA2
      CA1 = CA1/CA2
      CA3 = -ETA3 + I*ETA2
      CA4 = ETA3 + I*ETA2
      CA3 = CA3/CA4
      CA5 = I/(2.0D0*ETA2)
      CA6 = CDEXP(IETA2YD) * CDEXP(IETA2D)

500   WRITE(6,*) 'Input observation coord (Y)'
      READ (5,*) Y
      IF (Y .LT. -10.0D0) GOTO 3000
      Y = Y *1D-6

C      Calculate some more constants for the Green's function G.

      PHIA1 = -CA1 + 1.0D0
      PHIA2 = -CA1 * CDEXP(-I*ETA2*Y) + CDEXP(I*ETA2*Y)
      PHIB2 = CA6 + CA3*CDEXP(-IETA2YD)*CDEXP(-IETA2D)
      PHIA2D = CA3 * CDEXP(-2.0D0*IETA2D) * CDEXP(-I*ETA2*Y) +
1      CDEXP(I*ETA2*Y)
      PHIB2D = CA6 - CA1 * CDEXP(-IETA2YD) * CDEXP(IETA2D)
      PHIA3 = (CA3 + 1.0D0) * CDEXP(-IETA2D)

C      Now calculate the Green's function for each region.

      IF (Y .GE. 0.0D0) THEN
      GG = CA5 * PHIA1 * PHIB2 * DEXP(-ETA1*Y) / (-FDASH)
      DO 10 X = -(N/2-1), 0
      G = GG * CDEXP(-I*KQ*DFLOAT(X)*1D-7)
      WRITE(1,*) DFLOAT(X)*1D-1, Y*1D6, G
10     CONTINUE

      GG = CA5 * PHIA1 * PHIB2 * DEXP(-ETA1*Y) / FDASH
      DO 15 X = 1, N/2
      G = GG * CDEXP(I*KQ*DFLOAT(X)*1D-7)
      WRITE(1,*) DFLOAT(X)*1D-1, Y*1D6, G
15     CONTINUE

```

```

ENDIF

IF ((Y .GE. YDASH) .AND. (Y .LT. 0.0D0)) THEN
  GG = CA5 * PHIA2 * PHIB2 / (-FDASH)
  DO 20 X = -(N/2-1), 0
    G = GG * CDEXP(-I*KQ*DFLOAT(X)*1D-7)
    WRITE(1,*) DFLOAT(X)*1D-1, Y*1D6, G
20  CONTINUE

    GG = CA5 * PHIA2 * PHIB2 / FDASH
    DO 25 X = 1, N/2
      G = GG * CDEXP(I*KQ*DFLOAT(X)*1D-7)
      WRITE(1,*) DFLOAT(X)*1D-1, Y*1D6, G
25  CONTINUE
ENDIF

IF ((Y .LT. YDASH) .AND. (Y .GE. -D)) THEN
  GG = CA5 * PHIA2D * PHIB2D / (-FDASH)
  DO 30 X = -(N/2-1), 0
    G = GG * CDEXP(-I*KQ*DFLOAT(X)*1D-7)
    WRITE(1,*) DFLOAT(X)*1D-1, Y*1D6, G
30  CONTINUE

    GG = CA5 * PHIA2D * PHIB2D / FDASH
    DO 35 X = 1, N/2
      G = GG * CDEXP(I*KQ*DFLOAT(X)*1D-7)
      WRITE(1,*) DFLOAT(X)*1D-1, Y*1D6, G
35  CONTINUE
ENDIF

IF (Y .LT. -D) THEN
  GG = CA5 * PHIA3 * PHIB2D * DEXP(ETA3*(Y+D)) / (-FDASH)
  DO 40 X = -(N/2-1), 0
    G = GG * CDEXP(-I*KQ*DFLOAT(X)*1D-7)
    WRITE(1,*) DFLOAT(X)*1D-1, Y*1D6, G
40  CONTINUE

    GG = CA5 * PHIA3 * PHIB2D * DEXP(ETA3*(Y+D)) / FDASH
    DO 45 X = 1, N/2
      G = GG * CDEXP(I*KQ*DFLOAT(X)*1D-7)
      WRITE(1,*) DFLOAT(X)*1D-1, Y*1D6, G
45  CONTINUE
ENDIF

WRITE(1,*) ' '

GOTO 500

3000 WRITE(6,*) 'Another run with a different value of YDASH ?'
      READ (5,98) ANSWER
98  FORMAT(A1)
      IF (ANSWER .EQ. 'Y') GOTO 2000
      STOP
      END

```

APPENDIX L GF Program - Situation 2 - FT Calculation

PROGRAM GREEN_FUNCTION

C Program to compute the Green's function for a three layered
 C dielectric slab structure. The GF calculated is in the Fourier
 C domain, the spatial GF is determined using the IFFT_GREEN
 C program.

C Situation 2. Source point in N2 guiding layer.

DOUBLE PRECISION Y, YDASH, D, M
 DOUBLE PRECISION N1, N2, N3, NE, B
 DOUBLE PRECISION AETA1, AETA2, AETA3
 DOUBLE PRECISION KAPPA1, KAPPA2, KAPPA3
 DOUBLE PRECISION BETA, LAMBDA, INC, K0, KX, PI
 CHARACTER*1 ANSWER

COMPLEX*16 ETA2
 DOUBLE PRECISION ETA1, ETA3
 COMPLEX*16 A, A1, B1, A2, B2, A3, G
 COMPLEX*16 DENOM, IETA2D, IETA2YD
 COMPLEX*16 I, CA1, CA2, CA3, CA4, CA5, CA6

OPEN(5, FILE='/FTGF2 INPUT', FORM='FORMATTED')
 OPEN(1, FILE='/FTGF2 OUTPUT', FORM='FORMATTED')

WRITE(6,*) 'Input depth of N2 layer (d)'
 READ (5,*) D
 WRITE(6,*) 'Input N1, N2, N3'
 READ (5,*) N1, N2, N3
 WRITE(6,*) 'Input effective index estimate'
 READ (5,*) NE
 WRITE(6,*) 'Input the operating wavelength (um)'
 READ (5,*) LAMBDA
 WRITE(6,*) 'Input number of intervals (N = power of 2)'
 READ (5,*) N
 WRITE(6,*) 'Input freq. range of FT (eg 4= -4ko to 4ko)'
 READ (5,*) M

WRITE(1,*) N, M, LAMBDA

D = D * 1D-6
 LAMBDA = LAMBDA * 1D-6

I = DCMLX (0.0D0,1.0D0)
 PI = 4*ATAN(1.0D0)
 K0 = 2.0D0*PI/LAMBDA
 INC = 2.0D0*M*K0/N

C Calculate respective wavenumbers for each dielectric region.

BETA = NE*K0
 KAPPA1 = (N1 * K0)**2 - BETA**2
 KAPPA2 = (N2 * K0)**2 - BETA**2

```

KAPPA3 = (N3 * K0)**2 - BETA**2

2000 WRITE(6,*) 'Input source point coord (YDASH)'
      READ (5,*) YDASH
      YDASH = YDASH * 1D-6

500  WRITE(6,*) 'Input observation coord (Y)'
      READ (5,*) Y
      IF (Y .LT. -10.0D0) GOTO 3000

      Y = Y *1D-6
      DO 1000 J = 0, N-1
        KX = -M*K0 + DFLOAT(J)*INC

C      N2 > Ne > N3 > N1 Situation.

      AETA1 = KX**2 - KAPPA1
      AETA2 = KAPPA2 - KX**2
      AETA3 = KX**2 - KAPPA3

      ETA2 = DCMLPX(AETA2, 0.0D0)

      ETA1 = DSQRT(AETA1)
      ETA2 = CDSQRT(ETA2)
      ETA3 = DSQRT(AETA3)

C      Calculate some constants to be used in the Green's function G.

      IETA2D = I * ETA2*D
      IETA2YD = I * ETA2*YDASH

      CA1 = ETA1 + I*ETA2
      CA2 = ETA1 - I*ETA2
      CA1 = CA1/CA2
      CA3 = -ETA3 + I*ETA2
      CA4 = ETA3 + I*ETA2
      CA3 = CA3/CA4
      CA5 = 2.0D0*I*ETA2
      CA6 = CDEXP(IETA2YD) * CDEXP(IETA2D)
      DENOM = -(CA1*CDEXP(IETA2D) + CA3*CDEXP(-IETA2D))

C      Now calculate the coefficients A, A1, ..., A3

      B1 = (CA6 + CA3*CDEXP(-IETA2YD)*CDEXP(-IETA2D))/(CA5*DENOM)
      A1 = -CA1 * B1

      B2 = (CA6 - CA1*CDEXP(-IETA2YD)*CDEXP(IETA2D))/(CA5*DENOM)
      A2 = CA3 * B2 * CDEXP(-2.0D0*IETA2D)

      A = A1 + B1

      A3 = (A2 * CDEXP(IETA2D) + B2 * CDEXP(-IETA2D))
1      * DEXP(ETA3*D)

C      Now calculate the Green's function for each region.

      IF (Y .GE. 0.0D0) THEN
        G = A * DEXP(-ETA1*Y)
      WRITE(1,*) KX, Y, G
      ENDIF

```

```

KAPPA3 = (N3 * K0)**2 - BETA**2

2000 WRITE(6,*) 'Input source point coord (YDASH)'
      READ (5,*) YDASH
      YDASH = YDASH * 1D-6

500   WRITE(6,*) 'Input observation coord (Y)'
      READ (5,*) Y
      IF (Y .LT. -10.0D0) GOTO 3000

      Y = Y * 1D-6
      DO 1000 J = 0, N-1
        KX = -M*K0 + DFLOAT(J)*INC

C     N2 > Ne > N3 > N1 Situation.

      AETA1 = KX**2 - KAPPA1
      AETA2 = KAPPA2 - KX**2
      AETA3 = KX**2 - KAPPA3

      ETA2 = DCMLPX(AETA2, 0.0D0)

      ETA1 = DSQRT(AETA1)
      ETA2 = CDSQRT(ETA2)
      ETA3 = DSQRT(AETA3)

C     Calculate some constants to be used in the Green's function G.

      IETA2D = I * ETA2*D
      IETA2YD = I * ETA2*YDASH

      CA1 = ETA1 + I*ETA2
      CA2 = ETA1 - I*ETA2
      CA1 = CA1/CA2
      CA3 = -ETA3 + I*ETA2
      CA4 = ETA3 + I*ETA2
      CA3 = CA3/CA4
      CA5 = 2.0D0*I*ETA2
      CA6 = CDEXP(IETA2YD) * CDEXP(IETA2D)
      DENOM = -(CA1*CDEXP(IETA2D) + CA3*CDEXP(-IETA2D))

C     Now calculate the coefficients A, A1, ..., A3

      B1 = (CA6 + CA3*CDEXP(-IETA2YD)*CDEXP(-IETA2D))/(CA5*DENOM)
      A1 = -CA1 * B1

      B2 = (CA6 - CA1*CDEXP(-IETA2YD)*CDEXP(IETA2D))/(CA5*DENOM)
      A2 = CA3 * B2 * CDEXP(-2.0D0*IETA2D)

      A = A1 + B1

      A3 = (A2 * CDEXP(IETA2D) + B2 * CDEXP(-IETA2D))
1      * DEXP(ETA3*D)

C     Now calculate the Green's function for each region.

      IF (Y .GE. 0.0D0) THEN
        G = A * DEXP(-ETA1*Y)
      WRITE(1,*) KX, Y, G
      ENDIF

```

```
IF ((Y .GE. YDASH) .AND. (Y .LT. 0.0D0)) THEN
  G = A1 * CDEXP(-I*ETA2*Y) + B1 * CDEXP(I*ETA2*Y)
WRITE(1,*) KX, Y, G
ENDIF
```

```
IF ((Y .LT. YDASH) .AND. (Y .GE. -D)) THEN
  G = A2 * CDEXP(-I*ETA2*Y) + B2 * CDEXP(I*ETA2*Y)
WRITE(1,*) KX, Y, G
ENDIF
```

```
IF (Y .LT. -D) THEN
  G = A3 * DEXP(ETA3*Y)
WRITE(1,*) KX, Y, G
ENDIF
```

```
1000 CONTINUE
```

```
WRITE(1,*) ' '
GOTO 500
```

```
3000 WRITE(6,*) 'Another run with a different value of YDASH ?'
READ (5,98) ANSWER
98 FORMAT(A1)
IF (ANSWER .EQ. 'Y') GOTO 2000
STOP
END
```

APPENDIX M Kirchhoff- Huygen's Line Integral Program

PROGRAM KIRCHHOFF_HUYGEN_INTEGRAL

C Program to calculate the new field around a selected
 C contour surrounding a waveguide structure. The Kirchhoff-
 C Huygens line intgral formula is used in which the initial
 C field UFIELD and Green's Function G is used.

C The field values output in file 'SLABFD UMPDATA' from the
 C scalar finite diffrence program are stored in the UFIELD
 C array. The normal derivative du/dn is calculated and
 C stored in the array DUFIELD. The Green Function values
 C are read from the two corresponding GF programs.

C Finally the Kirchhoff-Huygen line integral is performed
 C around the waveguide structure and the new contour
 C field values are written into the file 'FILE FT09F001'
 C to be used for a subsequent run of the scalar finite
 C difference program.

C THE VARIABLES USED ARE:

C XCOORD : 1xN array of the x coordinates.
 C XSTART : Start value of the x coordinate.
 C DELTAX : Discrete increment of the x coordinate.
 C GREEN : NxNY+2xNY array of the IFT GF g.
 C DGREEN : NxNY+2xNY array of the normal derivative of the GF
 C UFIELD : NxNY array of the electric field values calculated
 C from the program SLABFD.
 C DUFIELD : NxNY array of the normal derivative of the UFIELD.
 C U, DU : 1x64 array of the contour field u & the derivative
 C G, DG : 1x64 array of the contour GF g & the derivative dg
 C UM : 1x64 array of the resulting new contour field.
 C H : Meshsize of the finite difference (=0.lum).

COMMON /DATA/ XCOORD
 COMMON /RDATA/ UFIELD, DUFIELD, U, DU
 COMMON /IDATA/ GREEN, DGREEN, G, DG

INTEGER N, NY, X, Y, YDASH
 DOUBLE PRECISION H, YCOORD, XCOORD (0:255)
 DOUBLE PRECISION XSTART, LAMBDA, DELTAX
 DOUBLE PRECISION UFIELD (1:13,0:255), DUFIELD (1:13,0:255)
 DOUBLE PRECISION UM (1:64), U (1:64), DU (1:64)

COMPLEX*16 GREEN (0:14, 0:255, 1:13), DGREEN (0:14, 0:255, 1:13)
 COMPLEX*16 G(1:64, 1:64), DG(1:64, 1:64)
 COMPLEX*16 GN, GM

C Read N (no. of intervals in the FT), FT freq. range and wavelen

OPEN(1, FILE='/IFTGF2 UMPDATA', FORM='FORMATTED')
 OPEN(2, FILE='/SLABFD UMPDATA', FORM='FORMATTED')
 OPEN(10, FILE='/GF2 UMPDATA', FORM='FORMATTED')

```

READ(1,*) N, LAMBDA

H = 0.1
MID = N/2 - 1
DELTAX = H
XSTART = -(MID)*H
DO 5 X = 0, N-1
  XCOORD(X) = XSTART + X*DELTAX
5 CONTINUE

WRITE(6,*) 'How many values of ydash ?'
READ(5,*) NY

DO 10 Y = 1, NY
  DO 10 X = 0, N-1
    READ (2,*) XX, YCOORD, UFIELD(Y,X)
10 CONTINUE

C Now calculate values for du/dn matrix DUFIELD from the UFIELD
C matrix values.

DO 15 X = 1, N-2
  DUFIELD(1,X) = -(UFIELD(2,X) - UFIELD(1,X))/H
  DUFIELD(NY,X) = -(UFIELD(NY-1,X) - UFIELD(NY,X))/H
15 CONTINUE

DO 20 Y = 2, NY-1

  DO 25 X = 1, MID
    DUFIELD(Y,X) = -(UFIELD(Y,X) - UFIELD(Y,X-1))/H
25 CONTINUE

  DO 30 X = MID+1, N-1
    DUFIELD(Y,X) = -(UFIELD(Y,X) - UFIELD(Y,X+1))/H
30 CONTINUE

20 CONTINUE

DO 35 YDASH = 1, NY
DO 40 Y = 0, NY+1

  DO 45 X = 0, N-1
    READ (1,*) XX, YCOORD
    READ (1,*) GN
    READ (10,*) XX, YCOORD
    READ (10,*) GM
    GREEN(Y, X, YDASH) = GN + GM
45 CONTINUE
40 CONTINUE

C Now calculate values for dg/dn matrix DGREEN from the GREEN
C matrix values.

DO 70 X = 1, N-2
  DGREEN(1,X,YDASH) = (GREEN(0,X,YDASH) - GREEN(1,X,YDASH))/H
  DGREEN(NY,X,YDASH) = (GREEN(NY+1,X,YDASH) - GREEN(NY,X,YDASH))
70 CONTINUE

DO 35 Y = 2, NY-1

  DO 75 X = 1, MID

```

```

75     DGREEN(Y,X,YDASH) = (GREEN(Y,X-1,YDASH) - GREEN(Y,X,YDASH))/H
      CONTINUE

      DO 80 X = MID+1, N-1
        DGREEN(Y,X,YDASH) = (GREEN(Y,X+1,YDASH) - GREEN(Y,X,YDASH))/H
80     CONTINUE
35     CONTINUE

      CALL CONTOUR (MID, NY)

      WRITE(6,*) 'Now performing KH integral calculation ...'

C     Now multiply the following  $u * dg/dn - g * du/dn$ 

      DO 90 X = 1, 64
        UM(X) = 0.0D0
        DO 95 Y = 1, 64
          UM(X) = UM(X) + U(Y)*DG(Y,X) - DU(Y)*G(Y,X)
95     CONTINUE
90     CONTINUE

C     Output the new contour field values in normalised form.

      CALL OUTPUT (UM)

      STOP
      END

```

C ***** SUBROUTINES *****

SUBROUTINE CONTOUR (MID, NY)

```

COMMON /DATA/ XCOORD
COMMON /RDATA/ UFIELD, DUFIELD, U, DU
COMMON /IDATA/ GREEN, DGREEN, G, DG

```

C This routine dumps the contour integral values of the
C GREEN, DGREEN, UFIELD, DUFIELD matrices into the relevant
C files and reads the dumped data back into the matrices
C G, DG, U and DU. This dumping of values and reading them
C back into the matrices was done for simplicity. The files
C used to store the dumped values are then deleted.

```

INTEGER M, N, NY, MID, X, Y, XDASH, YDASH
DOUBLE PRECISION UFIELD(1:13,0:255), DUFIELD(1:13,0:255)
DOUBLE PRECISION U(1:64), DU(1:64)
COMPLEX*16 GREEN(0:14,0:255,1:13), DGREEN(0:14,0:255,1:13)
COMPLEX*16 G(1:64, 1:64), DG(1:64, 1:64)

```

```

OPEN(3, FILE='/GREEN DATA', FORM='FORMATTED')
OPEN(4, FILE='/DGREEN DATA', FORM='FORMATTED')

```

WRITE(6,*) 'Now calculating contour points of integral ...'

CCC WRITE(3,*) 'Path 1 (xdash = -1.0 to 1.0, ydash = 0.1)'

DO 5 XDASH = 0, 20

```

DO 10 X = 0, 20
  WRITE(3,*) GREEN(1, MID+X-XDASH, 1)
  WRITE(4,*) DGREEN(1, MID+X-XDASH, 1)

```

```

10 CONTINUE

X = X - 1
DO 15 Y = 2, NY
  WRITE(3,*) GREEN(Y, MID+X-XDASH, 1)
  IF (XDASH .EQ. 20) THEN
    WRITE(4,*) -DGREEN(Y, MID+X-XDASH, 1)
  ELSE
    WRITE(4,*) DGREEN(Y, MID+X-XDASH, 1)
  ENDIF
15 CONTINUE

Y = Y - 1
DO 20 X = 19, 0, -1
  WRITE(3,*) GREEN(Y, MID+X-XDASH, 1)
  WRITE(4,*) DGREEN(Y, MID+X-XDASH, 1)
20 CONTINUE

X = X + 1
DO 25 Y = NY-1, 2, -1
  WRITE(3,*) GREEN(Y, MID+X-XDASH, 1)
  WRITE(4,*) DGREEN(Y, MID+X-XDASH, 1)
25 CONTINUE
WRITE(3,*) ' '
WRITE(4,*) ' '

5 CONTINUE

CCC WRITE(3,*) 'Path 2 (xdash = 1.0, ydash = -0.2 to -1.3)'

XDASH = XDASH-1
DO 30 YDASH = 2, NY

  DO 35 X = 0, 20
    WRITE(3,*) GREEN(1, MID+X-XDASH, YDASH)
    WRITE(4,*) DGREEN(1, MID+X-XDASH, YDASH)
35 CONTINUE

  X = X - 1
  DO 40 Y = 2, NY
    WRITE(3,*) GREEN(Y, MID+X-XDASH, YDASH)
    WRITE(4,*) -DGREEN(Y, MID+X-XDASH, YDASH)
40 CONTINUE

  Y = Y - 1
  DO 45 X = 19, 0, -1
    WRITE(3,*) GREEN(Y, MID+X-XDASH, YDASH)
    WRITE(4,*) DGREEN(Y, MID+X-XDASH, YDASH)
45 CONTINUE

  X = X + 1
  DO 50 Y = NY-1, 2, -1
    WRITE(3,*) GREEN(Y, MID+X-XDASH, YDASH)
    WRITE(4,*) DGREEN(Y, MID+X-XDASH, YDASH)
50 CONTINUE
WRITE(3,*) ' '
WRITE(4,*) ' '

30 CONTINUE

CCC WRITE(3,*) 'Path 3 (xdash = 0.9 to -1.0, ydash = -1.3)'

```

```
YDASH = YDASH-1  
DO 55 XDASH = 19, 0, -1
```

```
DO 60 X = 0, 20  
  WRITE(3,*) GREEN(1, MID+X-XDASH, YDASH)  
  WRITE(4,*) DGREEN(1, MID+X-XDASH, YDASH)  
60 CONTINUE
```

```
X = X - 1  
DO 65 Y = 2, NY  
  WRITE(3,*) GREEN(Y, MID+X-XDASH, YDASH)  
  WRITE(4,*) DGREEN(Y, MID+X-XDASH, YDASH)  
65 CONTINUE
```

```
Y = Y - 1  
DO 70 X = 19, 0, -1  
  WRITE(3,*) GREEN(Y, MID+X-XDASH, YDASH)  
  WRITE(4,*) DGREEN(Y, MID+X-XDASH, YDASH)  
70 CONTINUE
```

```
X = X + 1  
DO 75 Y = NY-1, 2, -1  
  WRITE(3,*) GREEN(Y, MID+X-XDASH, YDASH)  
  WRITE(4,*) DGREEN(Y, MID+X-XDASH, YDASH)  
75 CONTINUE  
  WRITE(3,*) ' '  
  WRITE(4,*) ' '
```

```
55 CONTINUE
```

```
CCC WRITE(3,*) 'Path 4 (xdash = -1.0, ydash = -1.2 to -0.2)'
```

```
XDASH = XDASH+1  
DO 80 YDASH = NY-1, 2, -1
```

```
DO 85 X = 0, 20  
  WRITE(3,*) GREEN(1, MID+X-XDASH, YDASH)  
  WRITE(4,*) DGREEN(1, MID+X-XDASH, YDASH)  
85 CONTINUE
```

```
X = X - 1  
DO 90 Y = 2, NY  
  WRITE(3,*) GREEN(Y, MID+X-XDASH, YDASH)  
  WRITE(4,*) DGREEN(Y, MID+X-XDASH, YDASH)  
90 CONTINUE
```

```
Y = Y - 1  
DO 95 X = 19, 0, -1  
  WRITE(3,*) GREEN(Y, MID+X-XDASH, YDASH)  
  WRITE(4,*) DGREEN(Y, MID+X-XDASH, YDASH)  
95 CONTINUE
```

```
X = X + 1  
DO 100 Y = NY-1, 2, -1  
  WRITE(3,*) GREEN(Y, MID+X-XDASH, YDASH)  
  WRITE(4,*) DGREEN(Y, MID+X-XDASH, YDASH)  
100 CONTINUE  
  WRITE(3,*) ' '  
  WRITE(4,*) ' '
```

80 CONTINUE

C Now dump out values of the field U and the derivative dU.

```
OPEN(7, FILE='/UFIELD DATA', FORM='FORMATTED')
OPEN(8, FILE='/DUFIELD DATA', FORM='FORMATTED')
```

CCC WRITE(7,*) 'Path 1 (xdash = -1.0 to 1.0, ydash = 0.1)'

```
DO 110 X = -10, 10
  WRITE(7,*) UFIELD(1, MID+X)
  WRITE(8,*) DUFIELD(1, MID+X)
```

110 CONTINUE

CCC WRITE(7,*) 'Path 2 (xdash = 1.0, ydash = -0.2 to -1.3)'

```
X = X-1
DO 115 Y = 2, NY
  WRITE(7,*) UFIELD(Y, MID+X)
  WRITE(8,*) DUFIELD(Y, MID+X)
```

115 CONTINUE

CCC WRITE(7,*) 'Path 3 (xdash = 0.9 to -1.0, ydash = -1.3)'

```
Y = Y-1
DO 120 X = 9, -10, -1
  WRITE(7,*) UFIELD(Y, MID+X)
  WRITE(8,*) DUFIELD(Y, MID+X)
```

120 CONTINUE

CCC WRITE(7,*) 'Path 4 (xdash = -1.0, ydash = -1.2 to -0.2)'

```
X = X+1
DO 125 Y = NY-1, 2, -1
  WRITE(7,*) UFIELD(Y, MID+X)
  WRITE(8,*) DUFIELD(Y, MID+X)
```

125 CONTINUE

```
CLOSE(3)
CLOSE(4)
CLOSE(7)
CLOSE(8)
```

C Now read in the values dumped out into the matrices
C G, DG, U and DU.

```
OPEN(3, FILE='/GREEN DATA', FORM='FORMATTED', STATUS='OLD')
OPEN(4, FILE='/DGREEN DATA', FORM='FORMATTED', STATUS='OLD')
OPEN(7, FILE='/UFIELD DATA', FORM='FORMATTED', STATUS='OLD')
OPEN(8, FILE='/DUFIELD DATA', FORM='FORMATTED', STATUS='OLD')
```

```
DO 130 N = 1, 64
  READ(7,*) U(N)
  READ(8,*) DU(N)
```

130 CONTINUE

```
DO 135 M = 1, 64
  DO 135 N = 1, 64
    READ(3,*) G(N,M)
    READ(4,*) DG(N,M)
```

135 CONTINUE

```
CLOSE(3, STATUS = 'DELETE')
CLOSE(4, STATUS = 'DELETE')
CLOSE(7, STATUS = 'DELETE')
CLOSE(8, STATUS = 'DELETE')
```

```
RETURN
END
```

```
SUBROUTINE OUTPUT (NEWU)
```

```
DOUBLE PRECISION NEWUMAX, NEWU(1:64)
```

```
C Find the maximum field value in the array
```

```
NEWUMAX = ABS(NEWU(1))
DO 10 I = 2, 64
  IF (ABS(NEWU(I)) .GT. NEWUMAX) THEN
    NEWUMAX = ABS(NEWU(I))
  ENDIF
```

```
10 CONTINUE
```

```
C Now normalise all the values in the array and output them
C into the file FILE FT09F001.
```

```
DO 20 I = 1, 64
  WRITE(9,*) NEWU(I)/NEWUMAX
```

```
20 CONTINUE
```

```
RETURN
END
```